國立交通大學
材料科學與工程學研究所
碩 士 論 文

多孔性及兩相式(MSQ/高溫起孔洞劑)低介電材料之吸水性與擴散行為研究

Moisture uptake and diffusion behavior of MSQ/high-temperature porogen hybrids and porous low-k materials

研 究 生：鄧鈞元

指導教授：呂志鵬　博士

中 華 民 國 九十六 年 十二 月

多孔性及兩相式(MSQ/高溫起孔洞劑)低介電材料之吸水性與擴散行為研究

Moisture uptake and diffusion behavior of MSQ/high-temperature porogen hybrids and porous low-k materials

研 究 生：鄧鈞元　　Student：Jun Yuan Teng
指導教授：呂志鵬　　Advisor：Dr. Jihperng (Jim) Leu

國 立 交 通 大 學
材 料 科 學 與 工 程 學 系
碩 士 論 文

A Thesis
Submitted to Department of Materials Science and Engineering
College of Engineering
National Chiao Tung University
in partial Fulfillment of the Requirements
for the Degree of Master
in

Materials Science and Engineering

December 2007

Hsinchu, Taiwan, Republic of China

中華民國九十六年十二月

多孔性及兩相式(MSQ/高溫起孔洞劑)低介電材料之吸水性與擴散行為研究

研究生: 鄧鈞元　　　　　　　　　　　　指導教授: 呂志鵬

國立交通大學材料科學與工程學系碩士班

摘要

本研究利用 Solid-First™ 製程以 Methylsilsesquioxane (MSQ)為介電材料的基材、poly (styrene-block-4-vinylpyridine) (PS-P4VP)以及 poly (styrene-block-butadiene-block- styrene) (PS-PB-PS)為高溫起孔洞劑。利用自行組裝之石英微量天坪探討下列三種低介電薄膜之吸水性及水氣擴散行為(1)不同製程溫度的 MSQ 膜(2) 製程溫度為 250 ^{o}C 之 MSQ/Porogen 混參膜(3)多孔性薄膜。

研究結果顯示孔隙率較大之多孔性薄膜有較高的吸水量乃是因為表面積與氫氧基較多之故。以 HMDS 改質孔隙率 19.3 %的多孔性薄膜則可降低約 17 %的吸水量。MSQ/PS-P4VP 混合膜的吸水性較多孔性薄膜高乃因 PS-P4VP 有較高吸水量之故且高溫起孔洞劑之砒啶與氫氧基之作用使得 MSQ/PS-P4VP 有較多之殘餘氫氧基。MSQ/PS-PB-PS 之吸水性比 MSQ/PS-4VP 差因為 PS-PB-PS 之吸水性較差之原故。

綜合 QCM、C-V、吸附脫附行為顯示水吸附於 MSQ 或 MSQ/Porogen 的方式以物理吸附為主。在本研究顯示水氣下列兩種方式吸附(1)以凡得瓦耳力附著於 MSQ 或起孔洞劑中、MSQ 與基材之介面以及起孔洞劑與基材之介面而此吸附方式佔總吸水量的 80 % (2)以氫鍵(Si-O……H_2O)附著此吸附方式佔總吸水量的 20 %。

水氣在薄膜中擴散行為大至符合 Fickian 擴散方式，但是各種薄膜有幾乎相同的擴散係數除了高含量高溫起孔洞的薄膜乃是因為孔洞型態改變之故。擴散係數在高溫起孔洞劑含量 20 wt%下保持不變是因為有一層緻密薄膜在表面形成且為速率控制。而此緻密薄膜可為擴散阻障層，保護 CVD、ALD 之先驅物擴散進入介電材料中。但是 PS-PB-PS 系統則無此緻密薄膜，本論文將提出 MSQ/PS-P4VP 表面緻密薄膜形成方式。

Moisture uptake and diffusion behavior of MSQ/high-temperature porogen hybrids and porous low-k materials

Student: Chun-Yuan Teng Advisor: Jihperng (Jim) Leu

Department of Materials Science and Engineering
National Chiao Tung University

Abstract

Incorporation of porosity into dielectric materials is a viable method to reduce k-value down to < 2.5. A Solid-First^{TM} scheme based on high-temperature porogen, poly (styrene-block-4-vinylpyridine) (PS-P4VP), poly(styrene-block- butadiene-block -styrene) (PS-PB-PS) and methyl-silsesquioxane (MSQ) as the matrix have been employed to prepare porous low-k dielectric in order to circumvent the reliability issues encountered in the integration of as-deposited porous dielectric. The impact of high-temperature porogens, their loadings, and porosities on the moisture uptake and diffusion behavior was investigated using a home-built quartz crystal microbalance (QCM). Three low-k dielectric systems were employed in this thesis to simulate interlayer dielectrics (ILD) at different stages of Solid-First^{TM} integration scheme; namely: (1) MSQ films cured at different temperatures up to 400 ^{o}C, (2) MSQ/porogen hybrid films cured at 250 ^{o}C with various porogen loadings, and (3) their corresponding porous films burned out at 400 ^{o}C.

The moisture uptake of porous films cured at 400 ^{o}C increased with porosity due to an increase of pore surface area and residual silanol, Si-OH groups. Further surface treatment of porous MSQ by hexamethlydisilazane (HMDS) eliminated

surface Si-OH groups and led to a 17% reduction of moisture uptake for porosity at 19.3%. In addition, moisture absorption of MSQ/PS-P4VP hybrid films cured at 250 ^{o}C were greater than porous MSQ ones because of the high water uptake in PS-P4VP (6.7 wt%) and the increased Si-OH concentration arisen from the interaction between the polar pyridine moiety of porogen with Si-OH in the MSQ matrix In contrast, moisture uptake of MSQ/PS-PB-PS hybrid films was much less than MSQ/PS-P4VP films because of the hydrophobic characteristic of PS-PB-PS.

Based on moisture uptake, sorption/desorption behavior, and HMDS pretreatment by using QCM and CV measurements, we concluded that the moisture uptake in porous MSQ films or MSQ/high-temperature porogens hybrid films in this thesis is solely physical sorption. The physical sorption of moisture uptake underwent by Van der Waals long range force with (1) available surface area within the MSQ or porogen matrix, inside the pores, and at the MSQ/substrate and porogen/substrate interfaces, which contributed < 80% of moisture uptake, and (2) available hydrogen-bonded Si-OH--H_2O sites, which were formed immediately after sample preparation, accounted for < 20% of moisture uptake.

Finally, the moisture diffusion in MSQ/PS-P4VP films and their corresponding porous MSQ films followed Fickian diffusion behavior with almost the same diffusion constant except in the high porogen loading region where pore morphology has changed. The constant diffusion constant at porogen loading below 20% could be attributed to the formation of a rate controlling, dense layer on the top of porous or hybrid low-k films. Such thin but dense layer could serve as a diffusion barrier layer beneficial in certain processing modules. In contrast, no skin layer was observed for MSQ/PS-PB-PS system. The formation mechanism of such a dense layer in MSQ/PS-P4VP system was proposed in the thesis.

誌謝

首先誠摯的感謝指導教授呂志鵬博士，老師悉心的教導使我得以一窺low-k領域的深奧，不時的討論並指點我正確的方向，使我在這些年中獲益匪淺。老師對學問的嚴謹更是我輩學習的典範。

兩年裡的日子，實驗室裡共同的生活點滴，學術上的討論、言不及義的閒扯、讓人又愛又怕的宵夜、趕作業的革命情感、因為睡太晚而遮遮掩掩閃進實驗室........，感謝眾位學長姐、同學、學弟妹的共同砥礪，你們的陪伴讓兩年的研究生活變得絢麗多彩。

感謝國原、kima、大龜、阿義學長、幸玲學姐們不厭其煩的指出我研究中的缺失，且總能在我迷惘時為我解惑，也感謝阿之、冠頭魚、欣源同學的幫忙，恭喜我們順利走過這兩年。實驗室的阿農、伯政、晉成、王聰明學弟、nikky、宜甄、先帝學妹們當然也不能忘記，妳的幫忙及搞笑我銘感在心。

女朋友小頭貞在背後的默默支持更是我前進的動力，沒有小頭貞的體諒、包容，相信這兩年的生活將是很不一樣的光景。

最後感謝國科會(計畫編號NSC95-2221-E009-309、NSC96-2221-E-009-216)及SRC(計畫編號SRC 2007-KJ-1301)於經費的贊助。

Contents

摘要....................i
Abstract.................... iii
Acknowledgements....................v
Table Caption.................... viii
Figure Caption.................... viii
Chapter 1 Introduction....................1
Chapter 2 Literature review....................3
2.1 low dielectric constant materials....................4
2.1.1 Dielectric constant....................6
2.1.2 Polarization of material....................7
2.2 Integration requirements of low-k materials....................10
2.3 Deposition of low-k films....................11
2.3.1 Chemical vapor deposition (CVD)....................11
2.3.2 Spin coating....................11
2.4 Introduction of low-k materials....................13
2.4.1 Silicon-base low-k polymer....................13
2.4.1.a Fluorinated silicate Glass (FSG)....................13
2.4.1.b Carbon doped oxide (CDO)....................14
2.4.1.c Hydrogen silsesquioxane (HSQ)....................16
2.4.1.d Methyl silsesquioxane (MSQ)....................18
2.4.2 Organic low-k polymer....................20
2.4.2.a SILK^{TM}....................20
2.5 Porous low-k materials....................21
(1) Sol-Gel method....................22
(2) Nano-clustering method....................23
(3) Template method....................23
2.6 Impact of porous materials on IC integration....................26
2.7 Impact of moisture on low-k materials.....................31
Chapter 3 Experimental....................32
3.1 Preparation of low-k films....................36
3.1.1 Chemicals....................36
3.1.2 Preparation of low-k precursor solution....................37
3.1.3 Deposition of low-k films....................38
3.2 Experimental techniques....................39

3.2.1 n&k analyzer 39
3.2.2 Specular reflectance Fourier-transform infrared spectroscopy (FIIR) 41
3.2.3 Capacitance measurement 41
3.2.4 Focus ion beam (FIB) 44
3.2.5 Quartz Crystal Microbalance (QCM) 45
Chapter 4 Result and Discussion 53
4.1 Optical properties of low-k films 54
4.2 Moisture uptake of low-k films..56
4.2.1 Moisture uptake of MSQ films with different curing temperature 56
4.2.2 Moisture uptake of porous films……………………………..………58
4.2.3 Moisture uptake of HDMS modified porous films and MSQ/PS-P4VP hybrid films…………………………………………………………...……60
4.2.4 Moisture uptake of MSQ/PS-PB-PS hybrid films 62
4.3 Dielectric properties..64
4.4 Diffusion behavior 68
Chapter 5 Conclusions 77
Reference 81
Appendix A 87
Appendix B 92

List of Tables

Table 2.1 Dielectric constants of typical materials at 20 ^oC 7
Table 2.2 Requirements of ILD properties 10
Table 2.3 Film properties of carbon-doped oxide and PECVD SiO_2 16
Table 2.4 Key material properties of HSQ and MSQ 20
Table 2.5 Summary of SiLK^{TM} properties 21
Table 2.6 Various surfactant(S)/inorganic(I) interaction and examples
including PH condition 25
Table 4.1 Moisture uptake of porous MSQ and HMDS modified porous
MSQ films..59
Table 4.2 Moisture uptake of MSQ/PS-PB-PS hybrid films 63

List of Figures

Figure 1.1 (a) dense low-k MSQ matrix cured at 400 °C, (b) solid-first^{TM}
MSQ matrix/porogen hybrids cured at 250 °C, and (c)
corresponding porous low-k MSQ films after removal of porogen at
400 °C 2
Figure 2.1 Structures of multilayer interconnect (a) Al metallization and (b)
copper metallization...3
Figures 2.2 Cross-sectional view of a three-layer interconnect with
orthogonal layout. 2
Figure 2.3 Relationship between generation node and RC-delay in gate and
interconnect for Al/SiO2 and Cu/lok k 4
Figure 2.4 (a) Capacitor in vacuum (b) Capacitor with dielectric 6
Figure 2.5 Electronic polarization...8
Figure 2.6 ionic polarization...8
Figure 2.7 orientation polarization 9

Figure 2.8 Relationship between dielectric constant and applied electric filed frequency 10
Figure 2.10 Chemical structure of fluorinated silicate glass at (a) low fluorine concentration and (b) high fluorine concentration 14
Figure 2.11 Chemical structure of carbon-doped oxide (CDO)..................14
Figure 2.12 Chemical structures of precursors for carbon doped oxide 15
Figure 2.13 Silsesquioxane preparative pathways 17
Figure 2.15 Chemical structures of (a) HSQ and (b)MSQ 20
Figure 2.17 Schematic illustratration of pore formation in nano-clustering23
silica 23
Figure 2.18 Pore was formed by thermally or chemically removing templating agent or porogen. 23
Figure 2.19 Ordered and disordered phases of microstructured materials ..24
Figure 2.20 SEM photographs of (a) delamination during CMP process and (b) delamination and failure after wire bonding 26
Figure 2.21 Penetration of copper into non-continuous sidewall of a porous dielectric..27
Figure 2.22 (a) TEM image of sidewall profile after pore sealing by a thin low dielectric layer , (b) The schematic diagram of sealing concept...28
Figure 2.23 Concept and process flow of Solid FirstTM scheme Figure 30
Figure 2.24 Low-k material thin film swells upon absorption of moisture .31
Figure 2.25 31
Figure 2.26 Leakage current of low-k thin films under wet and dry conditions...32
Figure 2.27 Schematic diagramd of water adsorption onto SiO2 with and without HMDS treatment..33

This chapter described the experimental methods and steps, including low-k precursor solution preparation, spin coating, thermal processed, quantitative measurement of moisture uptake in low-k films by quartz crystal microbalance, and collection of chemical bond information by FTIR, thickness and refractive index by n&k analyzer, pore morphology by SEM, and dielectric constant by CV-dot measurement. Flow-chart of experimental procedures was summarized in Figure 3.1 35

Figure 3.1 Flow-chart of experimental procedures....................35

Figure 3.2 Schematic illustration on the preparation of precursor solution.39

Figure 3.3 Typical curve of n&k measurement....................40

Figure 3.4 Schematic diagram of a specular reflectance infrared speectroscopy....................41

Figure 3.5 The process flow for fabricating a MIS sample for CV-dot measurement....................42

Figure 3.6 Shadow mask with three different diameters for CV-dot measurement....................43

Figure 3.7 The utilization of linear curve fitting of various dot sizes to minimize the errors from fringes effect and area measurement....................44

Figure 3.8 Schematic diagram of a FIB/SEM system....................45

Figure 3.9 Schematic diagram of QCM system for moisture uptake measurement....................50

Figure 3.10 The frequency change of the crystal resonator at 30 oC versus time during sorption and desoprtion for MSQ/PS-P4VP (10wt%) hybrid film....................51

Figure 3.11 Moisture uptake of MSQ/ PS-P4VP (10wt%) hybrid film as a

function of time....52
Figure 4.1 (a) Refractive index as a function of porogen loading and (b) Optical dielectric constant as a function of porogen loading....54
Figure 4.2 The correlation between porosity and porogen loading. 55
Figure 4.3 Moisture uptake behavior of MSQ films cured at 250°C and 400°C....56
Figure 4.4 FTIR spectra of MSQ films cured at at 250 ^{o}C and 400 ^{o}C 57
Figure 4.5 Moisture uptake of porous MSQ and HMDS modified porous MSQ films....58
Figure 4.7 The moisture uptake of MSQ/PS-b-P4VP hybrid films a function of porogen loadings....62
Figure 4.8 Moisture uptake of MSQ/PS-b-P4VP and MSQ/PS-PB-PS hybrid films 63
Figure 4.9 Dielectric constants of porous MSQ and HMDS-modified porous MSQ films at dry and RH 100 % conditions. 65
Figure 4.10 Dielectric constants of MSQ/PS-P4VP hybrid films at dry and RH 100% conditions....66
Figure 4.11 Series model, parallel model and EMA model of capacitance .67
Figure 4.12 Calculated dielectric constants based on three models: series model, parallel models, and EMA model as function of loading vs. experimental data....68
Figure 4.13 Typical fitting curve based on Fickian diffusion....70
Figure 4.14 Diffusion coefficients of various low-k films versus different porogen loadings....71
Figure 4.15 FIB/SEM topview of (a) as-cured, (b) after 5-second sputter etch and (c) cross-section view SEM of a porous MSQ film with 7.9 %

porosity based on PS-P4VP porogen. 72

Figure 4.16 Schematic diagram of a skin layer/porous low-k matrix stack under the diffusion of moisture..73

Figure 4.17 The proposed mechanism for skin layer formation in MSQ/PS-P4VP hybrid films..74

Figure 4.18 FIB/SEM top-view of as-cured MSQ/PS-PB-PS hybrid film with 5% porogen loading..74

Figure 4.19 (a) hydrogen-bonding between silanol and water and (b) condensation reaction of silanols..76

Chapter 1 Introduction

As device scaling continues, RC delay in the backend interconnect becomes the bottleneck [1]. In order to alleviate this problem, copper was first implemented, then low dielectric constant (low k) materials such as carbon-doped oxide or SiLK^{TM} (k~2.6-3.0) was introduced [2, 3]. For dielectric with k<2.2 which is required for 45 nm node and beyond, incorporation of porosity is inevitable to further reduce the k-value. However, porous low k thin film may encounter reliability issues such as (1) delamination and cracks during CMP and other process due to low mechanical strength, and (2) bias-temperature stressing (BTS) failure due to non-continuous side-wall coverage of barrier deposited by atomic layer deposition, chemical vapor deposition or physical vapor deposition process. To circumvent such reliability issues, a novel Solid-First^{TM} [4] approach in material design using high-temperature porogen and integration has been proposed to defer the formation of porous dielectric after the completion of a metal layer, then thermally remove the sacrificial, high-temperature porogen. Recently, Che et al. demonstrated porous ultra low-k materials (k~2.0) using an amphiphilic block copolymer (ABC) high temperature porogen, poly (styrene-block-4-vinylpyridine) (PS-P4VP) in the Solid-First^{TM} scheme [5]. In addition such approach offers better mechanical strength.

For porous dielectrics, there are additional concerns related to moisture and solvent uptake induced by processing steps such as CMP, post-etch cleaning, post-CMP cleaning or resist removal. The dielectric properties of porous low-k materials will be significantly degraded if residual H_2O (K_{water}~78) adsorbed in the matrix and porogen. In addition, the moisture outgassing may destroy diffusion barrier or etch-stop layer during thermal process [6] resulting in delamination or catastrophic fracture the die. However, there is still little understanding of the

adsorption behavior, moisture uptake, and outgassing behavior of low-k dielectric materials, especially porous dielectrics involving the matrix/high temperature porogen hybrid in Solid-First scheme at different stages.

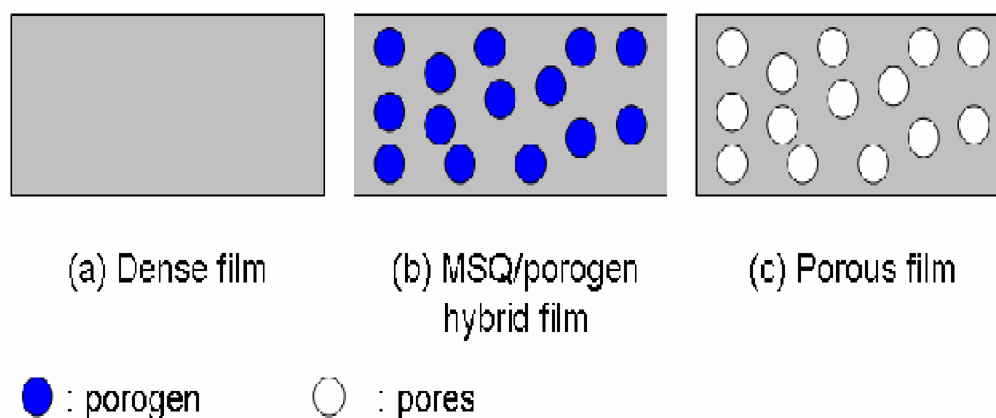

Figure 1.1 (a) dense low-k MSQ matrix cured at 400 °C, (b) solid-first^{TM} MSQ matrix/porogen hybrids cured at 250 °C, and (c) corresponding porous low-k MSQ films after removal of porogen at 400 °C

In this study, methylsilsesquioxane and high-temperature porogen, PS-P4VP, PS-PB-PS were used as low-k material matrix and template. Specifically, three types of low-k films namely (a) dense low-k MSQ matrix cured at 400 °C, (b) solid-first^{TM} MSQ matrix/porogen hybrids cured at 250 °C, and (c) corresponding porous low-k MSQ films after removal of porogen at 400 °C, schematically illustrated in Figure 1.1 were employed to investigate the impact of porogens and porosity on the moisture uptake and diffusion behavior using quartz crystal microbalance (QCM). The implication of moisture uptake and diffusion with ILD processing will be also discussed.

This thesis includes chapter 1 Introductions and Motivation, chapter 2 Literature Review, chapter 3 Experimental Method, chapter 4 Results and Discussion, chapter 5 Conclusions.

Chapter 2 Literature review

As the device dimension continuously shrinks towards small size according to **Moore's law** [7], the unit area of silicon wafer contains more and more transistors, and the chips performance is enhanced. Therefore, the chip price can be lowered by increasing the number of chips on each silicon wafer. On the signal propagation within a chip, the signal delay was controlled not only by gate delay but also by signal propagation within the multilayer interconnect such as Al/SiO2 and Cu/low-k interconnects as shown in Figures 2.1(a) and (b), respectively.

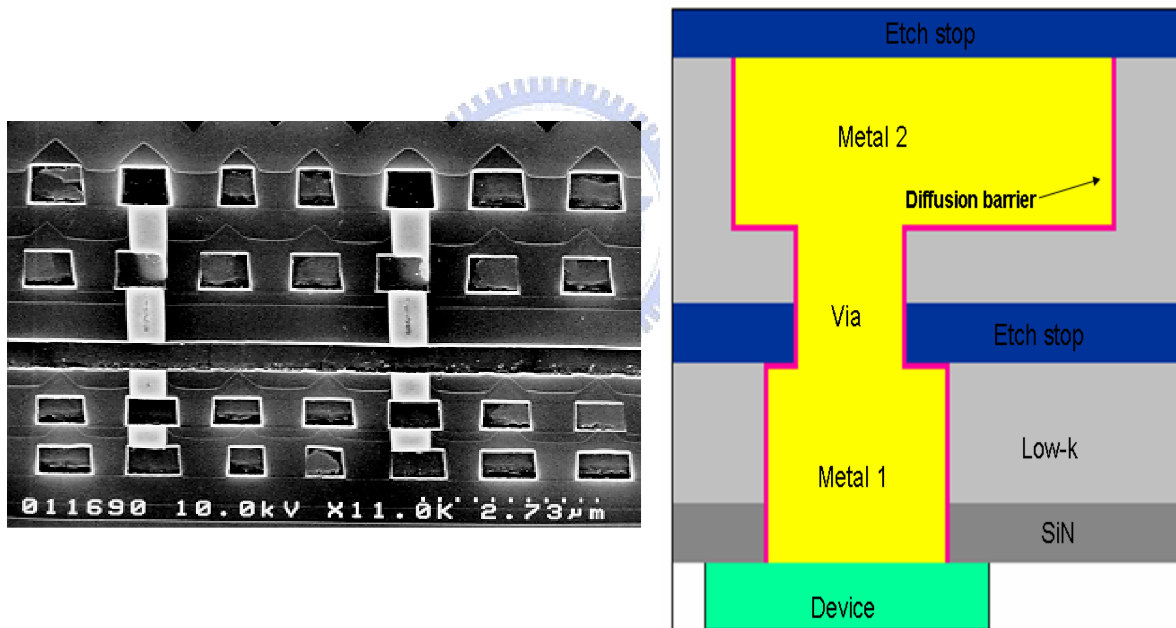

Figure 2.1 Structures of multilayer interconnect (a) Al metallization and (b) copper metallization

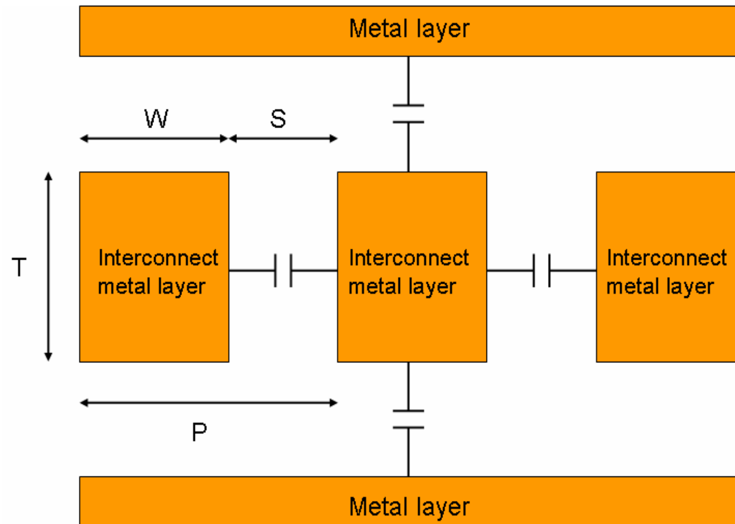

Figures 2.2 Cross-sectional view of a three-layer interconnect with orthogonal layout.

In the simple first-order, the RC-delay in the interconnect could be expressed by Equation (2.1) [2].

$$RC_{delay} = 2 \cdot \rho \cdot \kappa \cdot \varepsilon_0 \cdot \left(\frac{4L^2}{P^2} + \frac{L^2}{T^2} \right) \tag{2.1}$$

Where P: line pitch,

W: the metal line width,

S: the spacing between line to line

T: the thickness of metal line

ρ: metal resistively

ε_0: the vacuum permittivity,

k: the relative dielectric constant of dielectrics

L: the length of the metal line.

Moreover, the power consumption of device could be obtained by Equation 2.2.

$$P_c = \left(\frac{1}{2}\right) f_d C V^2 f \qquad (2.2)$$

where C: total capacitance

V: the supply voltage

f: the operation frequency

f_d: the fraction of gate that switches during a clock period.

In general, device scaling increased RC-delay and power consumption due to the increase of line-to-line capacitance. In the previous technology nodes (> 250 nm), interconnect signal delay based on Al aluminum (ρ=2.67 μΩ-cm) and silicon oxide (k = 4), could be ignored as compared to gate delay since the dimension of metal wire was large enough as illustrated in Figure 2.3. When the device dimensions scaled below than 250 nm node, the interconnect RC delay of Al/SiO_2 became the bottleneck of signal propagation while power consumption became the critical issue of device performance. In contrast, Cu/low-k interconnect illustrated in Figure 2.3 showed that RC delay was greatly reduced compared to Al/SiO_2 at < 250 nm nodes [8]. By employing (1) copper with low resistivity as interconnect metal line and (2) materials with low relative dielectric constant, the problem of RC-delay of interconnect could be contained. In addition, utilizing low dielectric materials could reduce cross-talk and power consumption. Therefore, low dielectric materials were more important for RF devices.

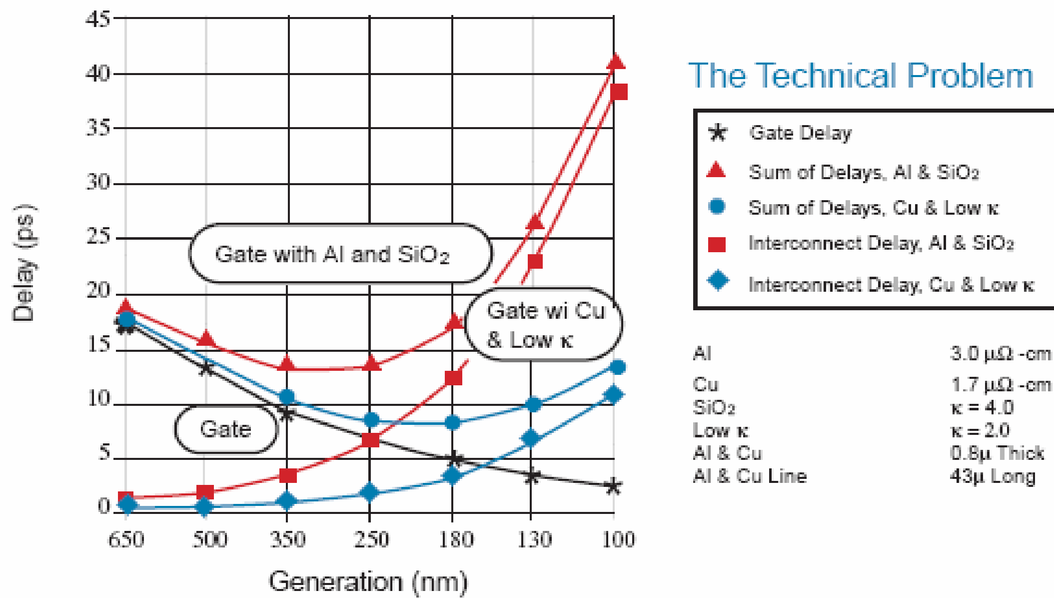

Figure 2.3 Relationship between generation node and RC-delay in gate and interconnect for Al/SiO2 and Cu/lok k [9]

The industry first introduced copper to replace aluminium into the backend technology in 1997 by International Business Machine Corp (IBM). However, the migration from silicon oxide to low-dielectric constant (low-k) materials was gradual due to its great impact on integration. As a result, the early adoption of low-k preferred the modification of silicon oxide such as fluorinated silicate glass (FSG) (k ~3.5-3.7), then carbon-doped oxide (CDO) (k ~3.2-2.5). Unfortunately, dielectric constants of viable, dense carbon-doped oxides were limited to ≥ 2.5. In order to further lower dielectric constants, the incorporation of pores into low-k materials became necessary since dielectric constant of air was about 1.

However, integrating porous, low dielectric materials into copper dual damascene structure and processes had many problems such as:

(1) The mechanical strength of porous low-k was much worse than silicon dioxide.or FSG

(2) Discontinuous barrier coverage at the trench sidewall of porous low-k

materials would cause reliability issues.

Therefore, the mitigation of mechanical strength and reliability issues in the integration and process development of porous low-k dielectrics is the most critical task in the backend technology of 45 nm node and beyond.

2.1 low dielectric constant materials

2.1.1 Dielectric constant

While electrical filed was applied on a parallel-plate capacitor in vacuum as shown in Figure 2.4 (a), the capacitance C_0 of capacitor was expressed as Equation 2.3.

$$C_0 = \frac{Q}{V} = \varepsilon_0 \frac{A}{d} \quad \text{(2.3)}$$

Where

Q: charge

V: voltage

A: parallel-plate (electrode area)

d: distance between the parallel-plate

ε_0: vacuum permittivity, 8.85E×10^{-12} F/m

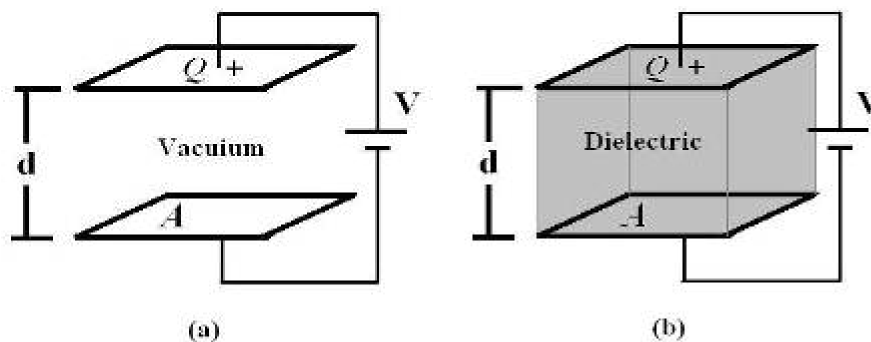

Figure 2.4 (a) Capacitor in vacuum (b) Capacitor with dielectric

The capacitances depended on geometry of the capacitor. It was directly proportional to the area A of electrode and inversely proportional to their separation *d*. The A and d were constant for a given capacitors, and ε_0 was also a universal constant.

When matter was present between the plates, it would affect the capacitance. For the same capacitor, the ratio of C to C_0 was called dielectric constant of the materials, defined as Equation 2.4 below

$$K = \frac{C}{C_0} \quad \text{.............................(2.4)}$$

Where C: the capacitance with dielectric present in parallel plate

The dielectric constant *K* is pure number. Table 2.1 listed the dielectric constants of some commonly used materials [10].

Table 2.1 Dielectric constants of typical materials at 20 °C [10]

Material	*K*	Material	*K*
vacuum	1	poly(vinyl chloride)	3.18
air (1 atm)	1.00059	germanium	16
Teflon	2.1	water	80.4
polyethylene	2.25	poly (propylene)	1.5
Benzene	2.28	poly (styrene)	2.4~2.6

2.1.2 Polarization of material [11]

The electric field applied on a material in the parallel plate capacitors would result in redistribution of electric charge, and then would induce an electric dipole. The phenomenon, redistribution of positive and negative charges within the dielectric material, was called polarization [11]. The materials dielectric properties were mainly

determined by polarizability. The dipole moment in unit volume represented the degree of polarization, which was called polarization strength.

The polarizations included electronic polarization, ionic polarization, orientation polarization and space charge [11]. The redistribution of outer atom electron and inter proton in materials in an electric field was called electronic polarization which was also called atomic polarization as shown in Figure 2.5. The electronic polarization phenomenon disappeared when the absence of the electric filed happened.

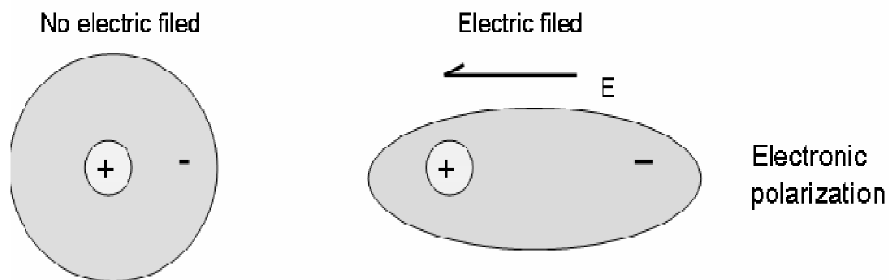

Figure 2.5 Electronic polarization

Ionic polarization, as shown in Figure 2.6, was caused by relative displacements between positive and negative ions in ionic crystals such as NaCl.

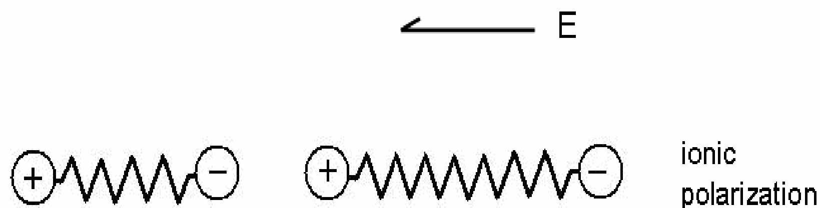

Figure 2.6 ionic polarization

When an electric filed was applied, the dipole of molecule would align electric filed which was called orientation polarization as shown in Figure 2.7. Space charge was in the dielectric, electrons, protons, and ions which moved around by the applied electric

filed. Charge tended to build up a discontinuous interface in the dielectric, such as the dielectric-electrode interface in film capacitors.

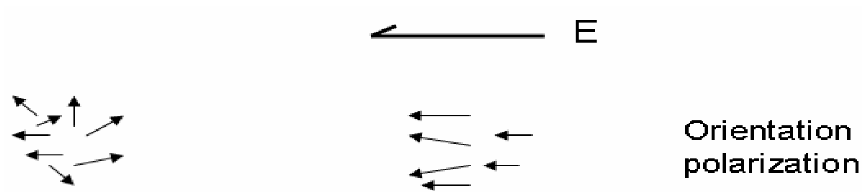

Figure 2.7 orientation polarization [11]

The dielectric constant related to polarization. When an electric filed was applied on parallel plate capacitor, polarizability *P*; then the capacitance increased as shown in equation 2.5.

$$C = \varepsilon_0 \frac{A}{d} + \frac{AP}{V} \quad \text{..................(2.5)}$$

By combining $k = 1 + \frac{Pd}{\varepsilon_0 V}$ with equation 2.5, we obtained equation 2.6.

$$C = k\varepsilon_0 \frac{A}{d} \quad \text{....................(2.6)}$$

Besides, the polarization also related to the frequency of electric filed**;** thus, the dielectric properties of materials were a function of operating frequency as shown in Figure 2.8. The dielectric constants of materials were dependent on operating frequency contributed to electronic, atomic and orientation polarization [12]. At the optical frequency, the primary contribution was electronic polarization because atomic and orientation polarization can not respond so fast.

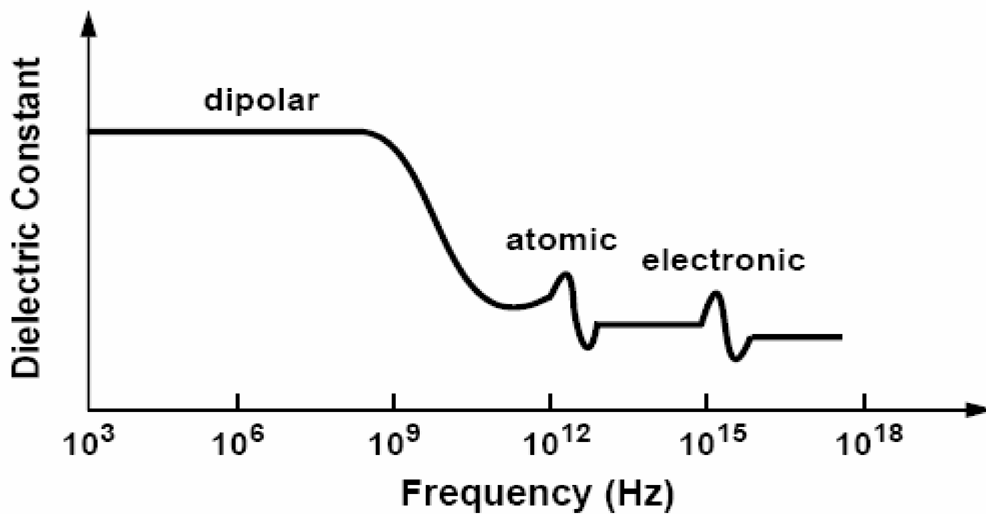

Figure 2.8 Relationship between dielectric constant and applied electric filed frequency [12]

2.2 Integration requirements of low-k materials

In order to reduce RC-delay, the k value of low-k materials must be lower than traditional SiO_2. However, the interlevel dielectric materials (ILD) needed not only good electrical properties, but also excellent chemical properties, mechanical properties and thermal stability. Desired properties [13] of ILD were shown in following Table 2.2.

Table 2.2 Requirements of ILD properties [13]

Electrical	Chemical	Mechanical	Thermal
Low dielectric constant Isotropic Low dissipation Low leakage current Low charge trapping High electric filed strength	Good chemical resistance Low moisture uptake <1% Etch rate and selectivity Low gas permeability No metal corrosion	Thickness uniformity Good adhesion Residual stress <100Mpa Low shrinkage Crack resistance Tensile modulus	High thermal stability CTE <50 ppm/^{o}C Low thermal shrinkage High thermal conductivity

2.3 Deposition of low-k films

There are two major methods, namely chemical vapor deposition and spin coating for depositing low-k thin films in the fabrication of silicon-based IC devices.

2.3.1 Chemical vapor deposition (CVD)

Chemical vapor deposition was a film deposition method, whose utilizing chemical reaction included pyrolysis, reduction, oxidation and/or nitridation on the substrates. The mechanism of CVD deposition consisted of three steps. The first was nucleation, and then the nucleus formed an island which grew into a big island later. Finally, continuous film formed when the island was large enough to contact the others. The films deposited, by low pressure CVD (LPCVD), with more uniform quality since low pressure had lager mean free path [14]. For low-k thin films used in the backend interconnect, plasma-enhanced chemical vapor deposition (PECVD) was commonly employed at 350-450 ^{o}C due to the consideration of lowered thermal budget.

2.3.2 Spin coating

The most simple and common technique of depositing thin films onto wafer was spin coating. Spin coating was applied in many applications such as dielectric and photoresist in semiconductor fabrication, magnetic disk coating, flat screen display coating, and tube phosphor and antireflection coating of television. There were four stages of the spin coating process schematically illustrated in Figure 2.9. The first stage was deposition of coating solution onto the substrate, and then the speed accelerated to desired rotation speed. In the third stage, speed rate was constant; the last stage was evaporation of solvent, which dictated the film thickness. Typically, this was followed by a prebake step at intermediate temperature (100-200 ^{o}C) to drive out the solvents then a curing step at 350-425 ^{o}C to form the final dielectric structure

through, for example, crosslinking reaction in the case of methylsilsesquioxane (MSQ). In this thesis, spin coating was employed for the deposition of low-k thin films.

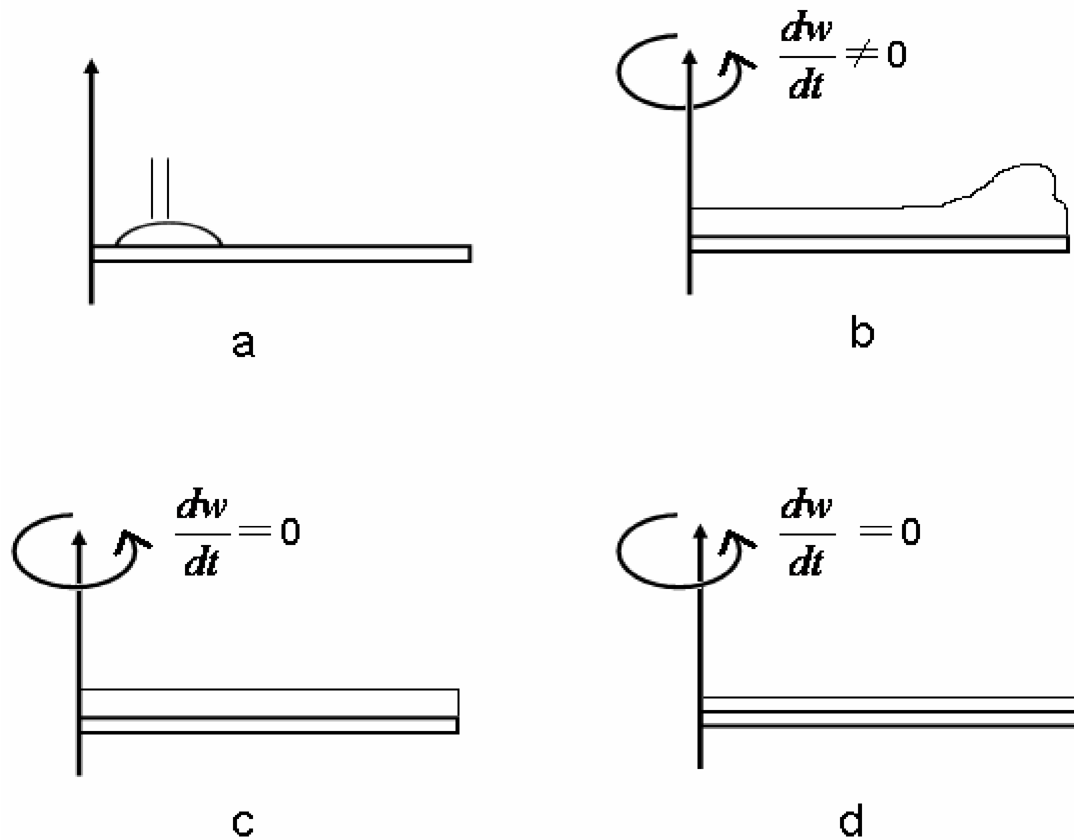

Figure 2.9 (a) Deposition on substrate, (b) acceleration to desired rotation speed, (c) spin at constant speed (d) solvent evaporation

2.4 Introduction of low-k materials

There were two commonly used low dielectric materials; one was silicon-based dielectric, the other was organic-based polymeric dielectric. Both possessed low poarizability and high thermal resistance. In the following sections, typical low-k materials already implemented in IC production or under development will be briefly reviewed.

2.4.1 Silicon-based low-k dielectrics

2.4.1.a Fluorinated silicate glass (FSG)

The dielectric constant of traditional silicon oxide was about 3.9~4.2. Fluorinated silicate glass (FSG) whose dielectric constant was about 3.5~3.9, was obtained by the incorporation of fluorine into silicon oxide [15]. Fluorinated silicate glass film could utilize either plasma-enhanced chemical vapor deposition (PECVD) or high-density plasma deposition (HDP) method [16] SiH_4 and fluorides, such as SiF_4, C_2F_6, CF_4 and triethoxyfluorosilicate (TEFS) were used as the gas sources for PECVD or HDP deposition of FSG thin films. FSG, with good gap-filling capacity, have been introduced into 0.25 and 0.18 μm IC production.

Terminal Si-F bond broke silicon oxide network structure as shown in Figure 2.10 and decreased the density of FSG film, which in turn the dielectric constant. The dielectric constant of FSG was also dependent on fluoride concentration. When concentration of fluoride increased, the dielectric constant decreased. However, FSG cannot stand in high temperature at which FSG released HF to react with Ti, Ta, TiN to form fluoride or volatile SiF_4 species. Therefore, the operating temperature of backend processing steps must be kept under 450 ^{o}C. In addition, too many Si-F bonds would also result in increased moisture adsorption

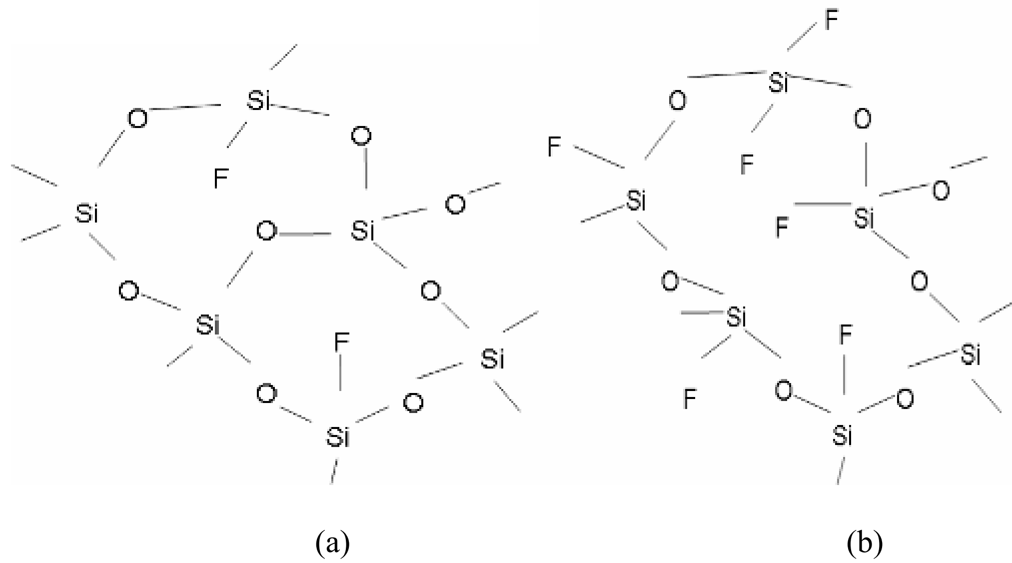

(a) (b)

Figure 2.10 Chemical structure of fluorinated silicate glass at (a) low fluorine concentration and (b) high fluorine concentration

2.4.1.b Carbon-doped oxide (CDO)

The chemical structure of carbon-doped oxide (CDO) was shown in Figure 2.11, in which the incorporation of Si-CH_3 terminal groups reduced the polarizability of SiO_2, thus lowered the dielectric constant.

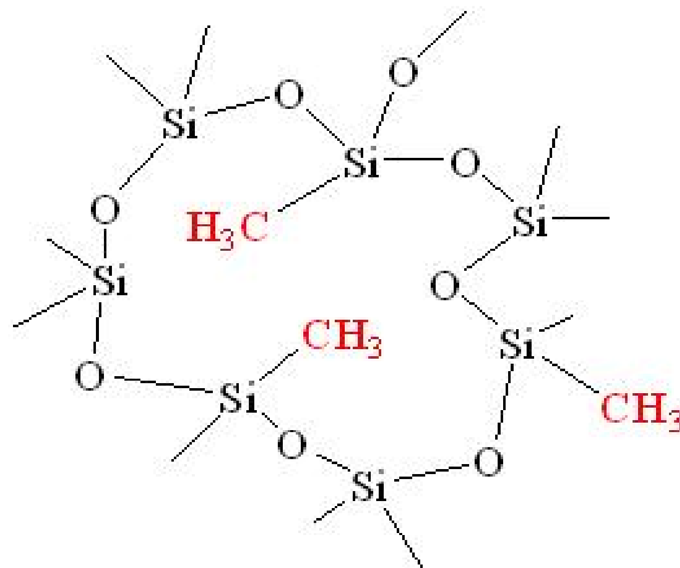

Figure 2.11 Chemical structure of carbon-doped oxide (CDO)

The CDO film was deposit by plasma enhanced chemical vapor deposition (PECVD).

Generally, there were two kinds of precursors**.** One contained oxygen in the chemical structure such as tetramethylcyclotetrasiloxane (TMCTS)[17], octamethlycyclotetrasilane (OMCTS) [18], dimethyldimethoxysilane (DMDMOS) [19], and methyltrimethoxysilane (MTOS) [20]; the other had no oxygen such as methylsilane (1MS), dimethylsilane (2MS), trimethylsilane (3MS) [21,22], and tetramethylsilane (4MS). These chemical structures were shown in Figure 2.12.

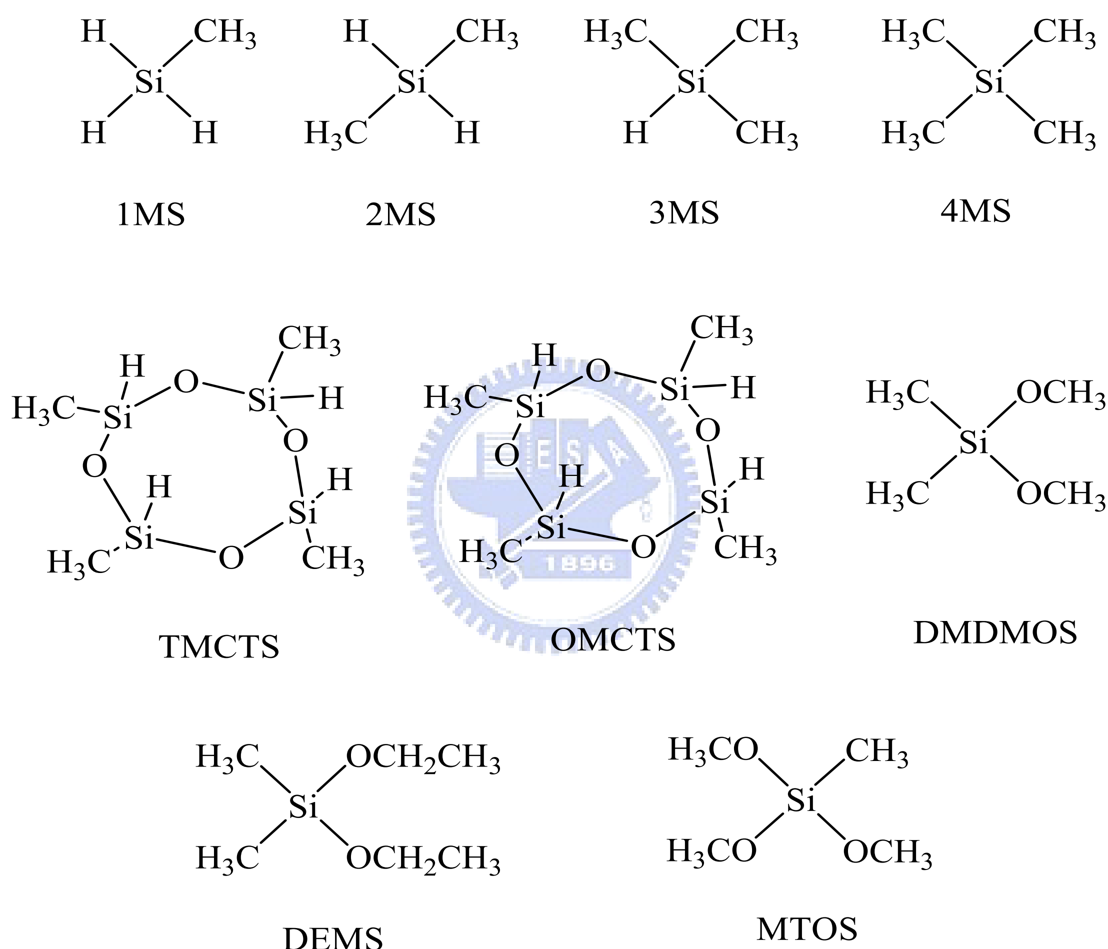

Figure 2.12 Chemical structures of precursors for carbon doped oxide

When 1MS, 2MS or 3MS were used as CDO precursors, the CDO deposition process needed oxygen or N_2O as an oxidant to oxidize precursors. Dielectric constant of CDO was about 2.6~3.3 which depended on the amount of methyl groups. In general, the amount of increased methyl groups could reduce dielectric constant of CDO.

However, too many methyl groups themselves as terminated group would also reduce mechanical strength.

The representative film properties of COD and SiO_2 films were summarized in Table 2.3 [18]**.** Since the thermal expansion coefficient of CDO was close to copper (Cu) and titanium nitride (TiN)**,** CDO was compatible for copper integration. The commercial CDO materials such as CORAL^{TM} were from Novellus Inc., Black Diamond^{TM} from Applied Materials Inc. and Auroua^{TM} from Tokyo Electron Inc. [23~25]

Table 2.3 Film properties of carbon-doped oxide and PECVD SiO_2 [18].

Property	**CDO**	**PECVD SiO_2**
Dielectric constant	< 3	4.2
Refractive index	<1.42	1.46
stress	Tensile	Compressive
Young's modulus	<10 GPa	70~80 GPa
Hardness	<2 GPa	7~9 GPa
Density	<1.4 g/cm^3	2.2 g/cm^3
Thermal conductivity	<0.4 W/mC	~1 W/mC
CTE	<10 ppm/^{o}C	<1 ppm/^{o}C

2.4.1.c Hydrogen silsesquioxane (HSQ)

Empirical formula of silsesquioxane was $(RSiO_{1.5})_n$ [26], where R was aromatic group, alkyl group or hydrogen. The procedure for the preparation of silsequioxane materials was shown in Figure 2.13. First step was hydrolysis of monomers, in which haloid or alkyloxy group was converted into hydroxyl groups. Then monomers went

through polycondenation with hydroxyl groups to become a larger molecule. Finally, the oligomers, which covered high molecular weight, would be cured at high temperature. However, the final product contained T8, T10, and T12 [27] structure which was dependent on the reaction condition, as illustrated in Figure 2.14.

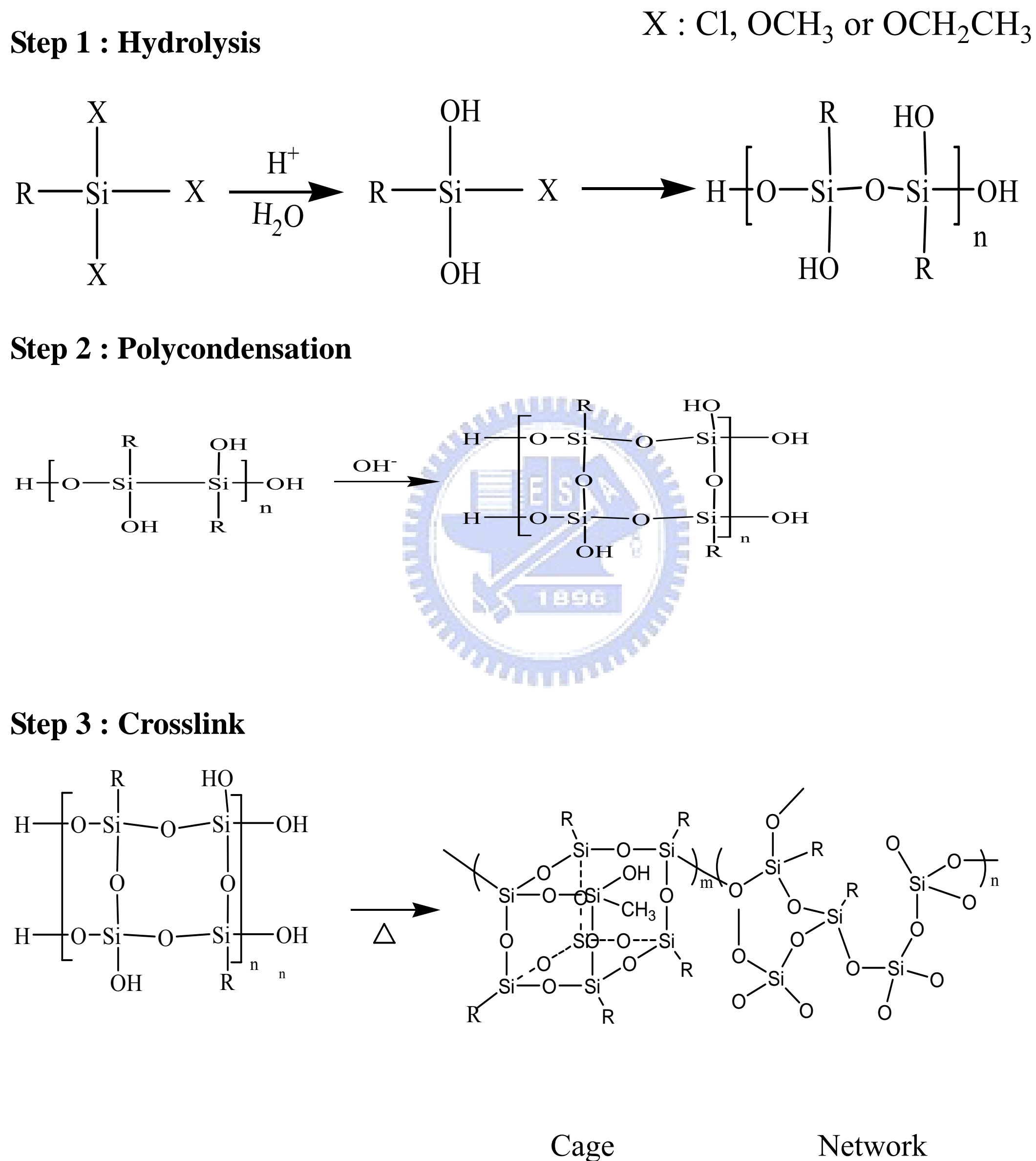

Figure 2.13 Silsesquioxane preparative pathways [28].

When R was hydrogen, the silsesquioxane was called hydrogen silsesquioxane as shown in Figure 2.15.a. Hydrogen silsesquioxane (HSQ) contained cage structure

which had larger free volume than silicon dioxide network structure. Hydrogen attaching on Si atom reduced its poarizability. This is the reason why HSQ had low dielectric properties. However, Si-H bond was sensitive to oxygen. If oxygen existed during the curing process, Si-H bond would convert to Si-OH bond, making HSQ become more hydrophilic. In curing process, temperature was also an important parameter. The modulus and hardness would increase since high curing temperature made cage structure convert to network structure [29]. However, increasing curing-temperature would degrade dielectric properties.

2.4.1.d Methyl silsesquioxane (MSQ) [28]

When R was methyl group, the final product was called methyl silsesquioxane (MSQ) which was shown in Figure 2.15.b. [28]. MSQ synthesis commonly used methyltrimethoxysilane (MTOS) illustrated in Figure 2.12, as monomer, whose reaction steps were illustrated in Figure 2.13. The reason why dielectric constant of MSQ was lower than HSQ was that polarization of methyl group attaching on Si atom was lower than hydrogen and methyl group, which had larger free volume. Si-CH_3 bond was more stable than Si-H, and therefore MSQ thermal stability and chemical resistance were greater than HSQ. Tables 2.4 listed the key materials properties of HSQ and MSQ.

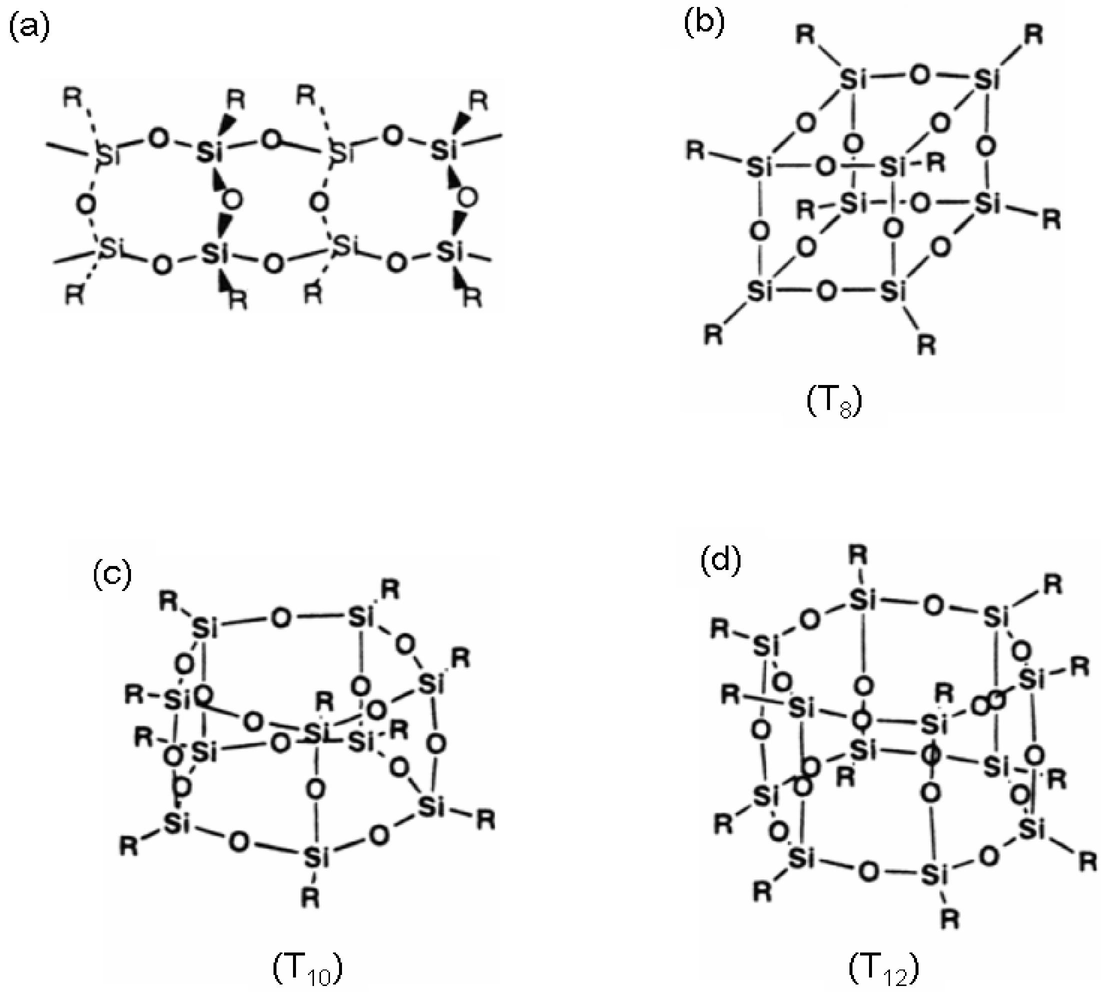

Figure 2.14 (a) ladder structure, (b)~(d) cage structure of T8, T10, T12[27]

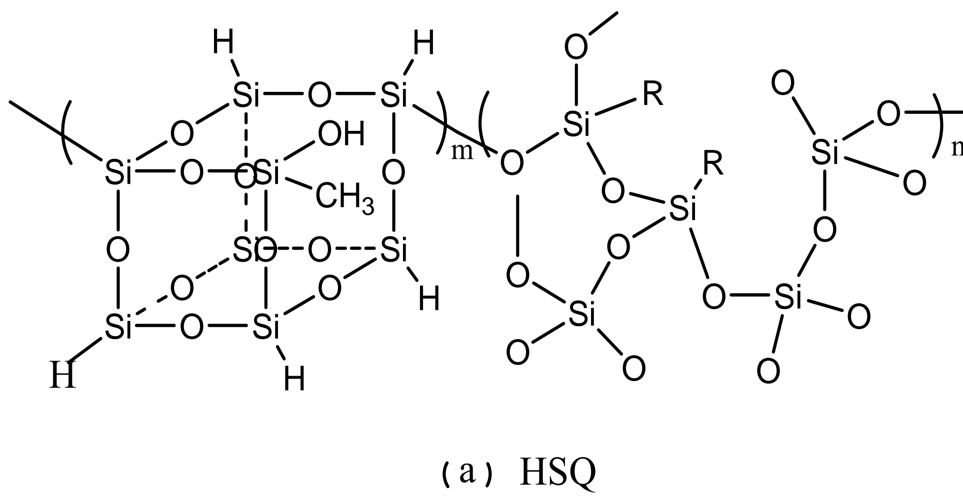

(a) HSQ

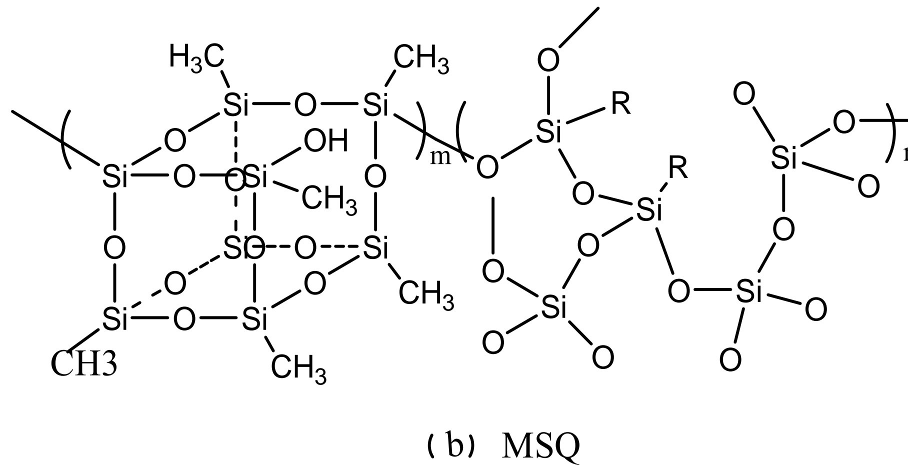

Figure 2.15 Chemical structures of (a) HSQ and (b)MSQ

Table 2.4 Key material properties of HSQ and MSQ [29]

Property	HSQ	MSQ
Dielectric constant	3 at 1MHz	2.8 at 1MHz
Modulus	6 GPa	3~5 GPa
Density	1.4~1.5 g/cm^3	1.2~1.3 g/cm^3
Tensile strength	80 MPa	50 MPa

2.4.2 Organic-based low-k polymeric dielectrics

2.4.2.a SiLK^{TM}

SiLK^{TM} was developed by Dow Chemical Company in 1996. SiLK^{TM} was a solution of low molecular weight aromatic thermosetting polymer (polynaphthalene) **[30]**. Dielectric constant of SiLK^{TM} was about 2.65, and it also had good gap filling, mechanical strength and good thermal stability. In April 2000, IBM announced SiLK^{TM} could be commercially fabricated in copper dual damascenece backend structure in IC devices **[26]**. The properties of SiLK^{TM} were summarized in Table 2.5.

Table 2.5 Summary of SiLK^{TM} properties [30]

Property	Value
Dielectric constant	2.65
Leakage current at 1MV/cm	4 MV/cm
Refractive index	1.63
Moisture uptake at 20°C RH 80%	0.24 %
Thermal stability	>425 ^{o}C
Weigh loss at 450°C	0.7 wt%/hr
Thermal conductivity	0.19 W/ mk at 25°C
Glass transition	>490°C
Young's modulus	2.45 GPa
Strength	90 MPa
Ultimate strain	11.5 %
Hardness	0.38 GPa
Toughness	0.62 MPa m
Residual stress at RT	56 MPa
CTE	66 ppm/^{o}C

However, the implementation of SiLK^{TM} IBM suffered a temporary setback in April, 2004 due to reliability issue caused by the unexpected, large coefficient of thermal expansion (CTE) mismatch at high temperatures (300-400 ^{o}C), until a modified version SiLK D^{TM} was introduced later in 2004. [31]

2.5 Porous low-k materials

The dielectric constant of production-worthy, dense dielectric materials was limited to 2.5-2.6. In order to achieve lower dielectric constant, incorporation of pores into dielectrics matrix was necessary and essential. Pore, introduced into matrix, could reduce dielectric constant more rapidly because k_{air} was about 1. There were three

methods to produce porous materials: (1) Sol-Gel method, (2) Nano-clustering method, and (3) Templating method, which would be described briefly below:

(1) Sol-Gel method

Sol-Gel method [32] was a synthesis process of solid materials. The precursor commonly had a metal or Si in center such as $Al(OH)_4$, tetramethyloxysilane, which included –OH as reactive groups. The first step was poly-condensation of precursor forming colloids, and colloids dispersion in liquid solution or solvent. Then particles continuously reacted with others which formed three-dimension network structure as schematically illustrated in Figure 2.16.

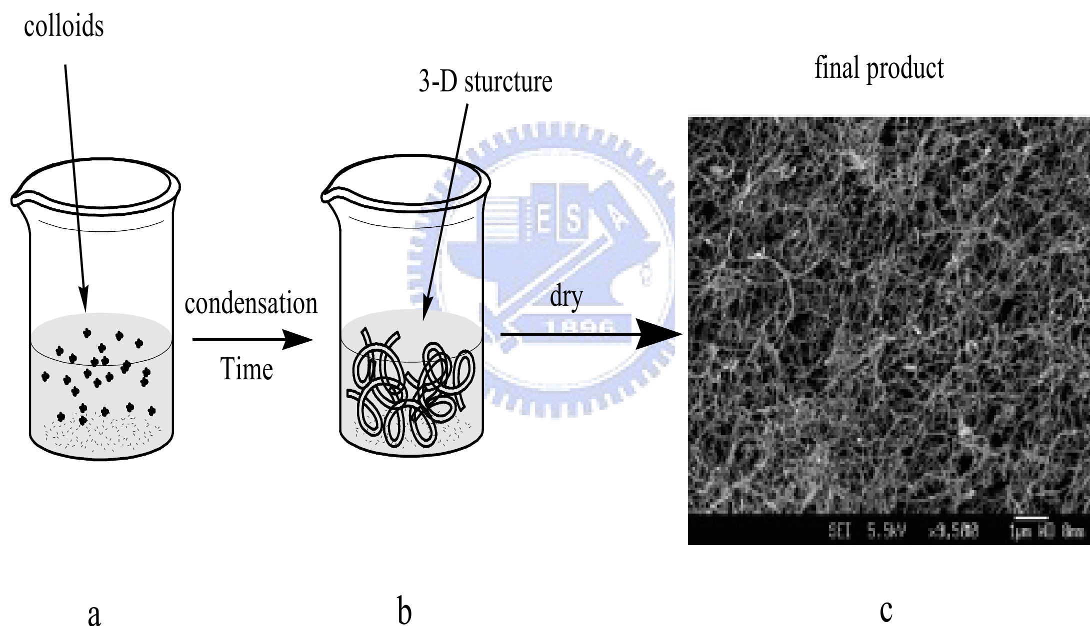

Figure 2.16 Sol-Gel processes (a) Sol, (b) Gel, (c) SEM picture of aerogel [33]

During the aging stage, the gel network became stronger. In drying process, the liquid in pore was replaced with gas or air. The gel could be dried with two main methods called aerogel and xerogel [32]. Aerogel referred to the gel, which was obtained when the liquid in pore was removed by supercritical drying. The network remained unchanged. Xerogel referred to drying by conventional or ambient drying. The sol-gel

method was difficult to control pore size of the prepared porous materials.

(2) Nano-clustering (NCS) method

The pore formation method for NCS was schematically illustrated in Figure2.17 [34]. The silica monomers were hydrolyzing by the compounds and silica which aggregated into a small size cluster in a solution. After spin coating, the nano-clusters polymerized during the subsequent curing process.

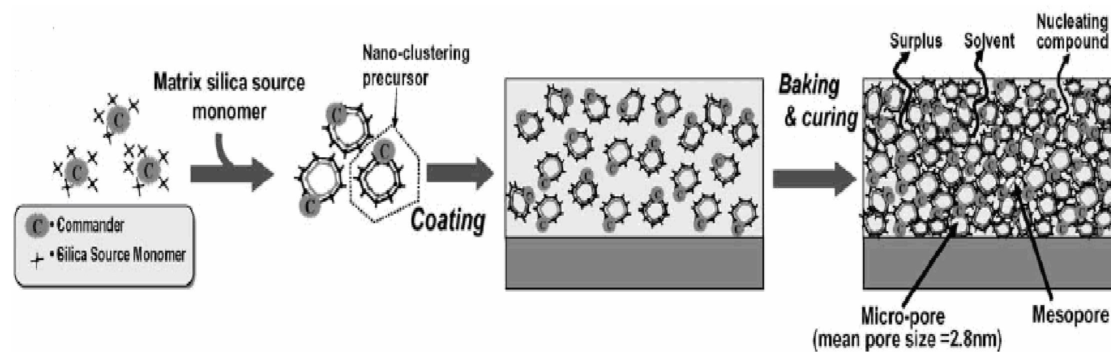

Figure 2.17 Schematic illustratration of pore formation in nano-clustering silica [34]

(3) Template method

Porous low-k dielectrics with high porosity and ordered pore geometry could be prepared by self- assembly surfactant template method, as illustrated in Figure 2.18. The porosity and pore size could was controllable by adjusting molecular size or template agent loading. The microstructure of template materials could be ordered or disorder with lamellar, cubic or hexagonal structure [35-41].

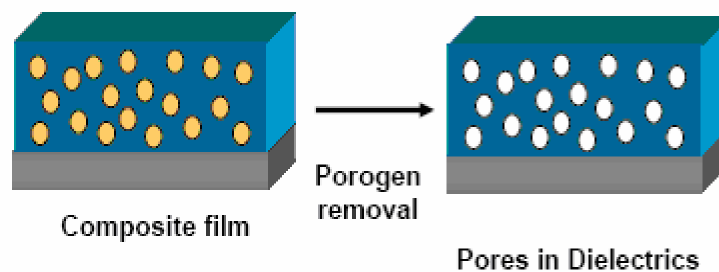

Figure 2.18 Pore was formed by thermally or chemically removing templating agent or porogen.

Examples of ordered and disordered structure reported in literature were illustrated in Figure 2.19. [35-41]

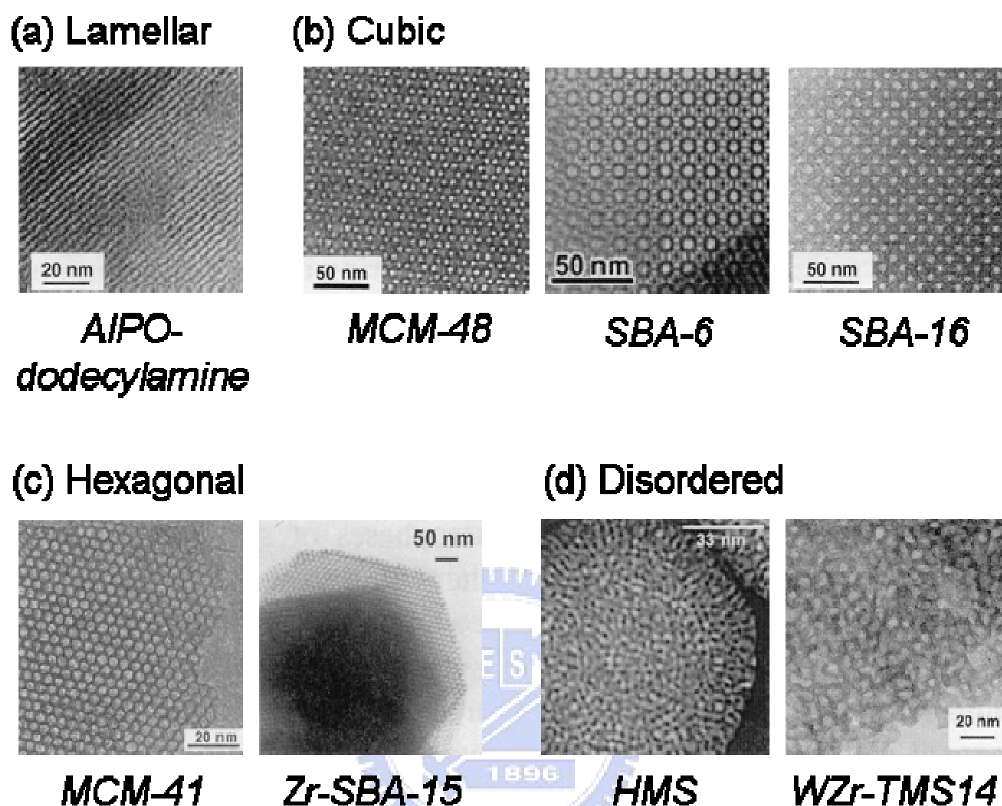

Figure 2.19 Ordered and disordered phases of microstructured materials [35-41]**.**

The formation of these microstructure involved surfactant (S)/inorganic (I) interaction. The interaction include electrostatic, (S^+I^-, S^-I^+, $S^+X^-I^+$, $S^-M^+I^-$)[42-45], hydrogen bonding (S^0I^0, N^0I^0)[46,47], hydrogen bonding/electrostatic [(S^0H^+)(X^-I^+)][48,49] and covalent (S-I) [50]. Various surfactant(S)/inorganic(I) interaction and examples were in Table 2.6. For example, MCM-41 and M41S [42,43] materials were synthesized by S^+I^- interaction under basic condition. The interaction between the cationic ammonium surfactant (S^+) and the hydrated silica (I^-) led to formation of hexagonal array. However, ionic and neutral amine surfactant were typical toxic and expensive, and impractical for used in IC industries.

Table 2.6 Various surfactant(S)/inorganic(I) interaction and examples including PH condition

Interaction	Example
S^+I^-	MCM-41 mesoporous SiO_2 (at basic pH)
S^-I^+	Al-dodecylphosphate mesostructure (at acidic pH)
$S^+X^-I^+$	SBA-3 mesoporous SiO_2 (at acidic pH)
$S^-M^+I^-$	Al-dodecylphosphate mesostructure (at basic pH)
S^oI^o	HMS mesoporous SiO_2 (at neutral pH)
N^oI^c	MSU-1 mesoporous SiO_2 (at neutral pH)
$(S^oH^+)(X^-I^+)$	SBA-15 mesoporous SiO_2 (at acidic pH)
S-I	Nb-TMS1 mesoporous Nb_2O_5

The nonionic amphiphilic surfactants including di-block and tri-block copolymers were relatively low cost, nontoxic and biodegradable [51]. Amphiphlic block copolymers (ABC) had hydrophilic and hydrophobic segment, and the pore size could be controlled by adjusting molecular weight or number of repeating unit. In this thesis, amphiphlic block copolymers (ABC) were employed as high-temperature porogens in the low-k methylsilsesquioxane (MSQ) matrix, which would be further described in details in Chapter 3.

2.6 Impact of porous materials on IC integration

Comparing to traditional silicon dioxide, porous materials possessed weaker mechanical properties and chemical resistance. Weak mechanical properties led to failure in the interconnect; for example, (1) the delamination of multilayer structures during chemical mechanical polish (CMP) process [52] as shown by Figure 2.20(a), and (2) the peeling or delamination of low-k layer during wire bonding as shown by Figure 2.20 (b) [53].

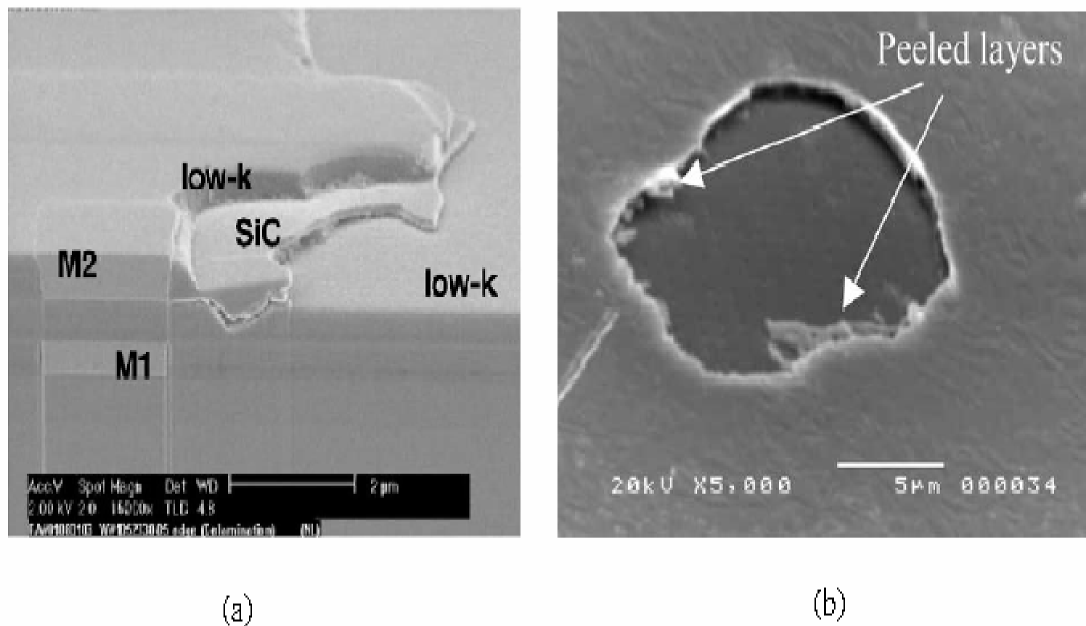

Figure 2.20 SEM photographs of (a) delamination during CMP process and (b) delamination and failure after wire bonding

Since etching rate of porous materials was faster than dense materials, the surface of porous materials would be rougher than that of the dense one after etching process. The non-continuous sidewall or open pores on the sidewall surface would make the barrier precursor penetrate into dielectrics so that the barrier could not prevent copper diffusion into dielectrics [55] as illustrated in Figure 2.21. Penetration of copper or barrier precursor, into dielectrics would cause degradation of electric

properties, such as increasing leakage current and decreasing breakdown voltage. Degradation of those electric properties could lead to circuit failure. To circumvent non-continuous sidewall issue, pore-sealing methods had been proposed. Two examples of pore-sealing were described below:

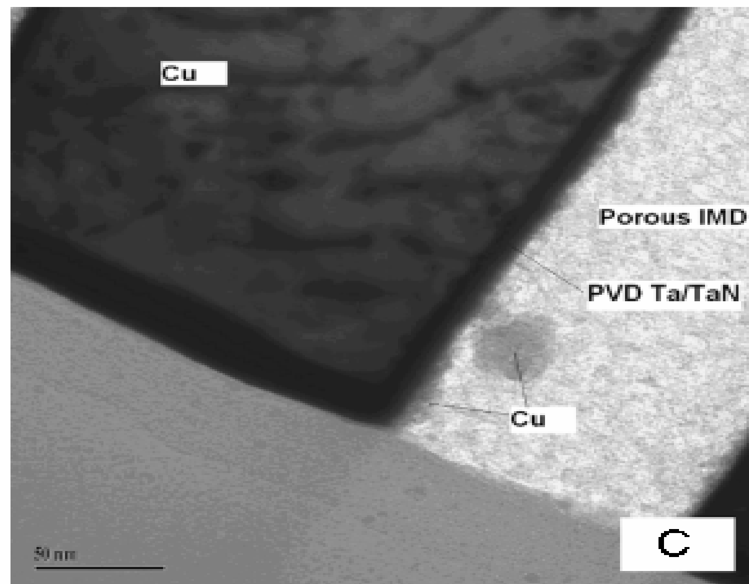

Figure 2.21 Penetration of copper into non-continuous sidewall of a porous dielectric

(1) Plasma pore sealing

Plasma pore sealing [55, 56] was utilized which the bombardment made the surface of porous films dense. The formation of thin layer on pore at sidewall prevented penetration of precursor into the dielectrics.

(2) Deposition of a thin layer on surface

Z. Chen *et al* [57], C. Jwzewski *et al* [58], and V. Jousseaume [59] demonstrated that effective pore sealing method could be achieved by applying a thin low dielectric layer such as SiC:H between the barrier and porous low-k, as shown in Figure 2.22 (a), to improve the non-continues sidewall. This sealing method was schematically illustrated in Figure 2.22 (b).

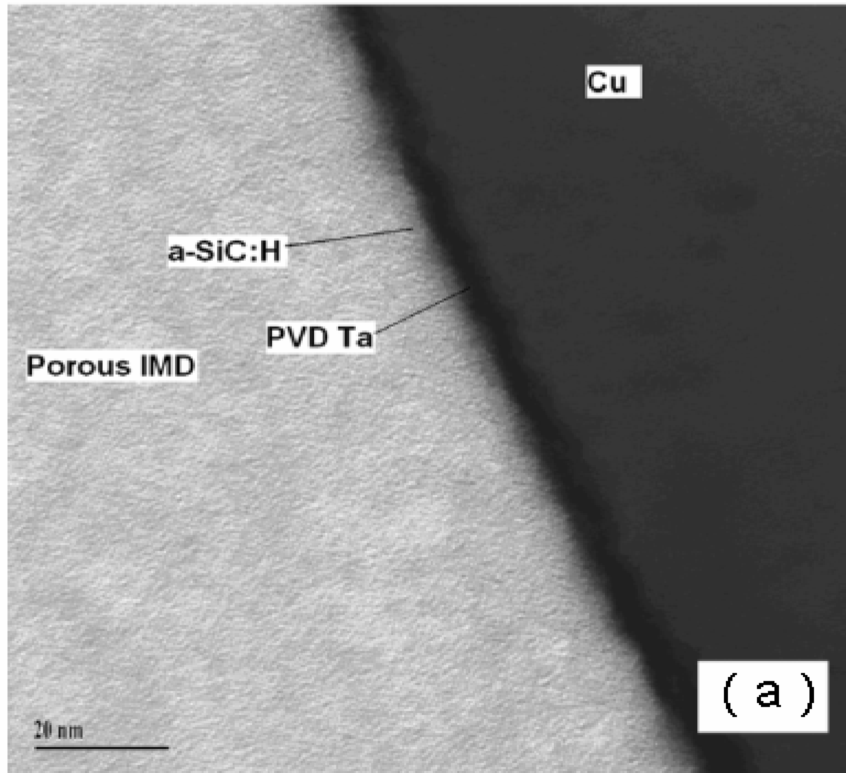

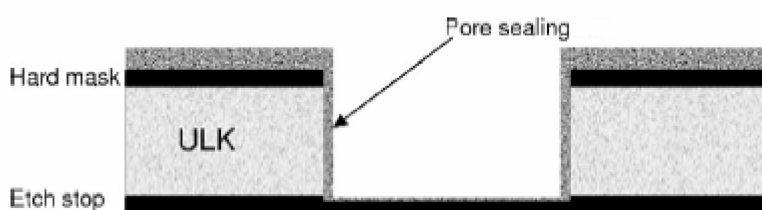

(b)

Figure 2.22 (a) TEM image of sidewall profile after pore sealing by a thin low dielectric layer [54] , (b) The schematic diagram of sealing concept [59]

However, the above-mentioned pore sealing required additional steps, such as thin layer and removal of such layer in via area, which incurred extra cost and reliability concern. Therefore, Shipey Company proposed a Solid-First^{TM} [60] scheme

to circumvent non-continuous sidewall issue, which was schematically shown in Figure 2.23. The first step of conventional porous low-k materials was to create pores at or immediately after deposition, but Solid First^{TM} scheme was to defer the removing of template agent or porogen in the final step, *i.e.* at the completion of a Cu/low-k layer. The sequence of Solid-First^{TM} process included (1) low-k film containing high temperature porogen was deposited, (2) patterning steps (lithography, etch, and clean), (3) metallization and CMP, and then (3) removal of high temperature porogen at 300-450 ^{o}C. The high temperature porogen (template agent) must possess high thermal stability for T > 300-350 ^{o}C commonly used in the backend processing steps..

Recently, Che *et al.* demonstrated porous ultra low-k materials (k~2.0) with poly styrene-block-4-vinylpyridine (PS-P4VP), an amphiphilic block copolymer (ABC), as a high-temperature porogen in the Solid-First^{TM} scheme [5]. The modulus of hybrid films below the critical porogen loading (< 30%) could pass chemical-mechanical polish (CMP) test (> 4.0 GPa). Thus, Solid-First^{TM} could solve not only the problem of non-continuous sidewall but also the low mechanical strength of porous films [5].

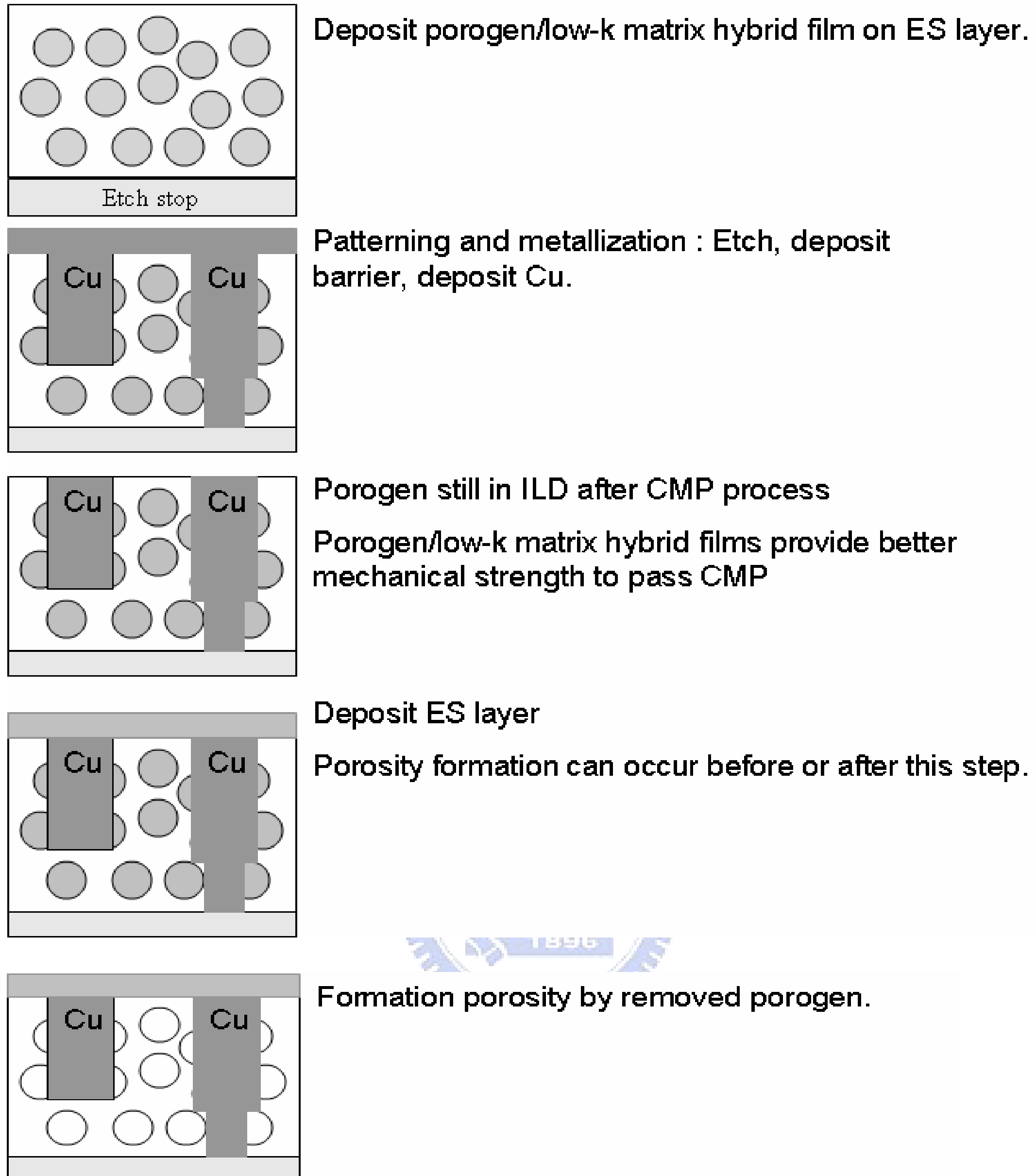

Figure 2.23 Concept and process flow of Solid First^{TM} scheme Figure

2.7 Impact of moisture on low-k materials.

Most low-k films had relative high coefficient of thermal expansion (CTE) compared to silicon substrate so that those films exhibited tensile stress. Water in films would reduce fracture resistance. By combining tensile stress with worse fracture resistance, low-k films with moisture uptake tended to crack [61]. Moreover, moisture adsorption made the low-k polymer swell, and thus increased the tensile stress as illustrated in Figure 2. 22.

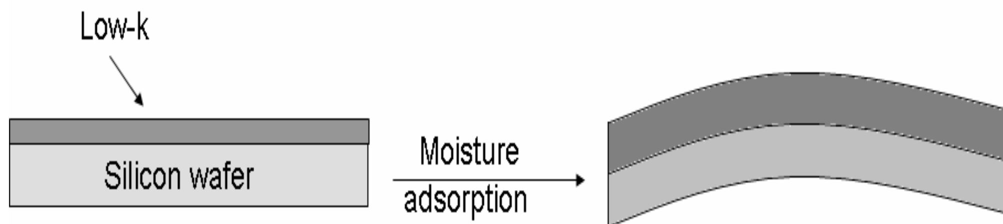

Figure 2.24 Low-k material thin film swells upon absorption of moisture

The moisture at interface may degrade the adhesion between the low-k films and cap layer [62]. In addition, the moisture outgassing may destroy the diffusion barrier or etch-stop layer during thermal process [63] as illustrated in Figure 2.23

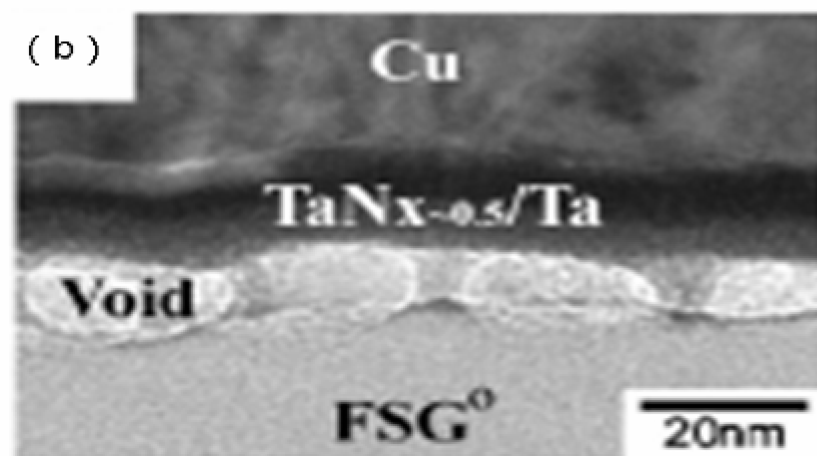

Figure 2.25 Void formation caused by moisture outgassing [58].

The dielectric properties of porous low-k materials would be significantly degraded if residual H_2O ($K_{water} = 78$) was adsorbed into the matrix and porogen. Water, in porous low-k films, also provided leakage path to lead to increasing leakage current and decreasing breakdown voltage as illustrated in Figure 2.24 [64, 65]. Thus, adsorption of moisture in low-k materials would reduce time dependent dielectric breakdown (TDDB) lifetime.

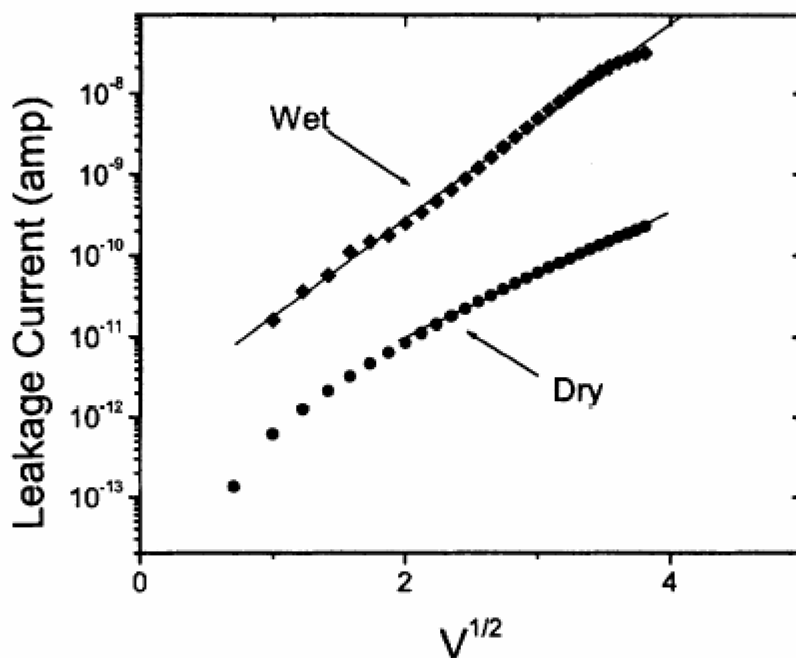

Figure 2.26 Leakage current of low-k thin films under wet and dry conditions

The mount of moisture adsorption of polar surface would be expected larger than non-polar surface, since high polarity of surface could induce multilayered adsorbents by long-range force such as Van der Waals force. For example, nanoporous silica xerogels contained unreacted hydroxyl (-OH) groups on surface that made the amount of moisture adsorption larger than that after the elimination of –OH groups of silica by HMDS treatment or TMCT treatment [66, 67], and high surface area could provide more sites for adsorbents as shown schematically in Figure 2.27 [67].

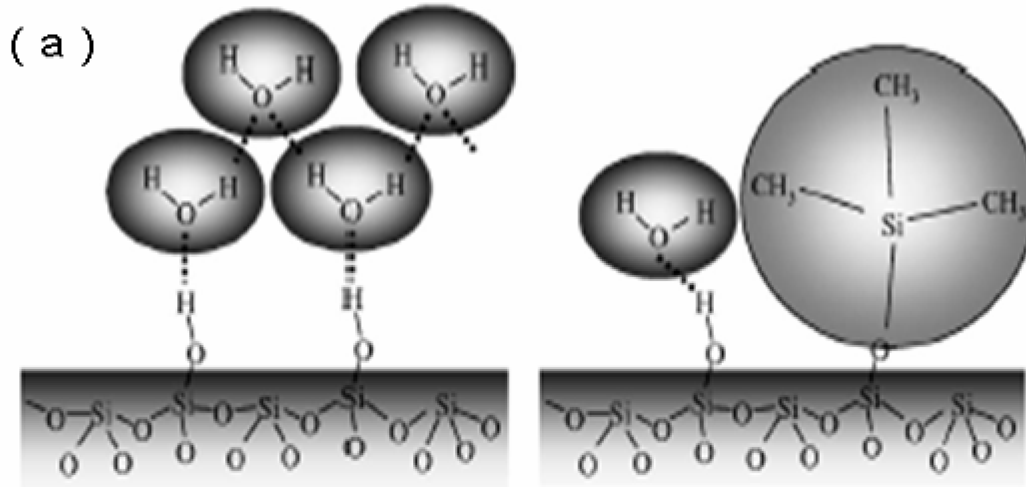

Figure 2.27 Schematic diagramd of water adsorption onto SiO2 with and without HMDS treatment [64].

In summery, we realized that integration of porous low-k materials had following reliability problems.

(1) Low mechanical strength cannot pass CMP process.

(2) Low chemical resistance led to corrosion or etch happen during wet cleaning.

(3) High surface area resulted in high moisture uptake and moisture outgassing made delamination of multilayer structure occur.

(4) Bias-temperature stressing (BTS) failure due to non-continuous sidewall coverage of barrier.

In order to circumvent non-continuous dielectric sidewall, Shipey Company proposed a Solid-First^{TM} approach that was the formation of porous dielectric after the completion of a metal layer, and then thermally removed the sacrificial high-temperature porogen. However, there was little understanding of moisture uptake about dielectrics, especially the porogen/low-k matrix hybrid films. During the integration process the dielectric films existed in the form of porogen/low-k matrix hybrid films, during CMP, post-etch cleaning, post-CMP cleaning or resist removal

process which contained a lot of water. Hence, the analysis of porogen/low-k matrix films and porous films on moisture uptake aspect was important.

It has been well known that quartz crystal microbalance (QCM) was a powerful tool to weight very small mass load in nano-gram scale. In this thesis, we employed QCM to characterize the moisture uptake and diffusion behaviors of low-k materials.

Chapter 3 Experimental

This chapter described the experimental methods and steps, including low-k precursor solution preparation, spin coating, thermal processed, quantitative measurement of moisture uptake in low-k films by quartz crystal microbalance, and collection of chemical bond information by FTIR, thickness and refractive index by n&k analyzer, pore morphology by SEM, and dielectric constant by CV-dot measurement. Flow-chart of experimental procedures was summarized in Figure 3.1

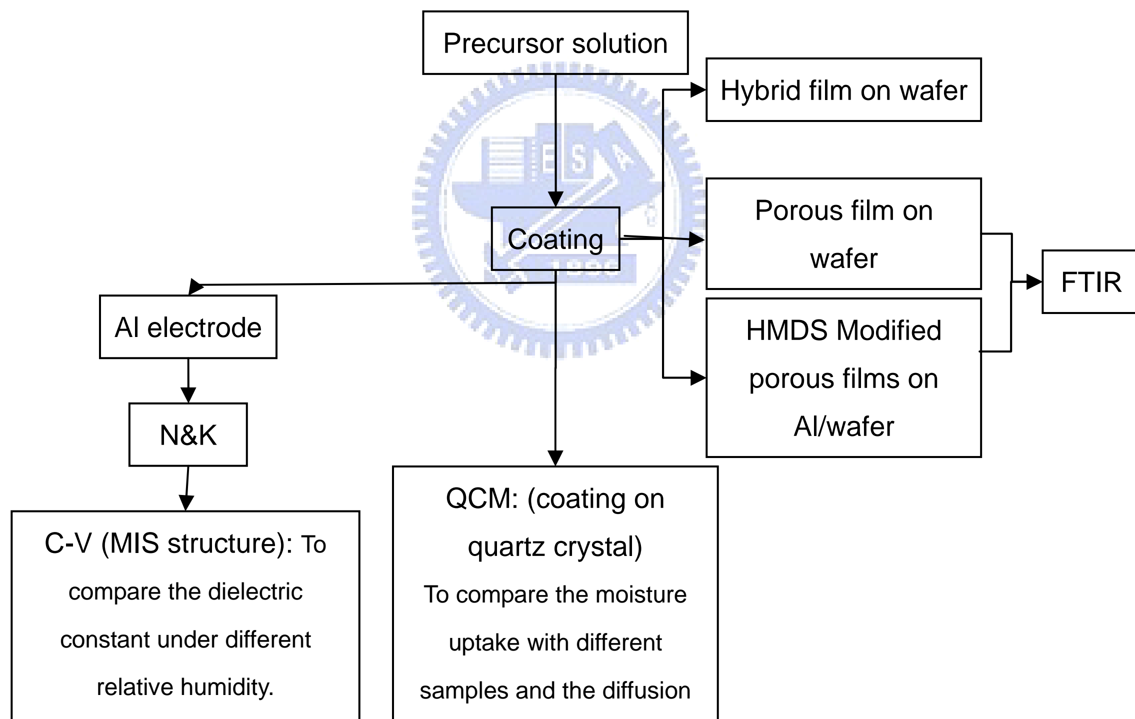

Figure 3.1 Flow-chart of experimental procedures

3.1 Preparation of low-k films

3.1.1 Chemicals

(1) Polymethylsilsesquioxane (MSQ) as low-k matrix.

MSQ, CAS No.68554-70-1, purity ≥95%, product by Gelest Inc.

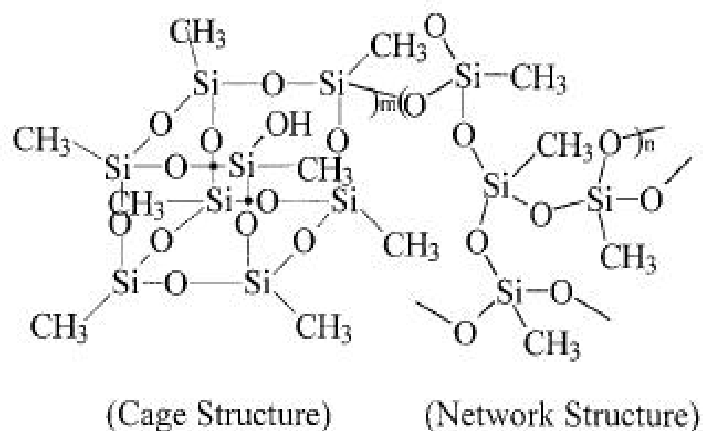

(2) High-temperature porogen was used as a template which was removed after the completion of a metal/low-k layer in the Solid-First™ scheme

(a) Polystyrene-block-poly(4-vinylprydine) as high-temperature porogen

PS-b-P4VP, 10% PS，CAS *No.*26222-40-2, Product by Sigma-Aldrich Co.

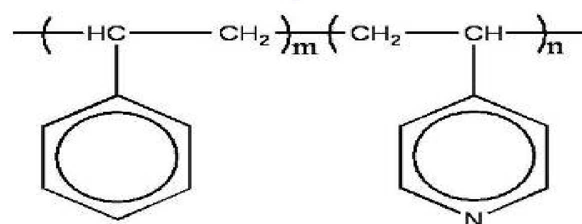

(b) Polystyrene-*block*-polybutadiene-*block*-polystyrene as high-temperature porogen

PS-PB-PS, CAS *No.*9003-55-8, Product by Sigma-Aldrich Co

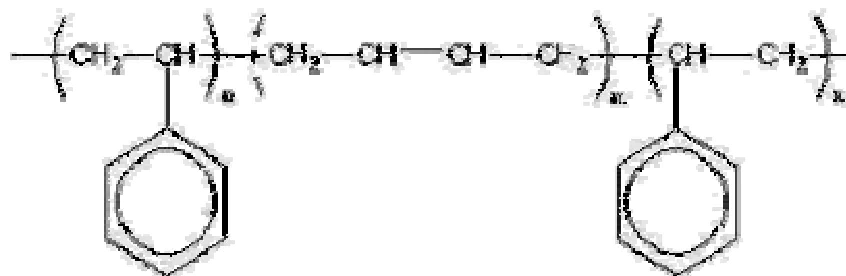

(3) n-Butanol as solvent.

CAS *No.*71-36-3, purity: ≥99.4, product by Scharlau

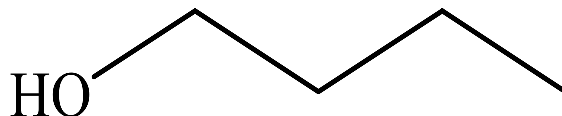

(4) Tetrahydrofuran as solvent

THF, CAS *No.*109-99-9, purity≥99.9, product by ECHO

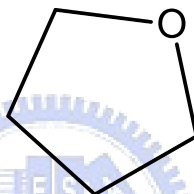

(5) Hexamethlydisilazane(HMDS) used as hydrophobic modifying agent, which was obtained from Sigma-Aldrich Co.

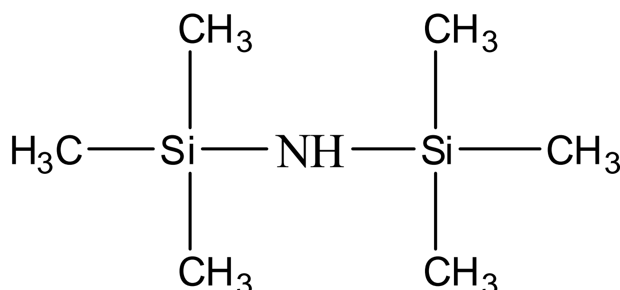

3.1.2 Preparation of low-k precursor solution

Methylsilsesquioxane (MSQ) was dissolved in n-butanol to form a 5 wt% solution which solution was as precursor of dense MSQ films. For hybrid films and porous films precursor, MSQ was first dissolved in solvent, and then high-

temperature porogen was mixed at various loadings to form a 5 wt% solution. The solvent of PS-PB-PS and PS-P4VP was tetrahydrofuran (THF) or n-butanol.

3.1.3 Deposition of low-k films

Before spin coating, the solution was initially filtered through a 0.2 μm PTFE filter (Millipore Inc.) in another bottle, and then placed in an ultrasonic bath for 1 minute as shown in Figure 3.2, to ensure no bubble in the solution. The precursor was spin coating onto silicon wafer or AT-cut quartz crystal (9 MHz resonant frequency, from Mercury Electronic Company). The dense, hybrid, and porous low-k films were prepared using different thermal process described in detail below.

(1) Preparation of dense polymethylsilsesquioxane (MSQ) films at 250 ^{o}C and 400 ^{o}C

The methylsilsesquioxane (MSQ) precursor was spin coating onto silicon wafer or AT-cut quartz crystal, and then cured at 250°C for 30 minutes for comparative study with the corresponding MSQ/porogen hybrid films at the same temperature (250 ^{o}C). This film was further cured at 400 ^{o}C for 60 minutes in a quartz tube furnace to be used as the control, dense low-k.

(2) Preparation of MSQ/porogen hybrid films

The solutions with various high-temperature porogen loadings were spin coating onto silicon wafer or AT-cut quartz crystal with, and then cured at 250°C for 30 minutes.

(3) Preparation of porous films

Precursors were spin coating onto silicon wafer and AT-cut quartz crystal, and then cured at 250 ^{o}C for 30 minutes. Then, the high-temperature porogen was removed at 400 ^{o}C for 60 minutes in quartz furnace

(4) Preparation of HMDS modified porous films

The porous low-k films on quartz and wafer of (3) were placed inside a Pyrex container and treated with saturated HMDS vapor under 70°C for 24 hours. Prior to the introduction of HMDS, low-k film was purged at N2 at high flow rate to ensure low moisture adsorbed on the surface.

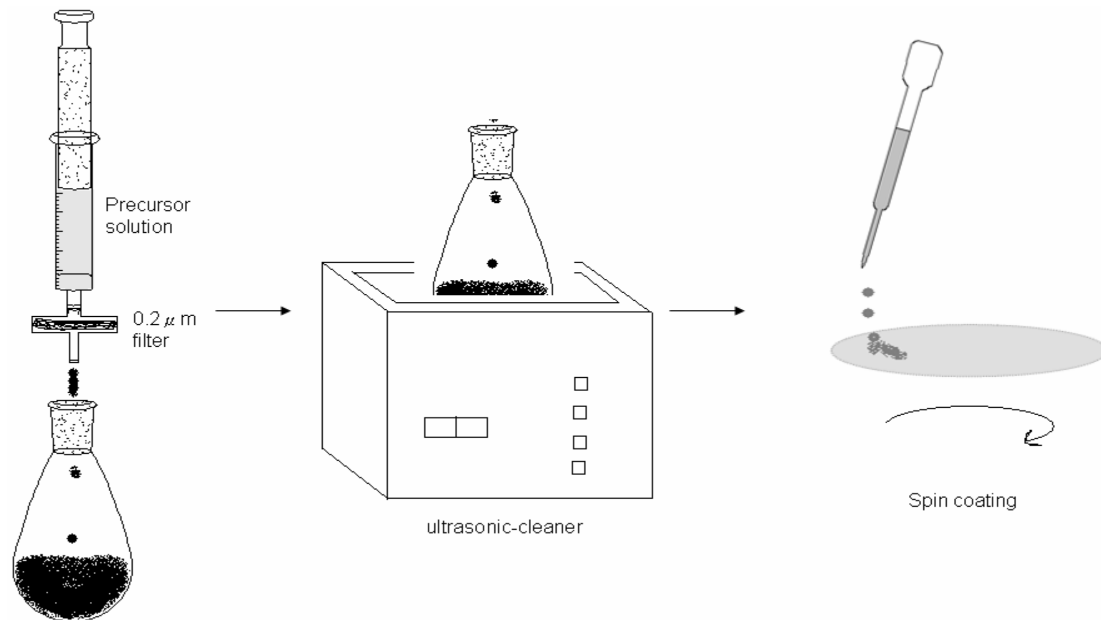

Figure 3.2 Schematic illustration on the preparation of precursor solution

3.2 Experimental techniques

3.2.1 n&k analyzer

The n&k analyzer 1200 was used in this study to obtain refractive index (n) and film thickness (d) information of low-k films. The experimental steps were listed below:

1. To scan standard sample as a baseline. (The wavelength ranged from 190 nm to 900 nm.)
2. To put sample wafer upside down on the n&k analyzer, and then scan again to collect the typical experimental curve illustrated in Figure 3.3.

The experimental curve was fitted using Forouhi-Boomer Dispersion relation [68] (Equation 3.1) to deduce refractive index (n) and film thickness (d).

$$n(E) = n(\infty) + \sum_{i=1}^{q} \frac{B_{0i}E + C_{0i}}{E^2 - B_i E + C_i} \qquad \text{..........(3.1)}$$

where

$$B_0 = \frac{A}{Q}\left[-\frac{B^2}{2} + E_g B - E_g^{\ 2} + C \right]$$

$$C_0 = \frac{A}{Q}\left[\left(E_g^{\ 2} + C\right)\frac{B}{2} - 2E_g C \right]$$

$$Q = \frac{1}{2}\left(4C - B^2\right)^{\frac{1}{2}}$$

E ： Incident energy of light

B, C ： Parameter which relate to electron structure of materials

q ： number of terms

n(∞) > 1

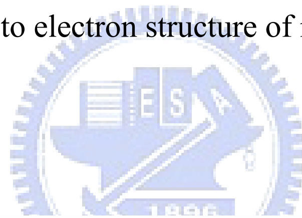

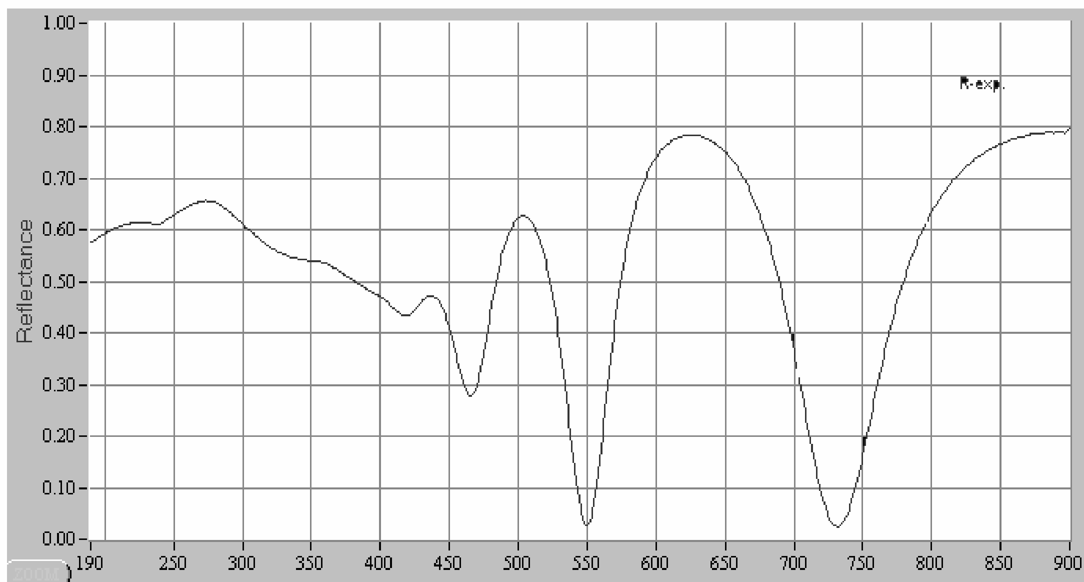

Figure 3.3 Typical curve of n&k measurement

3.2.2 Specular reflectance Fourier-transform infrared spectroscopy (FT-IR)

FTIR has been extensively applied to qualitative analysis of organic compounds due to the specific absorption wavelength by different vibration and rotation modes in the infrared wavelength range. The S/N ratio was very small for thin film measurement using transmission mode. Therefore specular reflectance FTIR apparatus VeeMAX [69] and PIKE 100 FTIR from PIKE Technologies Inc were employed for thin film characterization in this thesis.

The specular reflectance FTIR was schematically illustrated in Figure 3.4. The thin film samples were spun onto Al/silicon wafer substrate, where Al thin film was used as a reflective mirror. The spectrum was collected in 500~4000 cm^{-1} range at a resolution of 2 cm^{-1} and 30° incident angle.

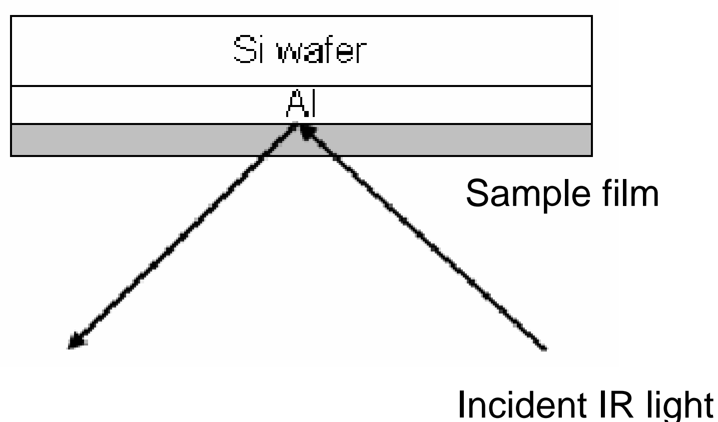

Figure 3.4 Schematic diagram of a specular reflectance infrared speectroscopy

3.2.3 Capacitance measurement

Metal-insulator-semiconductor (MIS) sample was used for measuring the dielectric properties. The fabrication steps of MIS samples were illustrated in Figure 3.5 and described below:

1. To deposit low-k materials on a p-type (100Ω㎝) silicon wafer and cure the film

at 250℃.

2. Al thin film (5000 A) to serve as an electrode, was then deposited onto dielectric film, which was covered with a shadow mask with various dot sizes as shown in Figure 3.6

The capacitance of low-k film in MIS structure was measured by a HP-4280 C-V meter. The capacitance value was then substituted into Equation 3.2, to obtain the dielectric constant (*k*).

$$C = K\varepsilon_0 \frac{A}{d} \quad \text{...(3.2)}$$

C : capacitance

ε_0 : Permittivity of free space, 8.85419 x 10^{-12} C^2/Jm

A : electrode area

d : dielectric thickness

k : dielectric constant

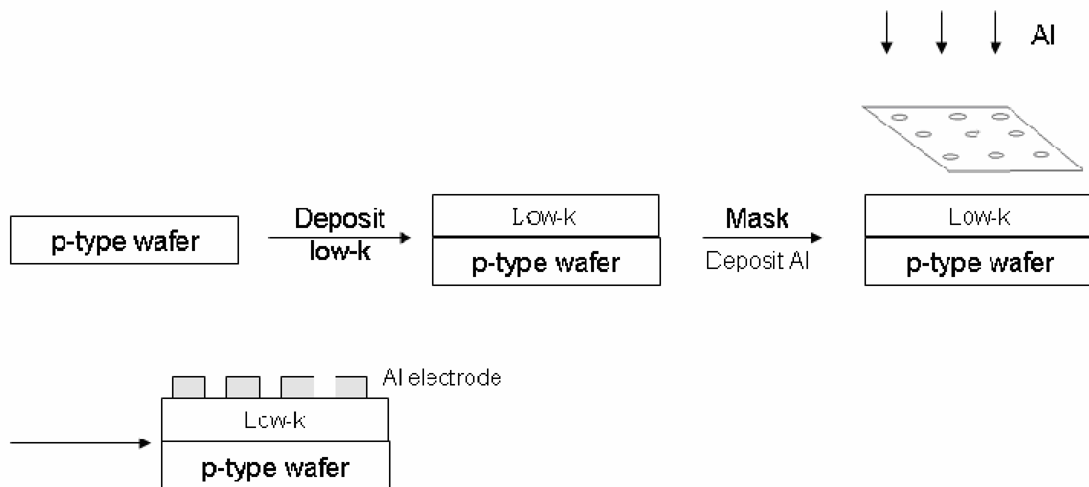

Figure 3.5 The process flow for fabricating a MIS sample for CV-dot measurement

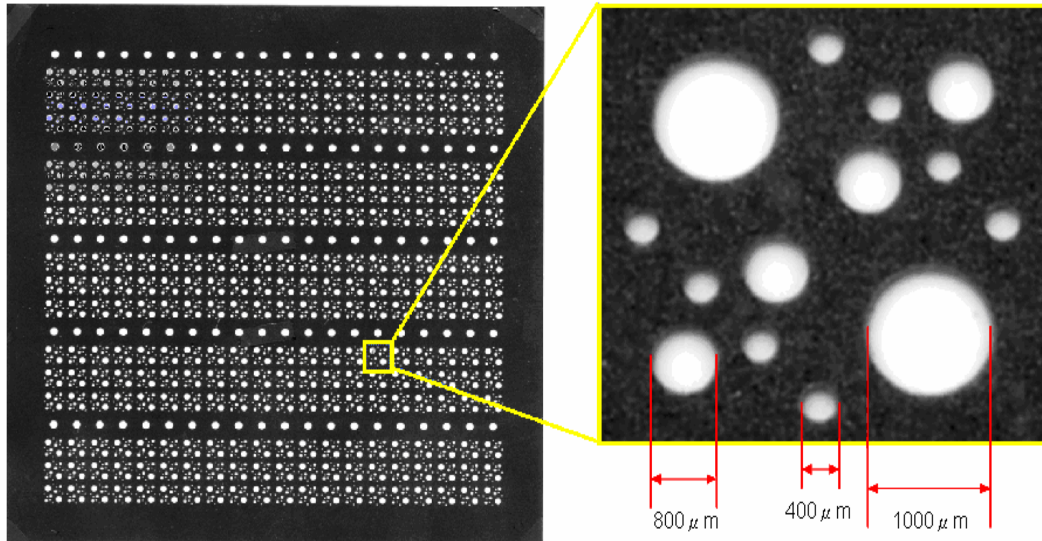

Figure 3.6 Shadow mask with three different diameters for CV-dot measurement

Electrode area and thin film thickness were two major sources of error in the dielectric constant measurement. In order to eliminate such measurement errors, linear curve fitting of capacitance versus area for various dot sizes was shown in Figure 3.7. Then the fitted value of slope was substituted into Equation 3.2 to obtain the dielectric constant.

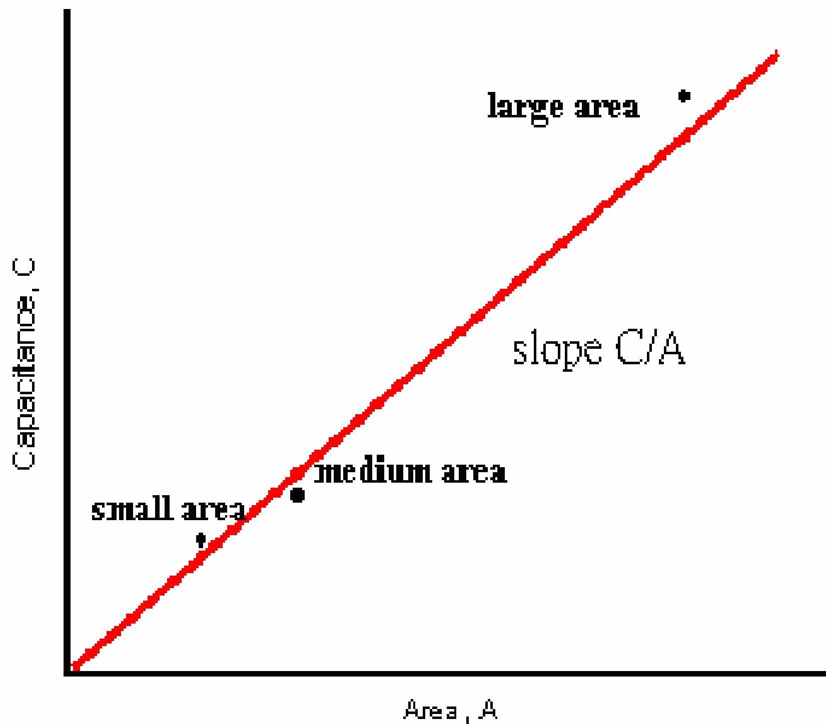

Figure 3.7 The utilization of linear curve fitting of various dot sizes to minimize the errors from fringes effect and area measurement

3.2.4 Dual beam (focused ion beam & electron beam) System (FIB/SEM)

Topography of porous low-k films was observed by FEI Nova 200 Dual beam, focused ion beam and electron beam System (FIB/SEM). The ion beam focused by electromagnetic lens to cut and etch in very small dimension. General ion beam used liquid metal Gallium (Ga) ion source, which had low melting point, low vapor pressure and large resistance of oxidation. Typical FIB system consisted of liquid metal source, electromagnetic lens, second ion detector, scanning electrode, X-Y-Z sample stage, and vacuum system schematically illustrated in Figure 3.8.

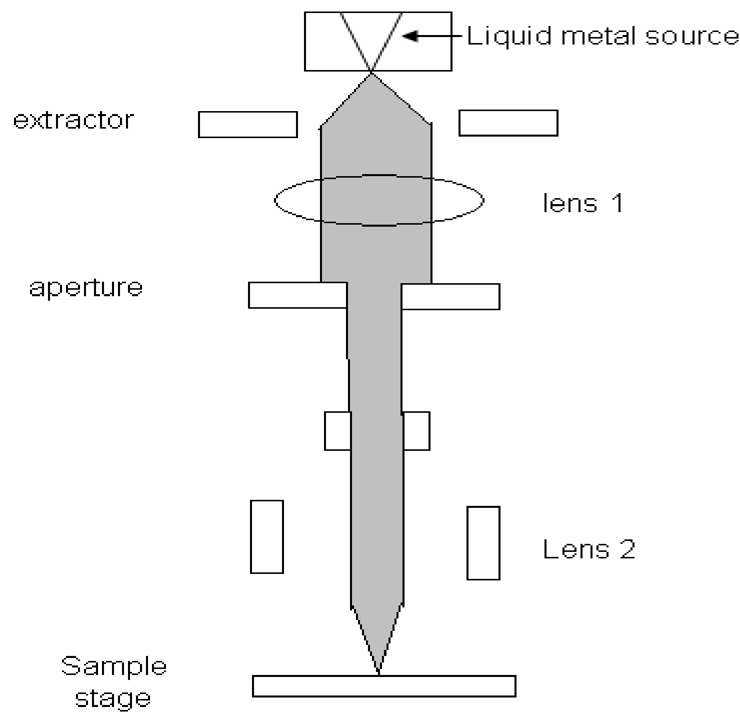

Figure 3.8 Schematic diagram of a FIB/SEM system

Liquid metal ion was extracted by electric field and through automatic variable aperture (AVA) to adjust the spot size. The FEI Nova 200 Dual beam system offered a function of not only focus ion beam but also electron beam. During ion cutting or etching, electron beam serviced as image probe (SEM) that precisely controlled cutting or etching process.

3.2.5 Quartz Crystal Microbalance (QCM)

Theory of Piezoelectric Quartz crystal microbalance

In Chapter 2 we realized that the dielectric properties of porous low-k materials would be significantly degraded if residual H_2O (k_{water}~78) adsorbed in the matrix and porogen. In addition, the moisture outgassing may cause delamination or catastrophic failure at low-k/diffusion barrier or low-k/etch-stop interface during the temperature cycling in subsequent processing steps. Thus, to understand the moisture uptake of

low-k films, especially in different stages of Solid-First^{TM} scheme, was important to devise the processing condition in order to eliminate catastrophic failure. In this study, a home-built quartz crystal microbalance (QCM) was employed to measure moisture uptake of low-k films. QCM was an extremely sensitive tool down to nano-gram level due to the application of piezoelectric effect. The quartz crystal would deform and had a specific resonant frequency while AC electronic filed was applied to quartz crystal. According to Sauerbrey equation [70], the mass load on crystal could be calculated by the measured resonant frequency. The quartz resonator was first explored by Sauerbrey, whose equation could be deduced as follows.

Sauerbrey Equation [70]

For a quartz crystal plate to oscillate in thickness shear mode, the following equation must be satisfied:

$$tq = \frac{\lambda q}{2} \quad \text{.....................(1)}$$

tq : thickness of the crystal

λq : wavelength of shear-mode elastic wave

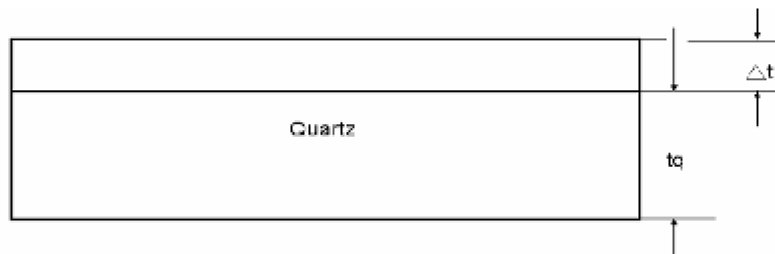

Speed of acoustic wave in the same material was a constant and could be described by the following equation:

$$v = \left(\frac{\mu q}{\rho q} \right)^{\frac{1}{2}} \text{…………………(2)}$$

v: wave speed

μq : the shear modulus of crystal

ρq : the density of crystal

If $v = f_0 \lambda$ substitute into (1), then

$$f_0 = \frac{v}{2tq} \text{…………………(3)}$$

Assume a thin layer with thickness, △t, was absorbed, then

$$\frac{\lambda q}{2} = tq + \Delta t$$

After adsorbed, wavelength became longer and wave speed would not change, we can get following equation:

$$\Delta f = -\frac{\Delta t}{tq} \text{…………………(4)}$$

Substitution of (3) into (4)

$$\frac{\Delta f}{f_0} = -\frac{f_0}{v} = -\frac{f_0 \Delta t}{\left(\frac{\mu q}{\rho q} \right)^{\frac{1}{2}}} \text{……………(5)}$$

Assume density of adsorbed layer equal to quartz crystal

$$\Delta m = A \Delta t \rho q \text{………………………(6)}$$

A : piezoelectric active area

△m : mass of adsorbs

Substitution of (6) into (5)

$$\Delta m = -A \frac{\sqrt{\rho_q \mu_q}}{2} \left(\frac{\Delta f}{f_0^{\ 2}} \right) \text{…………………} \qquad \text{Sauerbrey Equation (3.3)}$$

μ_q: the shear modulus of crystal(2.947×10^{11} $g.cm^{-1}.sec^{-2}$)

ρ_q: the density of crystal (~2.648 $g.cm^{3}$)

A: piezoelectric active area

△f: Frequency change before and after adsorption

△m: Mass loading

Quartz crystal microbalance (QCM) system

A home-built quartz crystal microbalance system, schematically illustrated in Figure 3.7, consisting of vacuum chamber, oscillator, frequency counter (HP 53131A), temperature controller, water vapor bubbler and computer-controlled data collection system, was used in this thesis. The AT-cut quartz crystal with 9 MHz resonant frequency (Mercury Electronics. Inc.) had a diameter and thickness of 0.8 cm and 200 μm, respectively. Diameter of active Au electrode was 0.4 cm. The measurement of moisture uptake was carried out under 100% relative humidity at 30 ^{o}C. The sensitivity of our QCM using a 9 MHz AT-cut quartz crystal is 1.72 ng/cm^2 based on the 1 Hz resolution of HP frequency counter according to Sauerbrey equation.

Sample preparation and moisture uptake measurement using QCM

Procedures of sample preparation and QCM system moisture uptake measurement were listed below:

1. Prior to the deposition of low-k film, crystal resonant frequency (f_0) was measured and recorded in the vacuum chamber.
2. Low-k precursor solution was spin coating onto a quartz crystal at a specific speed to obtain 0.5 μm thickness. Caution was taken to mask area excluding the top-side Au electrode using a tape to prevent poor electric contact caused by the contamination of precursor solution.
3. The low-k/quartz sample was then cured according to the curing processes

described in Section 3.1.3.

4. After curing, the low-k/quartz sample was placed into a QCM holder within the vacuum chamber. After the chamber was evacuated, a stable frequency value for low-k/quartz, called f_1 was measured and recorded.
5. When the water bubbler reached 100% saturation steady-state at 30 ^{o}C, the saturated moisture was introduced into the chamber to start adsorption process and *in-situ* measurement of resonance frequency as function of time through a computer-controlled data collection system as illustrated in Figure 3.10. The resonate frequency of quartz crystal decreased due to mass load on thin film when moisture was adsorbed in the low-k/quartz sample. As the adsorption of moisture reached steady state, a stable frequency value, called f_2, was recorded as shown in Figure 3.10.
6. Afterwards, the frequency was further monitored as function of time during the desorption process under pump down. Then, the stable frequency, called f_3, was recorded to check if moisture was fully desorbed or any chemical change if $f_3 \neq f_1$.

7. From the previous steps, amount of moisture uptake in low-k film could be calculated from $\triangle f = f_1 - f_2$ through Sauerbrey Equation. In this thesis, moisture uptake was expressed in term of wt%, i.e. $(f_1-f_2)/(f_0-f_1) \times 100\%$ as illustrated in Figure 3.11.

8. Moisture uptake of low-k/quartz sample after HMDS treated measurement was the same as low-k/quartz sample.

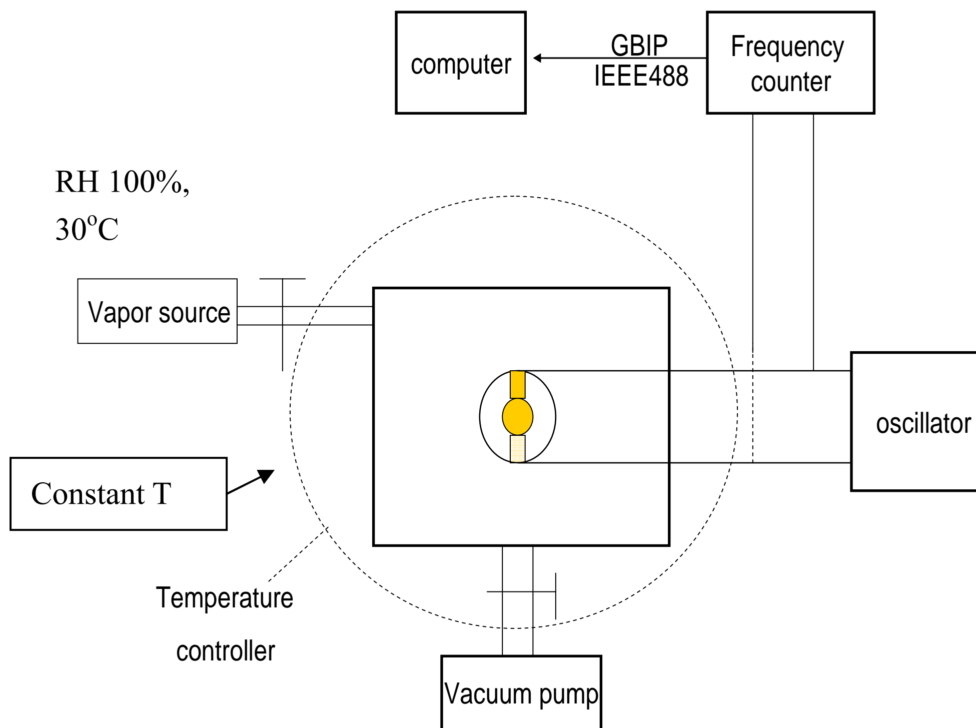

Figure 3.9 Schematic diagram of QCM system for moisture uptake measurement

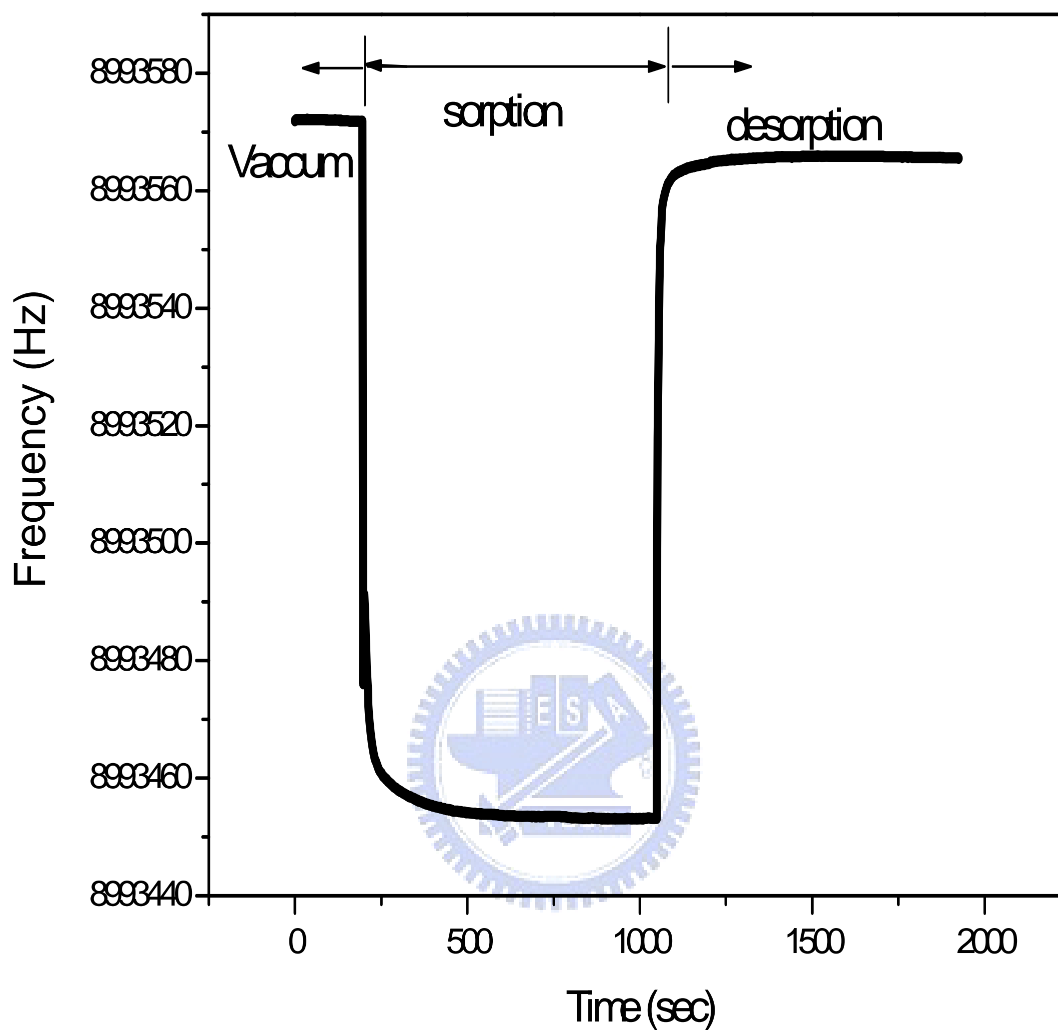

Figure 3.10 The frequency change of the crystal resonator at 30 oC versus time during sorption and desoprtion for MSQ/PS-P4VP (10wt%) hybrid film

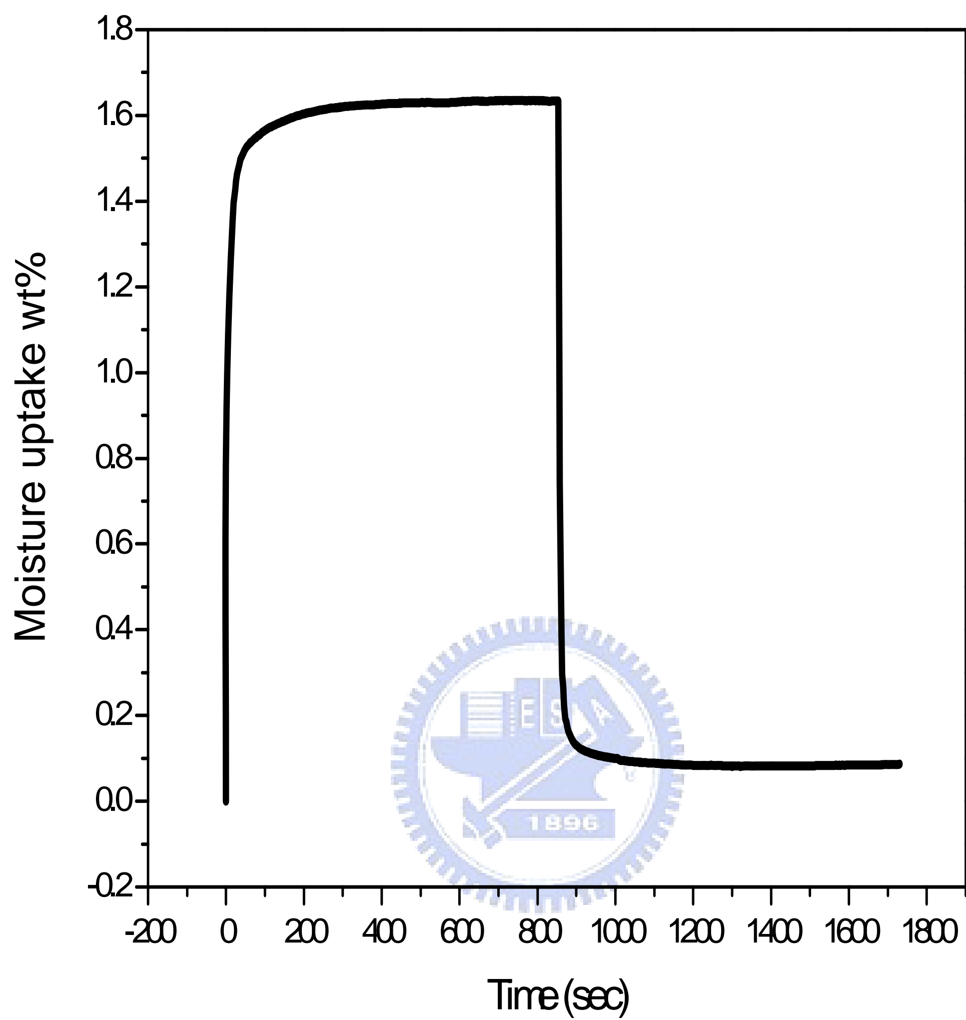

Figure 3.11 Moisture uptake of MSQ/ PS-P4VP (10wt%) hybrid film as a function of time

Chapter 4 Results and Discussion

In this thesis, the impact of high-temperature porogens, their loadings on the moisture uptake and diffusion behavior was investigated for low-k films based on Solid-First^{TM} approach. Specifically, di-block and tri-block copolymers such as PS-P4VP and PS-PB-PS were employed as the high temperature porogens, whose decomposition temperature was higher than 300 ^{o}C. Three low-k dielectric systems were comprehensively studied in this thesis, namely: (1) MSQ films cured at different temperatures, (2) MSQ/porogens hybrid films with various porogen loadings, cured at 250 ^{o}C, which simulated the starting ILD materials in the Solid-First^{TM} scheme, and (3) porous films after porogens were completely removed by burn-out at 400°C, which simulated the final porous low-k materials after the completion of Solid-First^{TM} integration scheme of Cu/low-k interconnect. We also examined the impact of porogen types and loading level on the moisture uptake in MSQ/high-temperature porogen hybrid films and its corresponding porous MSQ thin films representing the ILD films in different steps of Solid-First^{TM} scheme. The mechanism of moisture uptake in MSQ/porogen and porous MSQ thin films will be further studied and proposed**.** Moreover, the effect of moisture uptake on the dielectric property will be investigated, in comparison with that of moisture uptake by QCM. The diffusion behavior of moisture uptake and desorption in the MSQ/porogen hybrid and porous MSQ films were also studied. Assessment of moisture uptake in low-k films and appropriate steps in designing the process steps in Solid-First^{TM} scheme would be recommended.

4.1 Optical properties of low-k MSQ films

The porous MSQ films were prepared by burning out PS-P4VP poorgen at various loadings, unless the porogen was stated otherwise in this thesis. The refractive indices of porous films at different porogen loadings were shown as Figure 4.1(a). The refractive index decreased linearly with increasing porogen loading, which was replaced with air after the removal of porogens.

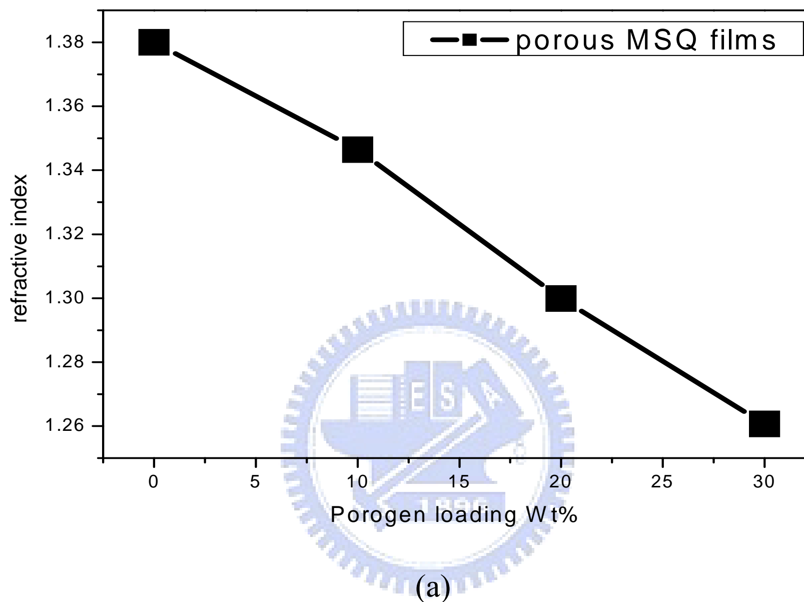

(a)

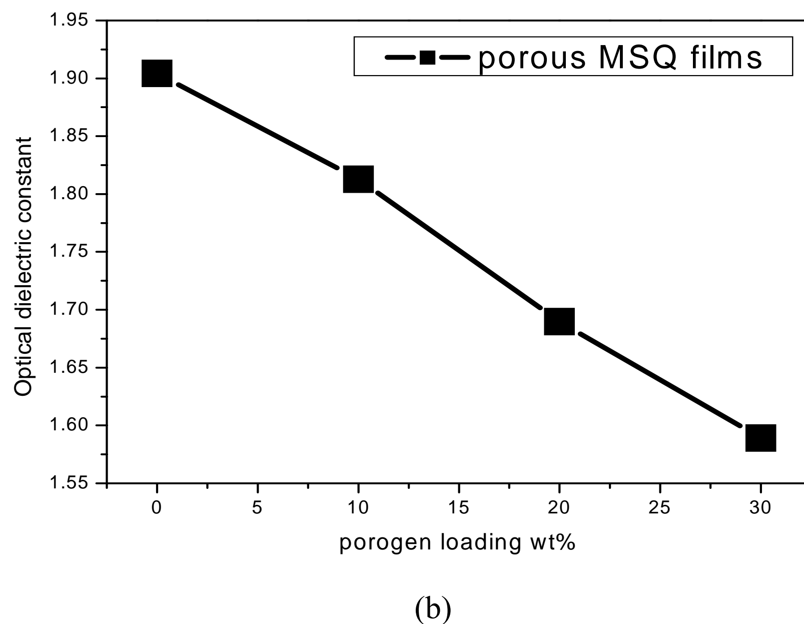

(b)

Figure 4.1 (a) Refractive index as a function of porogen loading and (b) Optical dielectric constant as a function of porogen loading

The dielectric constant at optical frequency range (optical dielectric constant) is equal to refractive index (n) square [71], expressed by Equation 4.1.

$$k = n^2 \quad \text{..............................(4.1)}$$

Therefore, the tendency of dielectric constant for various porogen loadings or different porosities could be predicated by refractive index as shown in Figure 4.1(b). Moreover, the porosities of porous MSQ films could be calculated using Lorentz-Lorenz Equation (4.2) [72] using the refractive indices measured by n&k Analyzer. The relation between porosity and porogen loading was shown in Figure 4.2.

$$\varphi = 1 - \frac{n_0^2 + 2}{n_0^2 - 1} \cdot \frac{n^2 - 1}{n^2 + 2} \quad \text{................ (4.2)}$$

Where φ: porosity

n_0: refractive index of dense film

n: refractive index of porous film.

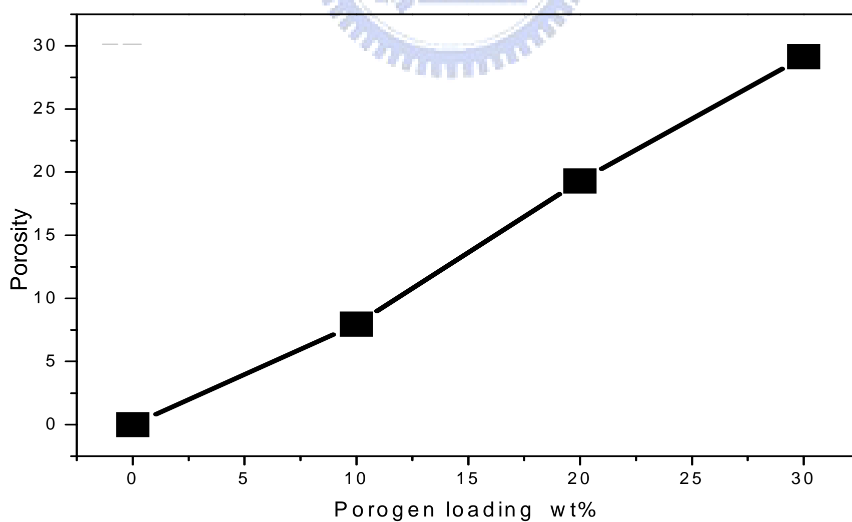

Figure 4.2 The correlation between porosity and porogen loading.

Porosity was found to linearly increase from 0% to 29% with increasing porogen form 0% to 30%.

4.2 Moisture uptake of low-k films

4.2.1 Moisture uptake of MSQ films cured at different temperatures

In the beginning, the moisture uptake behavior of dense MSQ films cured at different temperatures were examined. Based on measurement by quartz crystal microbalance, the moisture uptake as a function of time for dense MSQ films cured at 250 °Cand 400 °C were shown in Figure 4.3.

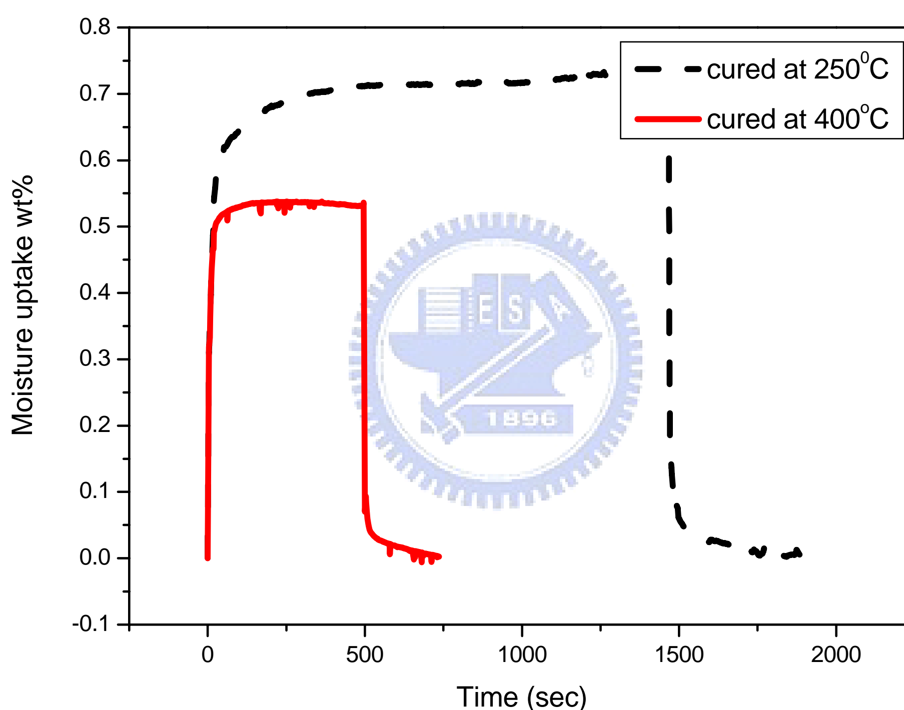

Figure 4.3 Moisture uptake behavior of MSQ films cured at 250°C and 400°C

The diffusion of moisture was extremely fast. It reached 95% of equilibrium level within 200 seconds for both cases. The desorption of moisture by pump-down brought the moisture level down to zero, indicating that there was no distinguishable or permanent chemical change when moisture was adsorbed onto dense MSQ films cured at 250 and 400 °C. In addition, the moisture uptake of MSQ films cured at

250°C and 400 °C were 0.7 wt% and 0.54 wt%, respectively. Densification of MSQ film cured at 400 °C may contribute to its low moisture uptake in part. Nevertheless, specular reflectance FT-IR spectroscopy was employed to examine the degree of cross-linking and chemical structures of dense MSQ films cured 250°C and 400 °C as shown in Figure 4.4 to understand why lower curing temperature possessed high moisture uptake.

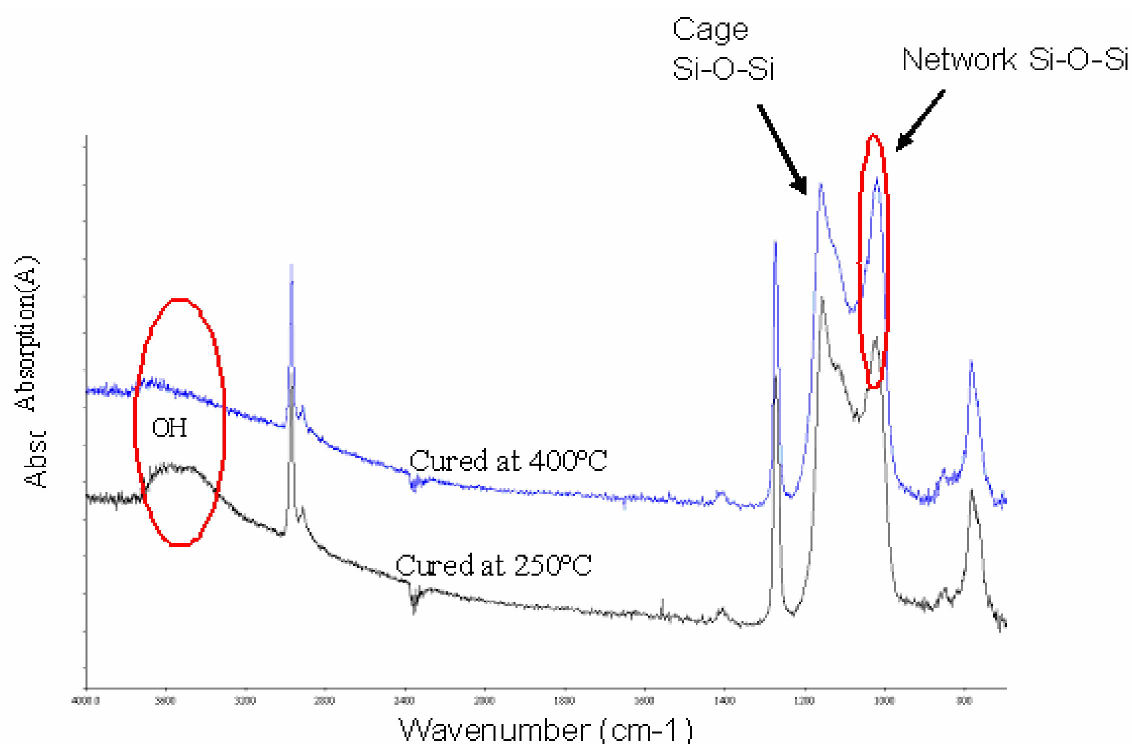

Figure 4.4 FTIR spectra of MSQ films cured at at 250 °C and 400 °C

FTIR spectra indicated the amount of hydroxyl groups (3000~3700 cm^{-1}) of MSQ film cured at 250°C was more than that cured at 400°C, yet the degree of crosslinking in MSQ film cured at 400°C was more than that cured at 250 °C judging from the network/cage Si-O ratio at 1030 cm^{-1} and 1130 cm^{-1}. Since MSQ cure was a polycondensation reaction, the existence of residual hydroxyl groups could be attributed to an incomplete reaction of condensation at 250 °C, which in turn decreased the degree of crosslinking or lower density. As a result, higher moisture

uptake in MSQ film cured at 250 °C could be attributed to (1) the polar hydroxyl groups which increased moisture uptake, and (2) lower density compared to films cured at 400 °C.

4.2.2 Moisture uptake of porous MSQ films

Next, the moisture uptake of dense MSQ film cured at 400 °C and porous MSQ films with various porosities after the removal of high-temperature porogen, PS-P4VP at 400 °C for 60 minutes. The moisture uptake of porous MSQ films as a function of porosity were shown in Figure 4.5 and Table 4.1, while their time-dependent moisture data curves were shown in Appendix A for reference.

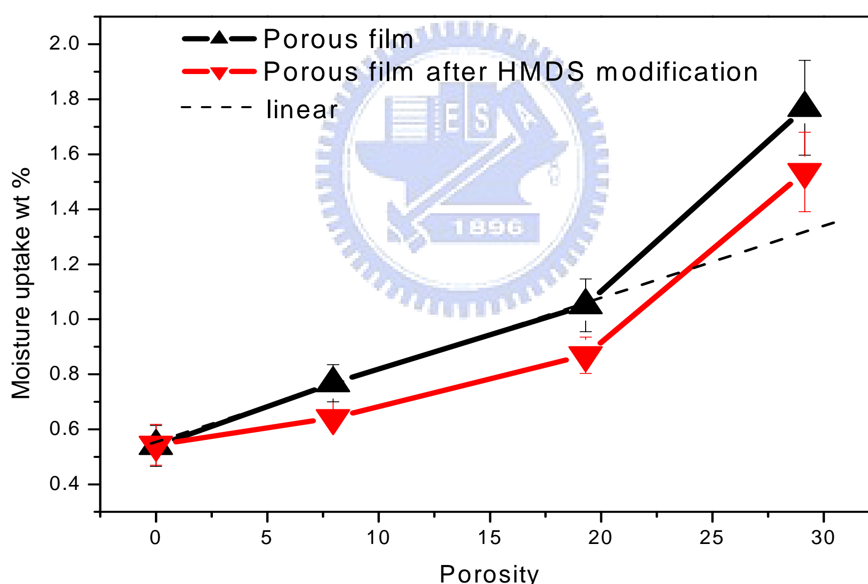

Figure 4.5 Moisture uptake of porous MSQ and HMDS modified porous MSQ films

The moisture uptakes of porous low-k films increased from 0.54 % to 1.77 % as porosity was raised from 0 % to 29 %. Yet, the moisture uptake, 1.77 wt% of porous MSQ film with 29% porosity is much higher than the liner fitting curve extrapolated from 0 to 20% porosity. The increased moisture absorption could be attributed to (1) increased surface area and (2) increased polarity such as Si-OH on the pore surface.

High surface area could provide more sites for adsorbents [66], while high concentration of Si-OH could form hydrogen bonding with H_2O and even induce multilayered adsorbents through Van der Waals force as previously illustrated in Fig. 2.27. It was speculated that the high-temperature porogen at 30% loading either changed the pore morphology and/or increased Si-OH at higher degree due to steric hindrance of high concentration of porogen to the polycondensation reaction of MSQ. More work will be required for elucidation of pore morphology and Si-OH concentration in separate study.

Table 4.1 Moisture uptake of porous MSQ and HMDS modified porous MSQ films

porosity	Moisture uptake in porous-MSQ	Moisture uptake in HMDS-modified	delta
0	0.54	0.54	0.00
8.0	0.77	0.64	0.13
19.3	1.05	0.87	0.18
29.1	1.77	1.56	0.21

4.2.3 Moisture uptake of HDMS-modified porous films and MSQ/PS-P4VP hybrid films

The porous MSQ films cured at 400 ^oC, with varying porosity were surface modified with HMDS to examine the level of surface polarity by Si-OH as a function porosity and further to minimize moisture uptake. The moisture uptake for HMDS-treated porous films was about 11 to 17% lower than those of as-prepared ones as shown in Figure 4.5. It indicated that more amount of hydroxide group (-OH) on the surface of modified porous film was replaced by $–Si(CH_3)_3$ after HMDS treatment [64] with increasing porosity as summarized in Table 4.1.

Specular reflectance FT-IR technique was employed to examine porous MSQ

(19.3 % porosity) before and after HMDS treatment as shown in Figure 4.6. For as-cured porous MSQ, the Si-O-Si stretching peaks at 1130 and 1030 cm^{-1} represented the cage and network structures, 791 cm^{-1} for Si-C stretching vibration of $-Si(CH_3)_3$, 2974 cm^{-1} for C-H stretching of $Si-CH_3$, 3000~3700 cm^{-1} for a broad –OH band, and the peak 940 cm^{-1} was attributed to Si-OH stretching. After HMDS treatment, infrared absorption peaks of Si-OH and –OH disappeared, implying that the surface of HMDS-treated, porous MSQ became hydrophobic. As porogen loading increased, it generated a steric barrier for MSQ molecular chains, and thus reduced the collision probability of MSQ molecular chains to further crosslinking. Therefore, the reduction in moisture uptake using HMDS treatment could be attributed to the elimination residual hydroxide group, which played a secondary role (< 20%) in the overall moisture uptake as compared to pore surface area accounted for physical absorption of moisture (<80%).

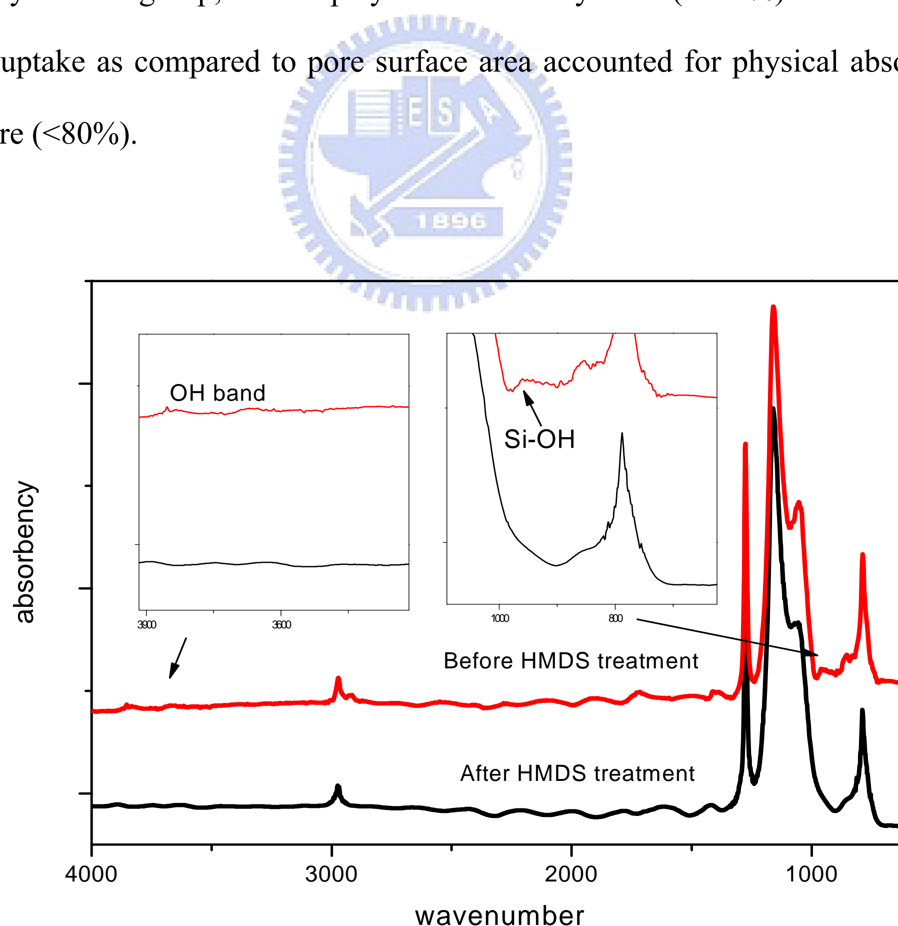

Figure 4.6 FTIR spectra of porous MSQ (19 % porosity) before and after HMDS treatment

The moisture uptake of MSQ/PS-b-P4VP hybrid films cured at 250 ^{o}C, which could be used as the starting ILD for copper damascene process, was studied using QCM and shown in Figure 4.7. The moisture uptake of dense MSQ film cured at 250°C was higher than that at 400 ^{o}C, because of its less degree of crosslinking illustrated in Figure 4.4. The moisture uptake of MSQ/PS-b-P4VP hybrid film increased with raising porogen loading. For example, at 10% loading, the amount of adsorbed water (1.67 wt%) was larger than its corresponding, porous film (0.77 wt%). The high uptake level in hybrid films was primarily attributed to the much increased amount of water sorption in porogen, 6.7 wt%. The free volume of the linear polymer, PS-P4VP was larger than the cross-linked MSQ, and PS-P4VP contained polar pyridine group, which had higher affinity toward moisture.

An ideal mixing rule of moisture uptake was applied to the MSQ/porogen hybrid films in order to further analyze any other factors contributing to the high-level of uptake, according the following expression:

$$wt\%_{hybrid} = wt\%_{porogen} * X + (1-X) * wt\%_{MSQ}$$

where X is the mass fraction of porogen, $wt\%_{porogen}$ (6.7 wt%) is the moisture uptake of pure porogen, $wt\%_{MSQ}$ (0.71 wt%) is the moisture uptake of MSQ film cured at 250 ^{o}C. The moisture uptakes of MSQ/porogen hybrid films were much higher than the values predicted by the ideal mixing rule and the deviations aggravated with increasing porogen loading as shown in Figure 4.7. The moisture uptake of hybrid films deviated from ideal mixing rule could be attributed to increased level of the residual Si-OH groups on the pores surface resulting from incomplete crosslinking at low cure temperature at 250 ^{o}C. The steric effect of high porogen concentration and interaction between the polar pyridine moiety of porogen with Si-OH in the MSQ matrix may also contribute to the increased level of Si-OH

sites. The other reason may involve an increase of moisture uptake at MSQ/PS-P4VP-Au substrate or porous MSQ-Au substrate interface. Such model had been proposed by J. Yao. *et. al* indicating that the moisture concentration near the interface of porous MSQ film and silicon substrate was much higher than the average level [74]. Lastly, the desorption curve of MSQ/PS-P4VP hybrid film could be reversed to initial state, shown in appendix A.

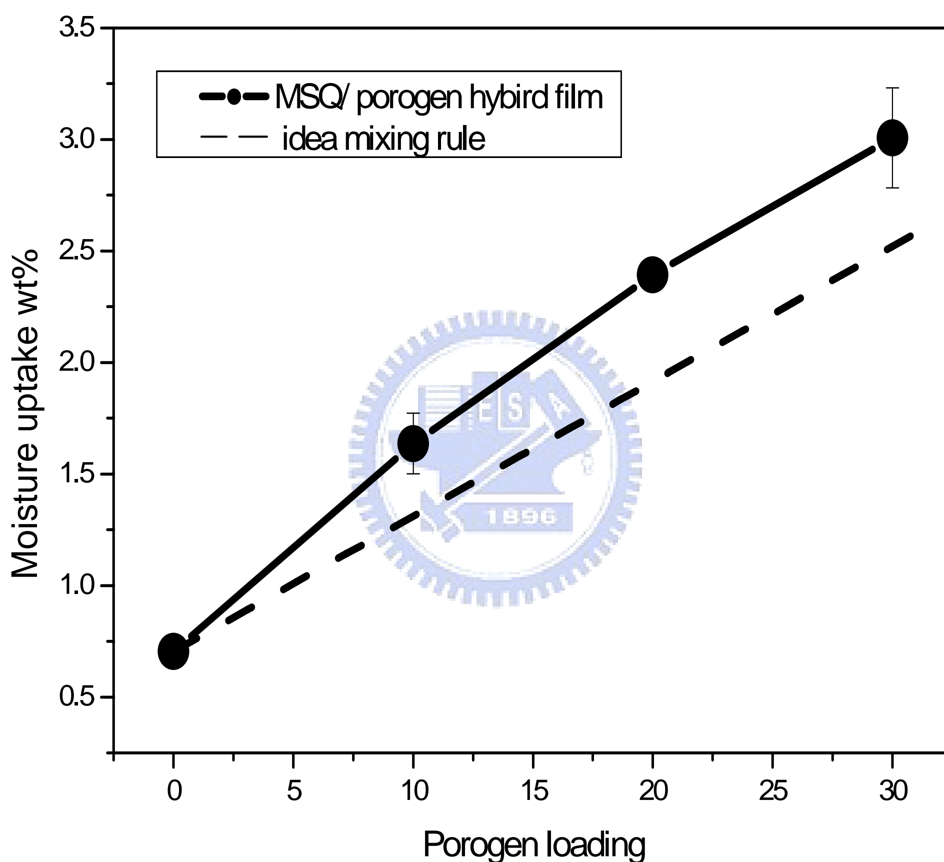

Figure 4.7 The moisture uptake of MSQ/PS-b-P4VP hybrid films a function of porogen loadings

4.2.4 Moisture uptake of MSQ/PS-PB-PS hybrid films

Next, a tri-block polymer, PS-PB-PS was used as a high-temperature porogen for comparison. The moisture uptakes of MSQ/PS-PB-PS compared to MSQ/PS-P4VP films were shown in Figure 4.8 and Table 4.2. The absorption and

desorption curves were attached in Appendix B as reference.

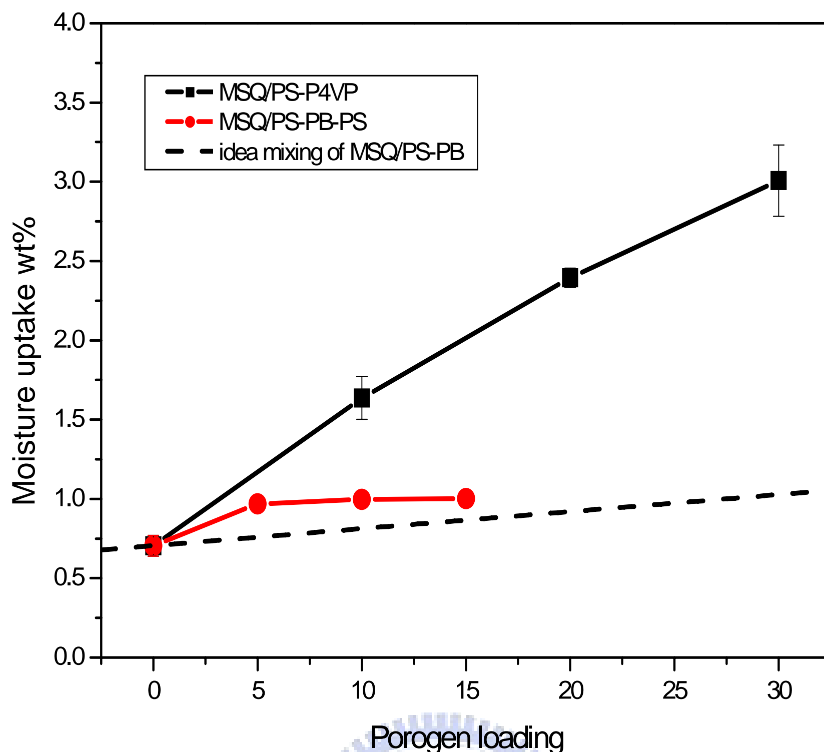

Figure 4.8 Moisture uptake of MSQ/PS-b-P4VP and MSQ/PS-PB-PS hybrid films

Table 4.2 Moisture uptake of MSQ/PS-PB-PS hybrid films

Loading	Moisture uptake (MSQ/PS-PB-PS), wt%
0	0.71
5	0.97
10	1.00
15	1.00

The moisture uptake in MSQ/ PS-PB-PS hybrid films were much lower, < 1.0 wt% as compared to <3 wt% MSQ/PS-P4VP hybrid films. For example, at 10% loading, the moisture adsorption of MSQ/PS-PB-PS films (1 wt%) was lower than MSQ/PS-P4VP films (1.67 wt%). The difference primarily originated from the low moisture uptakes of pure PS-PB-PS porogen, 1.8 wt% compared to 6.7 wt % in pure

PS-P4VP due to its polar pyridine moiety. We also observed that moisture uptake in MSQ/ PS-PB-PS hybrid films did not increase with increasing loading, instead remained relatively constant. The deviation from linear model could be attributed to increased level of moisture uptake at film/Au interface in QCM case. Overall, a hydrophobic PS-PB-PS as high temperature porogen could reduce moisture adsorption of hybrid films significantly as compared to PS-P4VP poorgen.

Finally, we also examined the desorption of moisture in MSQ/PS-PB-PS hybrid films. Similar to MSQ/PS-P4VP, the adsorption/desorption curve of MSQ/PS-PB-PS hybrid film could also reverse to its initial state. Thus, use of PS-P4VP and PS-PB-PS as high temperature porogen in MSQ/porogen hybrid ILD films had no difference after degassing under vacuum.

4.3 Dielectric properties

To understand the relationship between moisture uptake and dielectric properties, various porous MSQ films with and without HMDS treatment were measured at dry and RH 100% condition, shown in Figure 4.9. A porous MSQ films possessed a low dielectric constant of 2.46 when 30% porogen was added. The experimental data showed that dielectric constants of porous MSQ at dry condition were lower than those under RH 100% condition due to moisture adsorption. The amount of k reduction in dry condition increased with increasing porogen loading, in good agreement with the increasing trend of moisture uptake. After HMDS modification, the dielectric constants of porous MSQ films only slightly decreased when surface hydroxyl groups were eliminated by HMDS. This indicated after HMDS modified the surface became more hydrophobic. In addition, the number of polar Si-OH sites was relatively small compared to the total surface area in porous MSQ films. This observation was in good agreement with our finding from moisture uptake

study using QCM. Moreover, QCM method was more sensitive in qualitatively measuring the existence Si-OH compared to dielectric measurement using CV method.

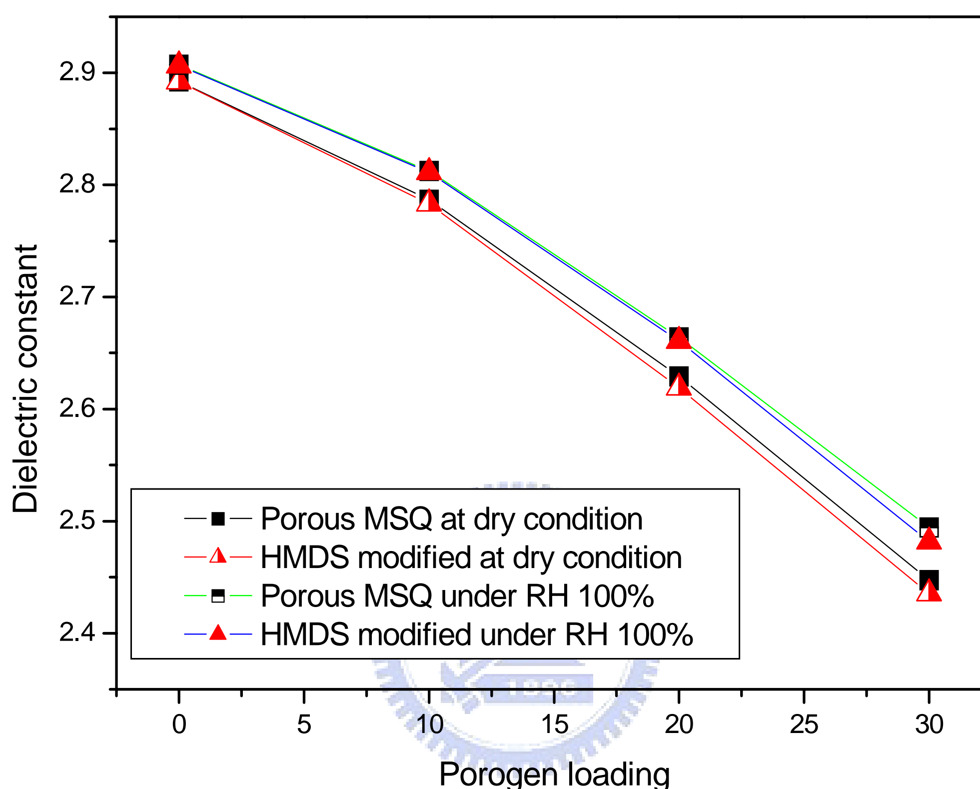

Figure 4.9 Dielectric constants of porous MSQ and HMDS-modified porous MSQ films at dry and RH 100 % conditions.

We then examined the dielectric properties of Solid-First^{TM} MSQ/porogen hybrid films cured at 250 ^{o}C under dry or wet conditions. The dielectric constants of MSQ/PS-P4VP hybrid films under dry and wet condition were shown in Figure 4.10.

The dielectric constants of hybrid films at RH 100% condition increased from 2.7 to 5.0 if porogen loading is increased from 0 to 30%. Their dielectric constants were much higher than those under dry condition, especially at high porogen loadings, due to high moisture uptake of hybrid film and k_{water}~78.

To sum up, the deviation of dielectric constant between HMDS modified and un-modified porous MSQ at dry and RH 100% films was very small, since the capacitance was strongly dependent on pore morphology and geometry. In contrast the HMDS modified and un-modified porous MSQ at dry and RH 100% films measured by QCM were more comparable and clear. Therefore, QCM was a powerful and sensitive tool for direct estimating amount of moisture adsorption in low-k films without further considered pore morphology and geometry.

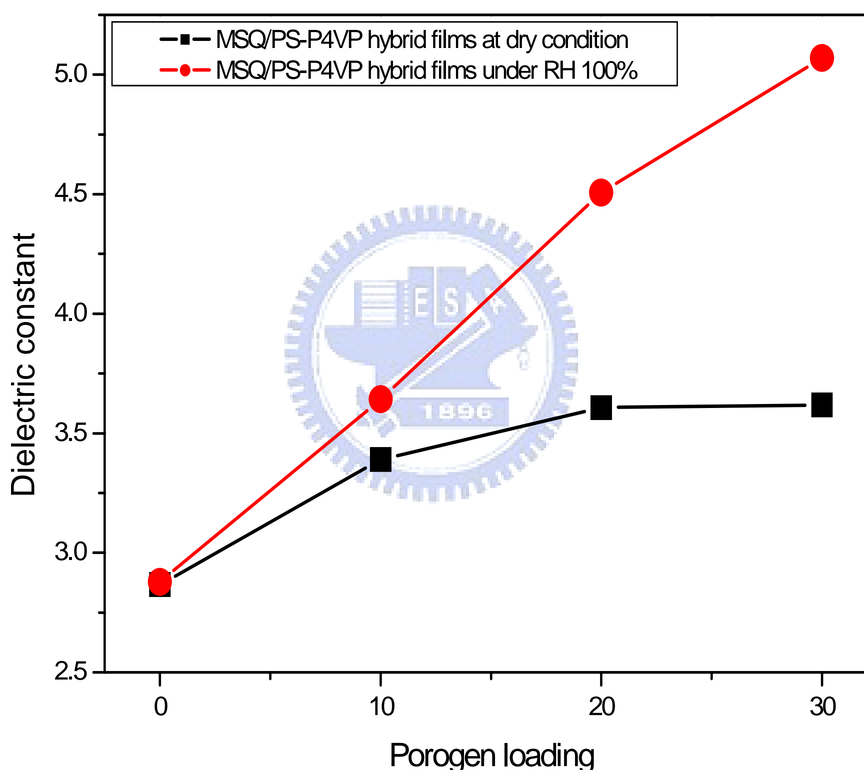

Figure 4.10 Dielectric constants of MSQ/PS-P4VP hybrid films at dry and RH 100% conditions

Model of dielectric constant of porous low-k materials

Since the amount of adsorbed H_2O bad been measured by QCM, the theoretic dielectric constants of porous MSQ films can by three different possible models such as (1) series model, (2) parallel model as shown by Figure 4.11, and (3) effective medium approximation (EMA model) assuming closed, spherical pores[64].

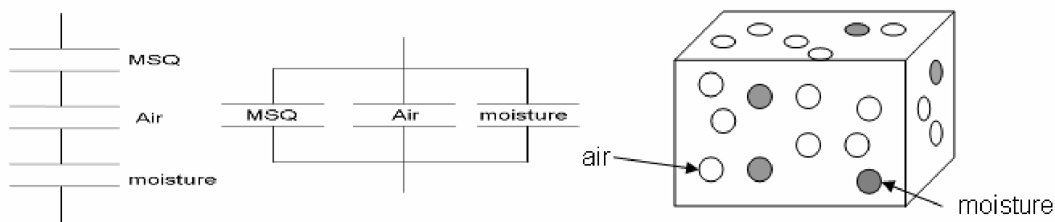

Figure 4.11 Series model, parallel model and EMA model of capacitance [64]

The total dielectric constants of the series and parallel models are expressed by Eq. 1 and 2, respectively

To calculate moisture induced dielectric constant difference, series and parallel model were employed. The models were shown in Figure 4.11

$$K_{film} = (1-x)K_{MSQ} + yK_{water} + (x-y)K_{air} \quad \text{...........(1)Parallel model}$$

$$\frac{1}{K_{film}} = \frac{(1-x)}{K_{MSQ}} + \frac{y}{K_{water}} + \frac{(x-y)}{K_{air}} \quad \text{................(2)Series model}$$

$$\frac{K_{film}-1}{K_{film}+2} = (1-x)\frac{K_{MSQ}-1}{K_{MSQ}+2} + (x-y)\frac{K_{air}-1}{K_{air}+2} + y\frac{K_{water}-1}{K_{water}+2} \quad \text{...(3)EMA model}$$

Where x is the porosity, y is the volume fraction of water, K_{MSQ} is the dielectric constant of MSQ, K_{water} and K_{air} are dielectric constants of water and air. The QCM moisture adsorption data and porosity were substituted into these three models to calculate the dielectric constants summarized in Figure 4.12. The calculations showed

that series and parallel models deviated significantly from experimental result, while EMA model strongly correlate with the dielectric properties of the porous MSQ in this study. This implied that the capacitance was strongly dependent on pore morphology and geometry. The pore morphology of these porous MSQ and MSQ/high-temperature hybrid films will be studied in the future.

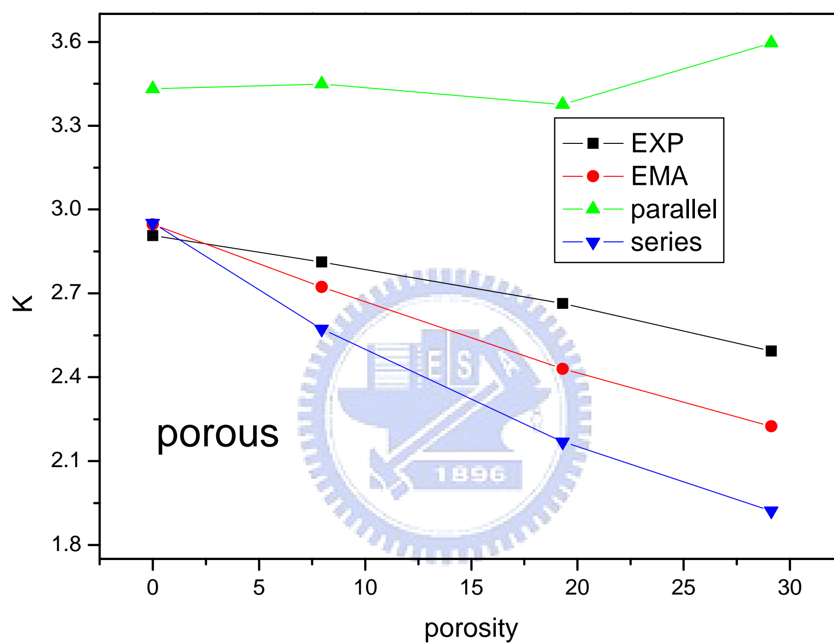

Figure 4.12 Calculated dielectric constants based on three models: series model, parallel models, and EMA model as function of loading vs. experimental data

4.4 Diffusion behavior

From manufacturing considerations, it was important to understand the diffusion behavior of moisture in dense MSQ, porous MSQ and the MSQ/porogen hybrids in order to design appropriate outgassing pretreatment prior to its subsequent processing steps, such as TaN barrier and etch-stop layer deposition to avoid any delamination caused by tremendous pressure from trapped moisture. In MSQ/PS-P4VP system, the moisture uptake of hybrid films could be desorbed or reversed to initial state (as illustrated in appendix A) completely within time scale (< 150 seconds), which made it easier for industry to add an additional outgassing step to eliminate trapped moisture. The outgassing time could be shortened at elevated temperature.

We attempted to characterize the diffusion coefficients and the diffusion mechanism of low-k films assuming that the diffusion followed Fickian diffusion behavior. Basically, the diffusion behavior could be modeled by following equation [75].

$$\frac{M_t}{M_\infty} = 1 - \frac{8}{\pi^2} \sum_{n=0}^{\infty} \frac{1}{(2n+1)^2} \exp\left[- \frac{(2n+1)^2 \pi^2 D t}{l^2} \right]$$

where M_t : the mass uptake at time t

M_∞: the equilibrium mass uptake

l: film thickness

D: diffusion coefficient.

A typical fitting curve illustrated in Figure 4.13 validated our assumption of Fickian

diffusion. Diffusion coefficient was then obtained from the fitting curve based on goodness of fit. Figure 4.14 summarized the diffusion coefficients of (1) MSQ/PS-P4VP hybrid films cured at 250 ^{o}C, (2) porous MSQ low-k films cured at 400 ^{o}C, and (3) Porous MSQ low-k films with HMDS treatment. Excluding the hybrid film with 30% porogen loading (D ~1.0×10^{-14} m^2/sec), the rest of diffusion coefficients were between $1x10^{-15}$ and $2x10^{-15}$ m^2/sec. Moreover, the diffusion coefficient of pure PS-P4VP porogen film cured at 250 ^{o}C, was extracted to be 2.4×10^{-14} m^2/sec, which was higher than low-k films due to its high free volume in PS-P4VP. For MSQ/hybrid films, one would expect its diffusion coefficient higher than dense MSQ film. Instead, to our surprise, diffusion coefficients of hybrid, porous and HMDS-treated films were almost the same except for hybrid film with 30% porogen loading. This implied that the diffusion process was dominated by a rate controlling step. A thin, but dense skin-layer on the surface of low-k films hypothesized.

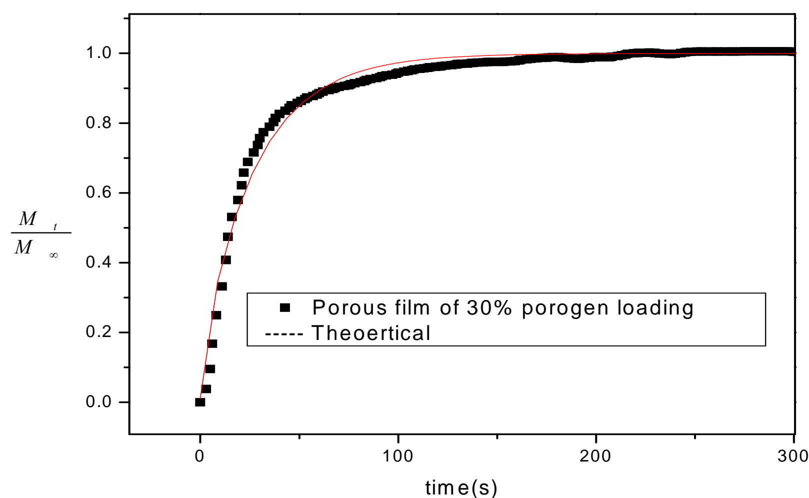

Figure 4.13 Typical fitting curve based on Fickian diffusion

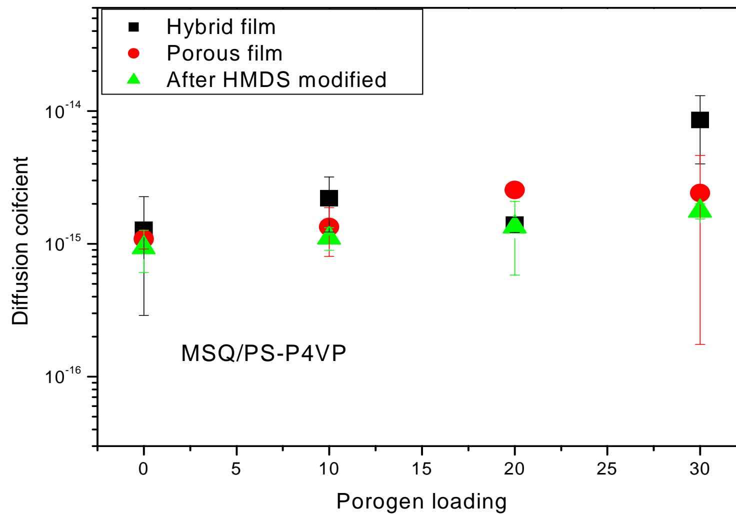

Figure 4.14 Diffusion coefficients of various low-k films versus different porogen loadings

This hypothesis was further confirmed by SEM viewgraphs of porous low-k films with 7.9 % porosity shown in Figures 4.15 (a)-(c) for (a) as-cured, (b) after FIB ion etching for 5 second with topview, and (c) cross-sectional view of as-cured porous MSQ film. No porosity was observed for as-prepared sample illustrated in Figure 14(a). In contrast, pore structures appeared after a short ion-etch, implying the existence of a skin layer in MSQ/PS-P4VP system, which was further confirmed by a cross-sectional SEM shown in Figure 14.15 (c). The skin layer was estimated to be 10-30 nm. However, detailed analysis by XRR will be carried out in a separate study.

Based on the physical evidence of a skin-layer by FIB/SEM and diffusion coefficient data, a bilayer low-k structure with a thin, but dense skin-layer was proposed and illustrated by Figure 4.16. The skin layer was speculated to be MSQ without porosity and behave as a rate controlling step in the moisture diffusion process.

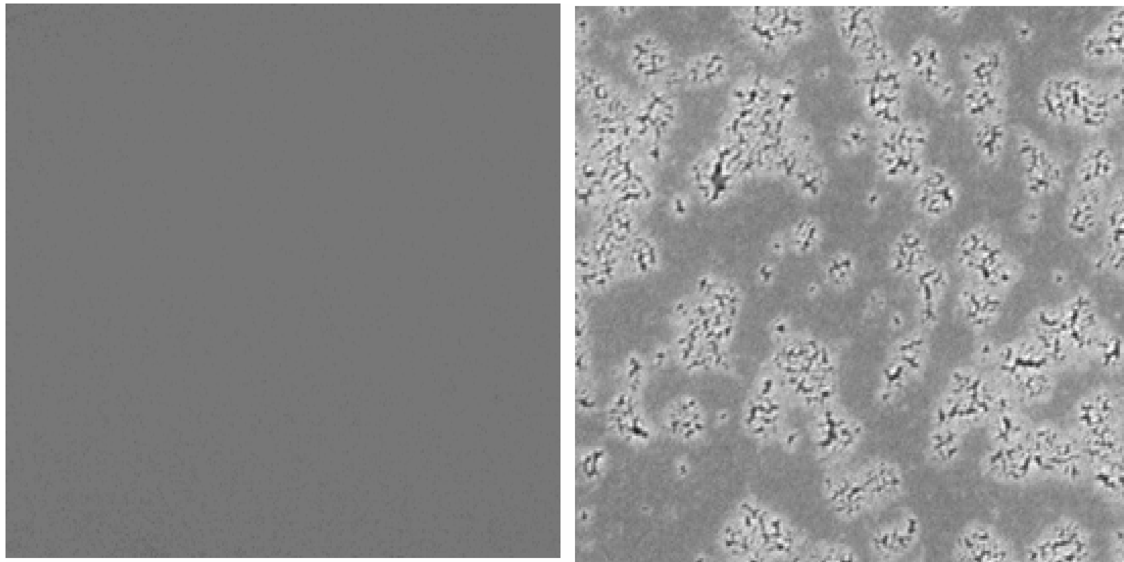

(a) as-cured; before etch (b) After etch 5 sec

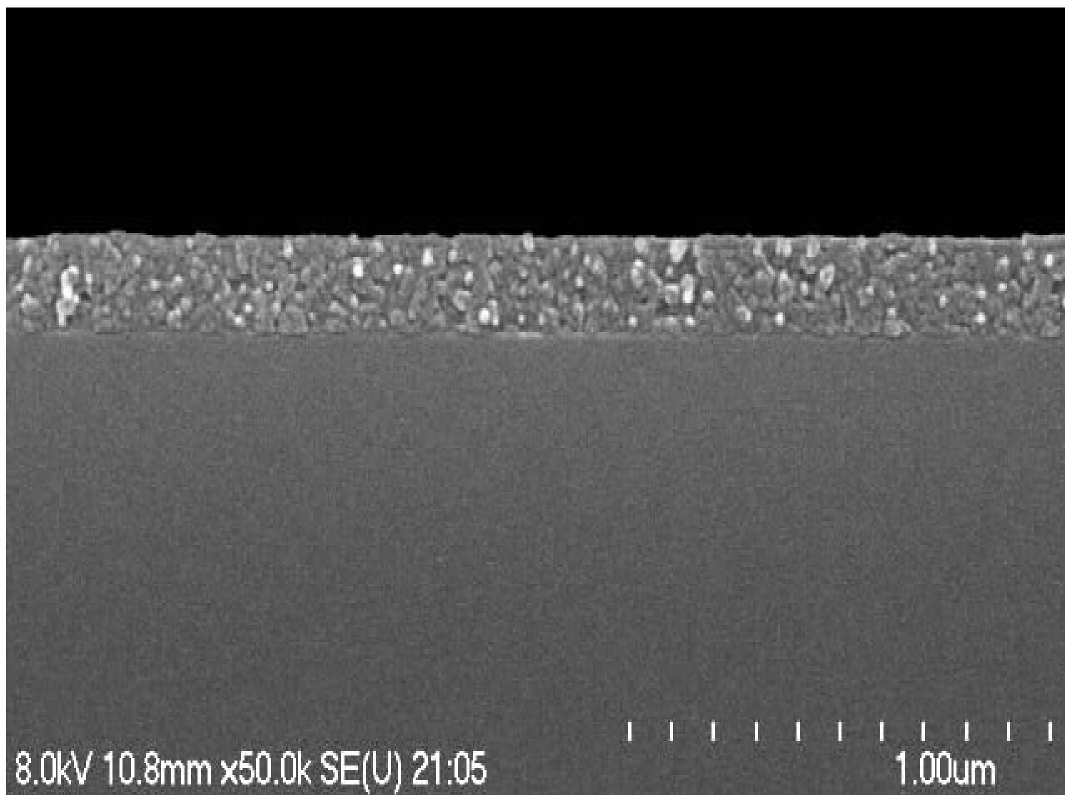

(c)

Figure 4.15 FIB/SEM topview of (a) as-cured, (b) after 5-second sputter etch and (c) cross-section view SEM of a porous MSQ film with 7.9 % porosity based on PS-P4VP porogen.

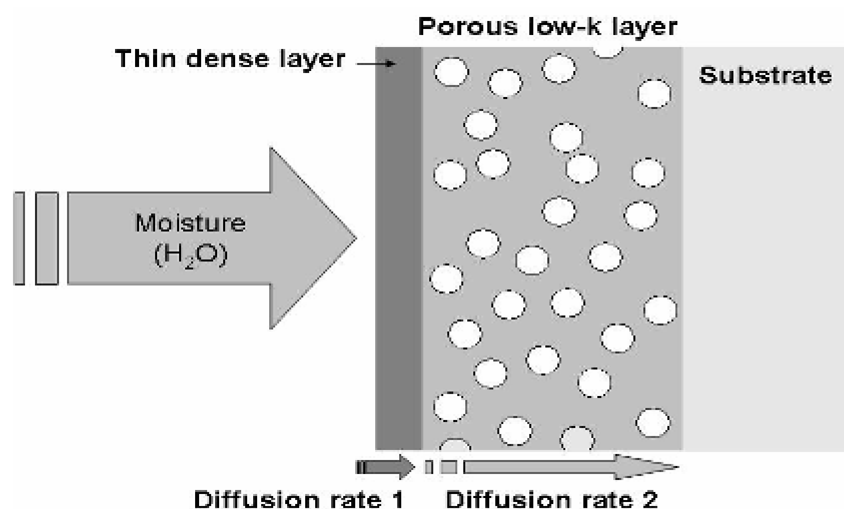

Figure 4.16 Schematic diagram of a skin layer/porous low-k matrix stack under the diffusion of moisture

In contrast, no skin layer was found in MSQ/PS-PB-PS hybrid films as shown in Figure 4.18. The possible mechanism of formation of skin layer in MSQ/PS-P4VP system was illustrated in Figure 4.17. During the spin-coating step, stable micelles were formed due to amphiphilic nature of PS-P4VP di-block copolymers, and then evaporation of solvent occurred at the top [76]. The concentration of solute species was much higher at surface, and thus solute species in sol-gel solutions tended to readily form a thin layer by condensation or cross-linking reactions. Within the matrix, the porogen would aggregate, if the inside of the gel did not undergo further condensation.

They were two reasons that there was no skin layer in MSQ/PS-PB-PS hybrid films. First, stable micelles could not form since hydrophobic PS and PB segment could not act as amphiphilic block copolymers. The other reason was the low boiling point (66 ^{o}C) of MSQ/PS-PB-PS solvent, tetrahydrofuran (THF). In contrast, the solvent for MSQ/PS-P4VP system, n-butanol possessed high boiling point, 117 ^{o}C. During the curing process of MSQ/PS-PB-PS, fast outgassing of bulk solvent made it

difficult to form any skin layer.

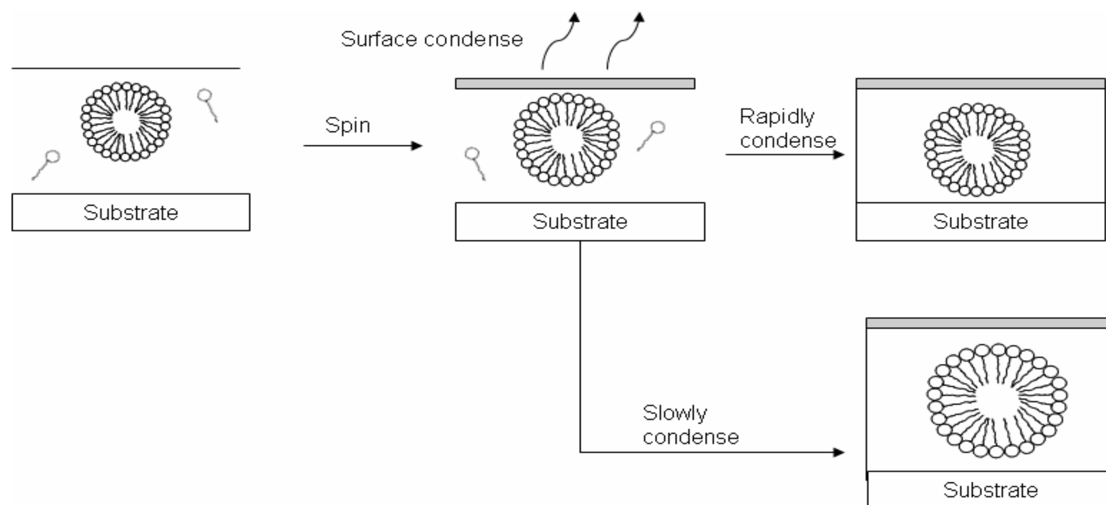

Figure 4.17 The proposed mechanism for skin layer formation in MSQ/PS-P4VP hybrid films

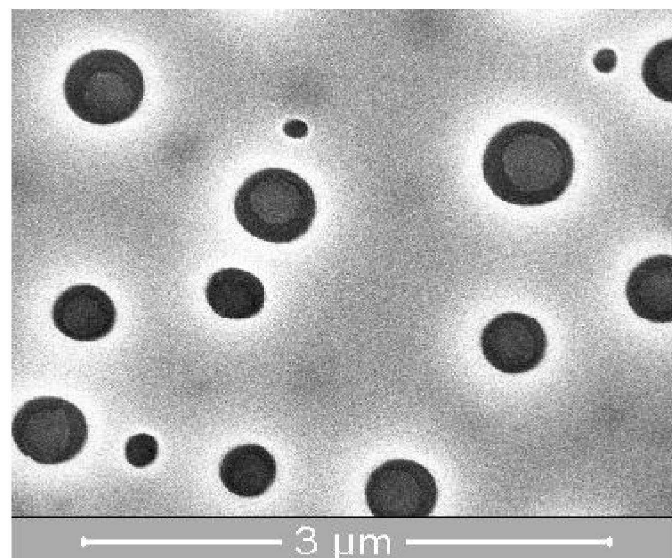

Figure 4.18 FIB/SEM top-view of as-cured MSQ/PS-PB-PS hybrid film with 5% porogen loading

Eliminating trapped moisture was an important pretreatment step for most of processing steps in low-k integration, several approaches such as nitrogen purge and thermal degas were proposed [77, 63]. A Solid-First^{TM} scheme based on MSQ/high-temperature porogen has been proposed to defer the removal of porogen until the completion of a Cu/low-k interconnect layer. However, there is still little

understanding of the adsorption behavior and outgassing behavior of Solid-First^{TM} low-k dielectric materials. From QCM measurement in this thesis study, the sorption/desorption curve showed that moisture adsorption in MSQ/PS-P4VP and MSQ/PS-PB-PS hybrid films could be reversed to initial state (0 wt%, desorption at ~10^{-3} torr) even though their moisture uptake were so different. The absorbed moisture could be desorbed or pumped out in a short time (<200 sec), which made it easier for industry to add a short outgassing step to eliminate the trapped moisture avoiding any blistering or delamination. The outgassing time could be further shortened if ougassing pretreatment was carried out at an elevated temperature. Moreover, a skin-layer was found in MSQ/PS-P4VP porogen hybrid films because of the amphiphilic nature of porogen and the high boiling point of n-butanol solvent. The skin layer, a dense MSQ layer behaved as a rate controlling step in the moisture diffusion process resulting in unvarying diffusion constants for porogen loading < 30% in MSQ/PS-P4VP hybrid films. The skin layer on the top of porous MSQ surface will offer the same barrier property and interfacial characteristics as the pure, dense MSQ.

Based on moisture uptake analysis using QCM and dielectric properties using CV-dot measurement, the mechanism of moisture uptake in porous MSQ films or MSQ/high-temperature porogen hybrid films could be summarized in two modes: physical sorption and chemical sorption. In physical sorption, the surface (1) within the MSQ or porogen matrix, (2) inside the pores, and (3) at the MSQ/substrate or porogen/substrate interface, interacted with the moisture adsorbent through a long range but weak Van der Waals force. In contrast, chemical sorption led to a formation of hydrogen bonding between silanol (Si-OH) and water as illustrated in Figure 4.19. This hydrogen bonding made the complete H_2O desorption from surface very difficult

unless high temperature (200~400 ^{o}C) was applied to overcome the bonding energy[78]. Our moisture sorption and desorption curves of the low-k films studied in this thesis all showed reversible behavior, indicating their adsorptions 30 ^{o}C were all in physical sorption mode. However, in Section 4.2.3, HMDS surface treatment could reduce moisture uptake further by 11-17% through chemical reaction to eliminate the polar Si-OH sites as previously illustrated by Figure 2.27. This implied that hydrogen bonding at residual Si-OH sites formed immediately after our samples were prepared, and remained intact in the subsequent moisture uptake and desorption processes. The hydrogen bonding Si-OH sites induced multilayered adsorbents through Van der Waals force, a physical sorption mode.

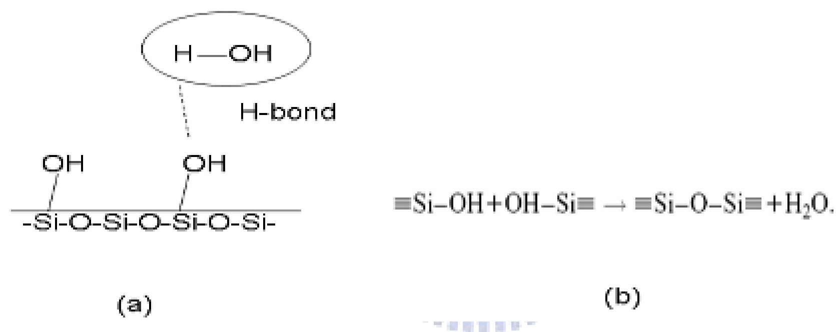

Figure 4.19 (a) hydrogen-bonding between silanol and water and (b) condensation reaction of silanols

Chapter 5 Conclusions

In this thesis, the impact of high-temperature porogens, their loadings on the moisture uptake and diffusion behavior was investigated for low-k films based on Solid-First^{TM} approach. Specifically, di-block and tri-block copolymers such as PS-P4VP and PS-PB-PS were employed as the high temperature porogens, whose decomposition temperature was higher than 300 ^{o}C. Three low-k dielectric systems were comprehensively studied in this thesis, namely: (1) MSQ films cured at different temperatures, (2) MSQ/porogens hybrid films with various porogen loadings, cured at 250 ^{o}C, which simulated the starting ILD materials in the Solid-First^{TM} scheme, and (3) porous films after porogens were completely removed by burn-out at 400°C, which simulated the final porous low-k materials after the completion of Solid-First^{TM} integration scheme of Cu/low-k interconnect. The moisture uptake of low-k films was investigated by using a home-built quartz crystal microbalance (QCM).

The moisture uptake of porous MSQ increased from 0.51 % to 1.77 % with raising porosity up to 29 %. The increased moisture absorption could be attributed to (1) increased surface area and (2) increased Si-OH sites on the pore surface due to increased surface area and increased polarity such as Si-OH on the pore surface due to incomplete crosslinking caused by the steric hindrance effect of porogen. High surface area could provide more sites for adsorbents [66], while high concentration of Si-OH could form hydrogen bonding with H_2O and even induce multilayered adsorbents through Van der Waals force. Moreover, the deviation of moisture uptake at 30% porogen loading from linearity was presumably caused by a change of pore morphology and/or increased Si-OH at higher degree, which required more in the future.

For MSQ/PS-b-P4VP hybrid low-k films cured at 250 ^{o}C, which could be used as the starting ILD for copper damascene process, the moisture adsorption were much larger than their corresponding porous MSQ. In addition, the deviation from ideal mixing rule increased with increasing porogen loading. Several factors contributed to such high moisture uptake; namely: (1) high moisture uptake of PS-P4VP porogen (6.7 wt%), (2) increased level of the residual Si-OH groups on the pores surface resulting from incomplete crosslinking at low cure temperature at 250 ^{o}C due to steric effect and additional interaction by the polar pyridine moiety of porogen, and possibly (3) increased moisture uptake at MSQ/PS-P4VP-Au substrate or porous MSQ-Au substrate interface.

For a tri-block copolymer, PS-PB-SP porogen, the moisture uptake in MSQ/PS-PB-PS hybrid films were much lower, ≤ 1.0 wt% as compared to MSQ/PS-P4VP hybrid films, ≤ 3 wt%. For example, at 10% loading, the moisture adsorption of MSQ/PS-PB-PS films (1 wt%) was lower than MSQ/PS-P4VP films (1.67 wt%). The difference primarily originated from the low moisture uptakes of pure PS-PB-PS porogen, 1.8 wt% compared to 6.7 wt % in pure PS-P4VP due to its polar pyridine moiety. We also observed that moisture uptake in MSQ/ PS-PB-PS hybrid films did not increase with increasing loading, instead remained relatively constant. The deviation from linear model could be attributed to increased level of moisture uptake at film/Au interface in QCM case. Overall, a hydrophobic PS-PB-PS as high temperature porogen could reduce moisture adsorption of hybrid films significantly as compared to PS-P4VP porogen.

HMDS pre-treated porous MSQ films cured at 400 ^{o}C showed 11-17% reduction in moisture uptake could be attributed to the elimination of residual silanol groups, which played a minor role (< 20%) in the overall moisture uptake. Based on our studies in the thesis, such moisture adsorption was believed to be physical sorption

mode by forming a multilayer H_2O adsorbent through long-range Van der Waals force with the hydrogen-bonded Si-OH--H_2O, which was formed immediately after sample preparation. Elimination of such Si-OH groups required either by high-temperature annealing (> 280 ^{o}C) or chemical reaction such as HMDS treatment employed in this thesis. Moreover, the variation of dielectric constant between HMDS modified and un-modified porous MSQ at dry and RH 100% films was very small. In contrast the HMDS modified and un-modified porous MSQ at dry and RH 100% films measured by QCM were more comparable and clear. Therefore, QCM was a powerful and sensitive tool for direct estimating amount of moisture adsorption in low-k films.

The diffusion behavior of moisture uptake and desorption in the MSQ/porogen hybrid and porous MSQ films were also investigated in this thesis. The sorption of moisture in porous MSQ and MSQ/high-temperature porogens (PS-P4VP and PS-PB-PS) was found to be Fickian diffusion and very fast (< 200 seconds) and the absorbed moisture could be completely desorbed or pumped out in a short time (< 200 sec), even though their equilibrium moisture uptake may Such reversible characteristics indicated the moisture sorption at 30 ^{o}C was purely in physical sorption mode. Therefore, for IC industry, a short outgassing pre-treatment step at room temperature or elevated temperature can be easily added in the low-k integration steps to eliminate the trapped moisture avoiding any blistering or delamination.

Furthermore, the diffusion constants of the MSQ/porogen hybrid and porous MSQ films were obtained by fitting the sorption curves based on Fickian diffusion. It was found that the diffusion coefficients of porous MSQ films (400 ^{o}C cure) at porogen loading ≤ 20% were relatively constant ranging from $1.0 \text{x} 10^{-15}$ to $2.0\ \text{x} 10^{-15}$ m^2/sec, while the diffusion coefficient of PS-P4VP porogen film was much higher at 2.4×10^{-14} m^2/sec. The unvarying diffusion coefficients in MSQ/PS-P4VP system could be attributed to the formation of a rate controlling, dense MSQ layer on the top

of the porous or hybrid porous low-k films. Such thin but dense layer could serve as a diffusion barrier layer to prevent precursor penetration from hybrids or porous films. The skin layer would be beneficial for MSQ/porogen hybrids in the Solid-First^{TM} scheme or porous MSQ to be processed in the damascene technology.

In contrast, no skin layer was observed for MSQ/PS-PB-PS system. The formation mechanism of such a dense layer in MSQ/PS-P4VP system was proposed based on the amphiphilic nature of porogen and the solvent evaporation rate as dictated by its boiling point. For spin-coated MSQ/PS-P4VP/n-butanol system, the top of the as-deposited film was first to form a thin layer due to fast evaporation of solvent near the top during spin-coating step, while the evaporation of bulk n-butanol solvent was still relatively low at room temperature. In contrast, no skin layer was found in MSQ/PS-PB-PS hybrid films because the low boiling point (66 ^{o}C) of MSQ/PS-PB-PS solvent, tetrahydrofuran (THF) would outgas relatively fast and made it difficult to form any skin layer.

Based on moisture uptake, diffusion behavior analysis using QCM at 30 ^{o}C and dielectric properties using CV-dot measurement, we concluded the moisture uptake in porous MSQ films or MSQ/high-temperature porogen hybrid films was sorely in physical sorption as evidenced by the reversible sorption/desorption behavior for all the samples in this thesis. The moisture uptake in our samples included the following physical sorption modes through Van der Waals long-range force with (1) available surface area within the MSQ or porogen matrix, inside the pores, and at the MSQ/substrate or porogen/substrate interface, which contributed < 80% of moisture uptake, and (2) available hydrogen-bonded Si-OH--H_2O sites, which were formed immediately after sample preparation, which contributed < 20% of moisture uptake.

References

1. M.T. Bohr, IEEE International Electronic Device Meeting, 241 (1995).
2. Y. H. Wang and R. Kumar, J. Electrochem. Soc. **151,** 73 (2004).
3. S. J. Martin, J. P. Godschalx, M. E. Mills, E. O Shaffer and P. H. Townsend, Adv Mater. **12**, 1769 (2000).
4. S. Malhouitre, C. Jehoul, J. V. Aelst, H. Struyf, S. Brongersma, L. Carbonell, I. Vos, G. Beyer, M. V. Hove, D. Gronbeck, M. Gallagher, J. Calvert and K. Maex, Micro. Eng. **70**, 302 (2003).
5. M. L. Che, C. Y. Huang, S. Choang, Y. H. Chen, Y. L. Wang, and J. Leu, ECS Trans. 6, 591 (2007)
6. C.C. Chang, S. K. Jangjian and J. S. Chen, J. Electrochem. Soc. **153**, 901 (2006).
7. International Technology Roadmap for Semiconductor, Executive summary, 2005.
8. National Technology Roadmap for Semiconductor (NTRS), 1997 edition (Semiconductor Industry Association, San Jose, California)
9. R. J Gutmann, IEEE Trans. Microw. Theory Tech. **47**, 667 (1999).
10. H. D. Young, R. A . Freedman, Physics (Addison-Wesley, Massachusetts 1995)
11. D. I. Bower, An Introduction to Polymer Physisc(Cambridge University, Chapter 9, 2002)
12. G. Huougham, G. Tesoro, A. Viehbeck and J. D. Chapple-Sokol, Macromolecules, **27,** 5964 (1994)
13. C. H. Ting, T.E. Seidel, Materials Research Society Symposium - Proceedings, Low-Dielectric Thin Films for Micoelectronics Applications, 1995

14. P.V. Zant, Microchip Fabrication : a practical guide to semiconductor processing (McGraw-Hill, 2001)
15. K. Mikagi, H. Ishikawa, T. Usami, M. Suzuki, K. inoue, N. oda, S. Chikaki, I. Sakai and T. Kikkawa, IEEE International Electronic Device Meeting, **365** (1996)
16. Y. L. Cheng, Y. L. Wang, C.P. Liu, Y. L. Wu, K. Y. Lo, C. W. Liu, J. K. Lan, Mater. Chem. Phys, 150, **83** (2004)
17. Y. H Wang and R. Kumar, J. Electrochem. Soc, **151**, 73 (2004)
18. C. C Chiang, M. C. Chen, L. J. Li, Z. C. Wu, S. M. Jang, and M. S. Liang, J. Electrochem. Soc, **151**, 612 (2004)
19. T. B. Casserly, K. K. Gleason, Plasma Process. Polym, **2,** 679 (2005)
20. Y. C. Sil, Y. Y. Hun, L. K. Man, L. H. Ju and C. C.Kyu, Thin Solid Films, **26**, 50 (2006)
21. Rusil, M. R. Wang, T. K. S. Wang, M. B. Yu and C. Y. Li, J. Electrochem. Soc, **152**, 838 (2005)
22. M. R. Wang, Rusil, J. L. Xie, N. Babu, C.Y. Li and K. Rakesh, J. Appl. Phys, **96**, 829 (2004)
23. A trademark of Novellus (www.novellus.com
24. A trademark of Applied Materials (www.appliedmateraials)
25. http://www.read-electronics.com/semiconductor/index.asp?layout=articlePrint &articleID=CA279106
26. R. H. Baney, M. Itoh, A. Sakakibara and T. Suzuki, Chem. Rev, 95, 1409 (1995)
27. R. Franco, A. K. Kandalam and R. Pandy, J. Phys. Chem, 106, 1709 (2002)
28. P. S. Ho, J. Leu and W. W. Lee, Low Dielectric Cinstant Materials for IC Application, Chapter 6 (Springer, 2002)

29. H. C. Liou and J. Pretzer, Thin Solid Films, 335, 186 (186)

30. S. J. Martin, J. P. Godschalx, M. E. Mills, E. O. Shaffer and P. H. Townsend. Adv. Mater, **23** , 1769 (2000)

31. http://www.eetimes.com/news/latest/showArticle.jhtml?articleID=18308274reference/EE times http://xx

32. R. W. Jones, Fundamental Principles of Sol-Gel Technology (London, The Institute of Metals, 1989)

33. S. Loo, S. Idapalapati, S. Wang. L. Shen and S. G. Mhaisalkar, Scripat Materials, 57, 1157 (2007)

34. I. Sugiura, N. Misawa, S. Otsuka, N. Nishikawa, Y. Iba, F. Sugimoto, Y. Setta, H. Sakai, Y. Koura, K. Nakata, Y. Mizushima, T. Suzuki, H. Kitada, N. Shimizu, S. Nakai, M. Nakaishi, S. Fukuyama, T. Nakamura, E. Yano, M. Miyajima and K. Watanabe, Micro. Eng, **82**, 380 (2005)

35. A. Sayari, I. Moudrakovski, J. S reddy, C. I. Ratcliffe, J. A. Pipmeester and K. F. Preston, Chem. Mat, **8**, 2080 (1996)

36. J. M. Thomas, O. Terasaki, P. L. Gai, W. Zhou and J. Gonzalez-Calbe, Accounts Chem, Res, **34**, 583 (2001)

37. Y. H. Sakamoto, M, Kaneda, o. Terasaki, D. Y. Zhou, J. M. Kim, G. Stucky, J. Shin and R. Ryoo, Nature, **408**, 449 (2000)

38. M. Kruk, M. Jaroniec, Y. Sakamoto, O. Terasaki, R. Ryoo and C. H. Ko, J. Phys. Chem. B, **104**, 292 (2000)

39. M.S. Wong, H. C. Huang and J. Y. Ying, Chem. Mat, **14,** 1961 (2002)

40. T. R. Pauly and T. J. Pinnavaia, Chem. Mat, **13,** 987 (2001)

41. M. S. Wong, E. S. Jeng and J. Y. Ying, Nano. Lett, **1**, 637 (2001)

42. C. T. Kresge, M. E. Leonowicz, W. J. Roth, J. C. Vartuil and J. S. Beck, Nature, **359**, 710 (1992)

43. J. S. Beck, J. C. Vartuil, W. J. Roth and M. E. Leonowicz, J. Am. Chem. Soc, 114, 10834 (1992)
44. Q. Huo, D. I. Margolese, U. Ciesla, D. G.. Demuth, and P. Feng, Chem. Mat, **6**, 1176 (1994)
45. Q. Huo, D. I. Margolese, U. Ciesla, P. Feng, T. E. Gier, and G. D. Stucky, Nature, **368**, 317 (1994)
46. P. T. Tanev and T. J. Pinnavaia, Science, **267**, 865 (1995)
47. S. A. Bagshaw, E. Prouzet and T. J. Pinnavaia, Science, **269**, 1242 (1995)
48. D. Y. Zhao, J. L. Feng, Q. S. Huo, N. Melosh, G. H. Fredrickson, B. F. Chmelka and G. D. Stucky, Science, **279**, 548 (1998)
49. D. Y. Zhao, Q. S. Huo, J. L. Feng, B. F. Chelka and G. D. Stucky, J. Am. Chem. Soc, **120**, 6024 (1998)
50. M. S. Wong and J. Y. Ying, Chem. Mat, **10**, 2067 (1998)
51. M. R. Porter, Handbook of Surfactant (Chapman and Hall, New york, 1991)
52. K. Mosig, T. Jacobs, K. Brennan, M. Rasco, J. wolf and R. Augur, Micro. Eng, **64**, 11(2002)
53. J. Tan, Z. W. Zhong and H. M. Ho, Micro. Eng, **81**, 75 (2005)
54. Z. Chen, K. Prasad, C. Li, N. Jiang and D. Gui, IEEE Trans. Device Mater. Reliab., **5**, 133 (2005)
55. T. Abell and K. Maex, Micro. Eng, **76**, 16 (2004)
56. A. M. Hoyas, J. Schuhmacher, C. M. Whelan, J. P. Celis and K. Maex, Micro. Eng, **76**, 32 (2004)
57. Z. Chen, K. Prasad, C. Y. Li, P. W. Lu, S. S. Su, L. J. Tang, D. Gui, S.Balakumar, R. Shu, and R. Kumar, Appl. Phys. Lett, **84** , 2442 (2004).
58. C. Jezewski, C. J. Wiegand, J. wiegand, D. Ye, A. Mallikarjunan, D. Liu, C. Jin, W. A. Lanford, G. C. Wang, J. J. Senkevich and T. M. Lu, J. Electrochem.

Soc, **151**, 157 (2004)

59. V. Jousseaume, M. Fayolle, C. Guedj, P. H. Haumesser, C. Huguet, F. Pierre, R. Pantel, H. Feldis and G. Passmard, J. Electrochem. Soc, **152**, 156 (2005)
60. S. Malhouitre, C. Jehoul, J. V. Aelst, H. Struyf, S. Brongersma, L. Carbonell, I. Vos, G. Beyer, M. V. Hove, D. Gronbeck, M. Gallagher, J. Calvert and K. Maex, Micro. Eng. **70**, 302 (2003).
61. E. G. Liniger and E. E. Simonyi, J. Appl. Phys, **96**, 3482 (2004)
62. J. Yao, A. Iqbal, H. Juneja and F. Shadman, J. Electrochem. Soc, **154**, 199 (2007)
63. C. C. Chang, S. K. Jangjian and J. S. Chen, J. Electrochem. Soc, **153**, 901 (2006)
64. T. Kikkawa, S. Kuroki, S. Sakamoto, K. Kohmura, H. Tanaka and N. Hate, J. Electrochem. Soc, **152**, 560 (2005)
65. A. P. Singh, D.D. Gandhi, E. Lipp, M. Eizenberg and Gramanath, J. Appl. Phys, **100**, 114504 (2006)
66. S. Rogojevic, A. Jain, W. N. Gill and J. Plawsky, Eeletrochem. Solid-state Lett, **5**, 22 (2002)
67. S. I. Kuroki and T. Kikkawa, J. Electrochem. Soc, **153**, 759 (2006)
68. A. R. Forouhi and I. Bloomer, Phys. Rev. B. **34**, 7018 (1986)
69. P. R. Griffiths and J. A. deHaseth, Fourier Transform Infrared Spectrometry. (wiley, 1986)
70. C. Lu and A.W. Czanderna, Applications of Piezoelectric Quartz Crystal Microbalance, (Elsevier, New York, 1984).
71. P. S. Ho, J. Leu, W. W. Lee, Low Dielectric Constant Materials for IC Application, chapter 2 (Springer 2002).
72. S. V. Nitta, V. Pisupatti, A. Jain, P. C. Wayner, W. N. Gill and J. L. Plawsky, J.

Vac. Sci. Technol B. **17**, 205 (1999)

73. C. Y. Wang, J. Z. Zheng, Z. X, Shen, Y. Xu, S. L. Lim, R. Liu and A. C. Huan, Surf. Interface Anal. **28,** 97 (1999).
74. J. Yao, A. Iqbal, H. Juneja and F. Shadman, J. Electrochem. Soc, **154**, 199 (2007)
75. J. Crank, The Mathematics of Diffusion, (Oxford University, London, 1975)
76. D. E. Haas, J. N. Quijada, S. J. Picone and P. Birnie, Proc SPIE Int Soc Opt Eng, **3943**, 280 (2000)
77. A. Iqbal, H. Juneja, J. Yao and F. Shadman, AICHE, **52**, 1586 (2006)
78. J. Proost, E. Kondoh, G. Vereeche, M. Heyns and K Maex, J. Vac. Sci. Technol. B, **16,** 2091 (1998)

Appendix A

QCM data curve of Moisture uptakes of porous, HMDS modified, MSQ/PS-P4VP hybrid films and PS-P4VP films.

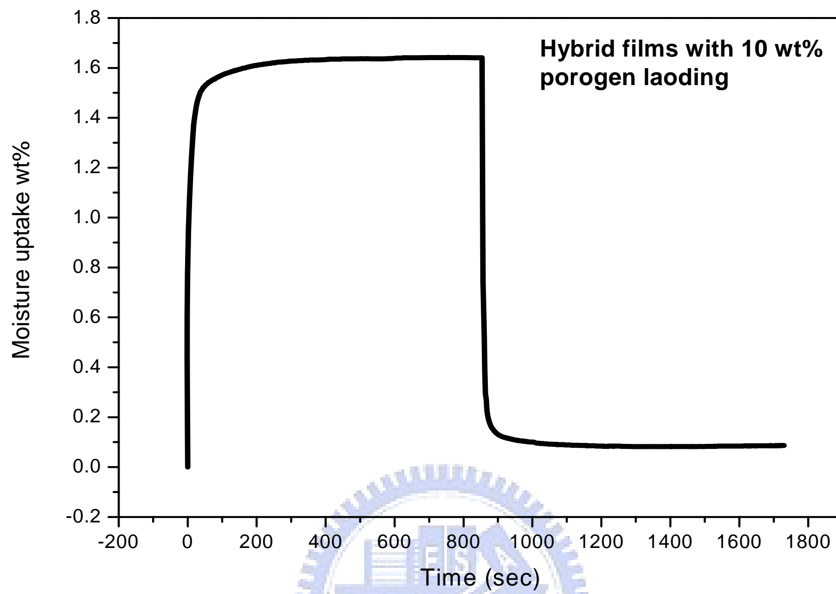

(a) Hybrid film with 10 wt% loading

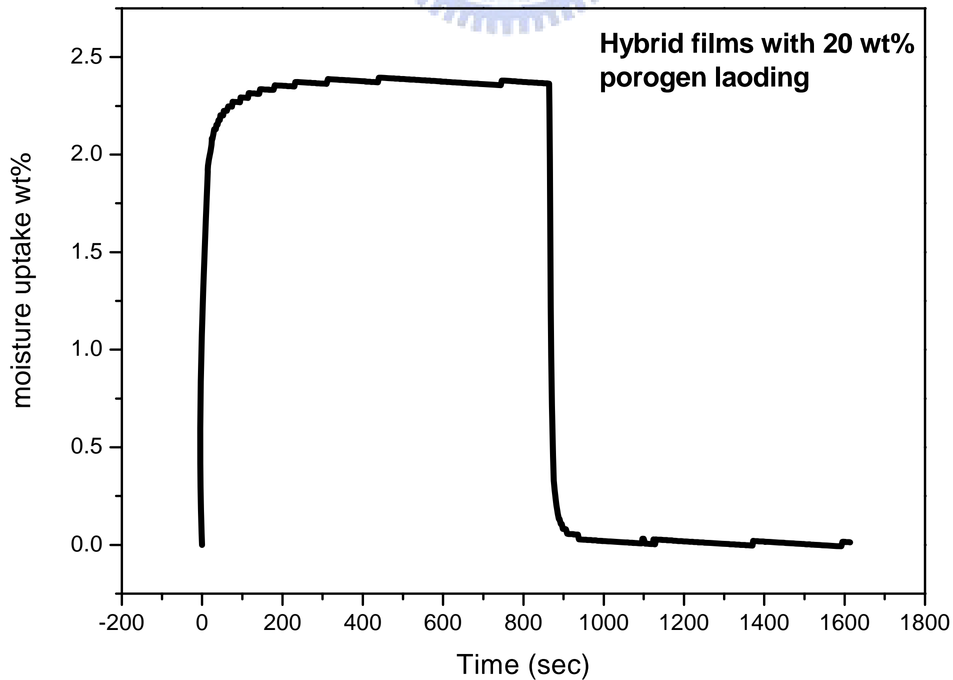

(b) Hybrid film with 20 wt% loading

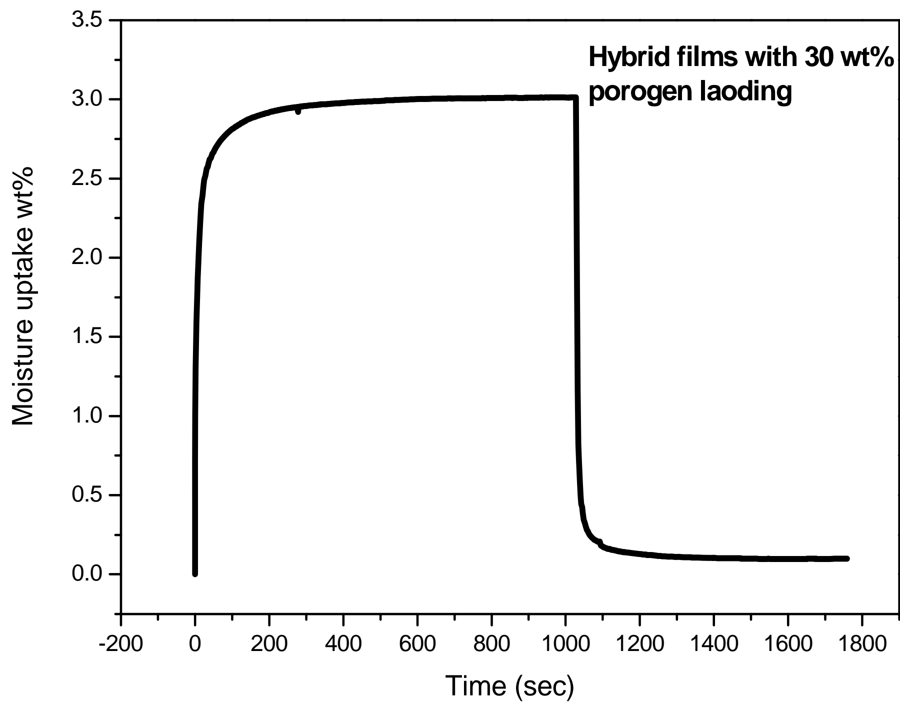

(c) Hybrid film with 30 wt% porogen loading

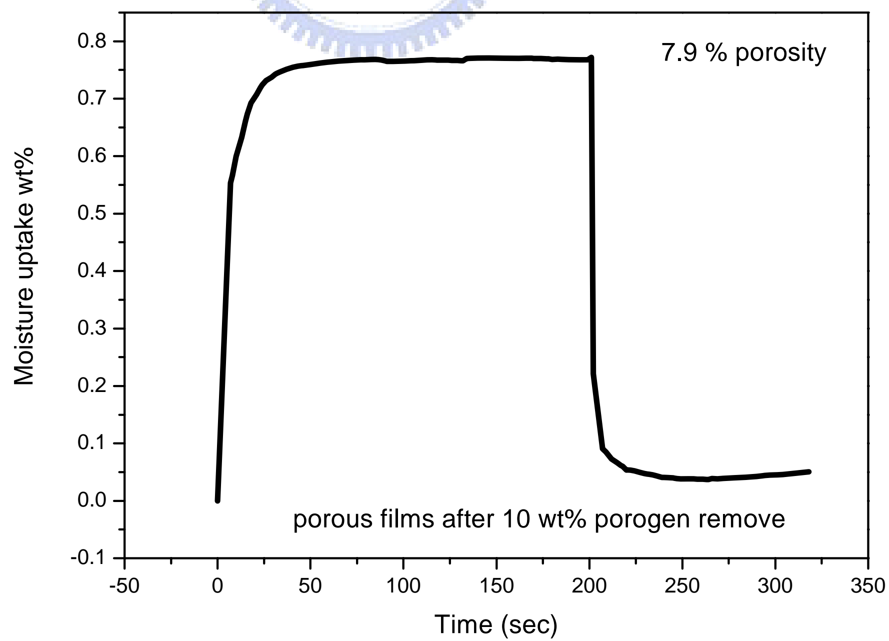

(d) Porous MSQ with 7.9 % porosity

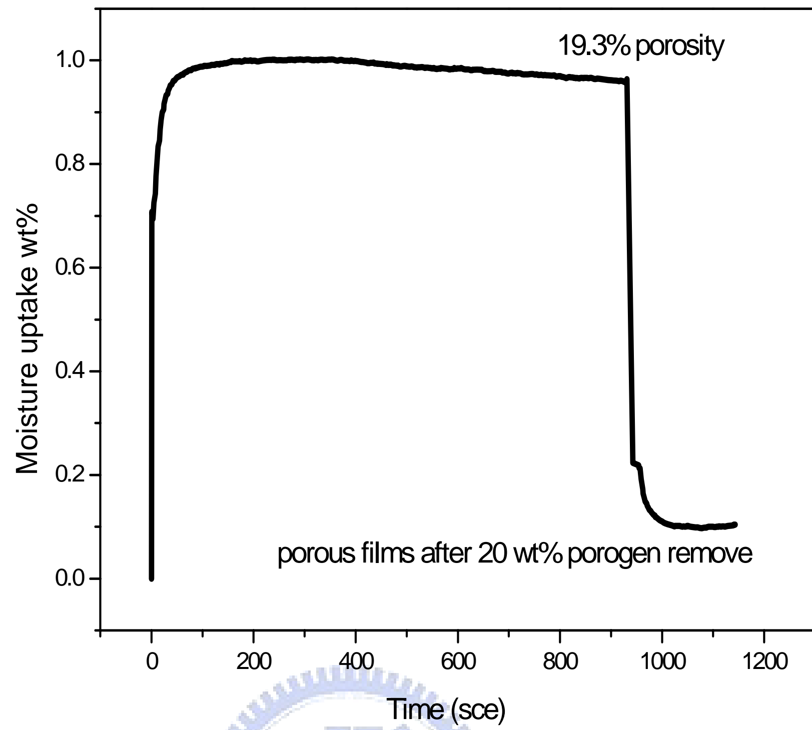

(e) Porous MSQ with 19.3 % porosity

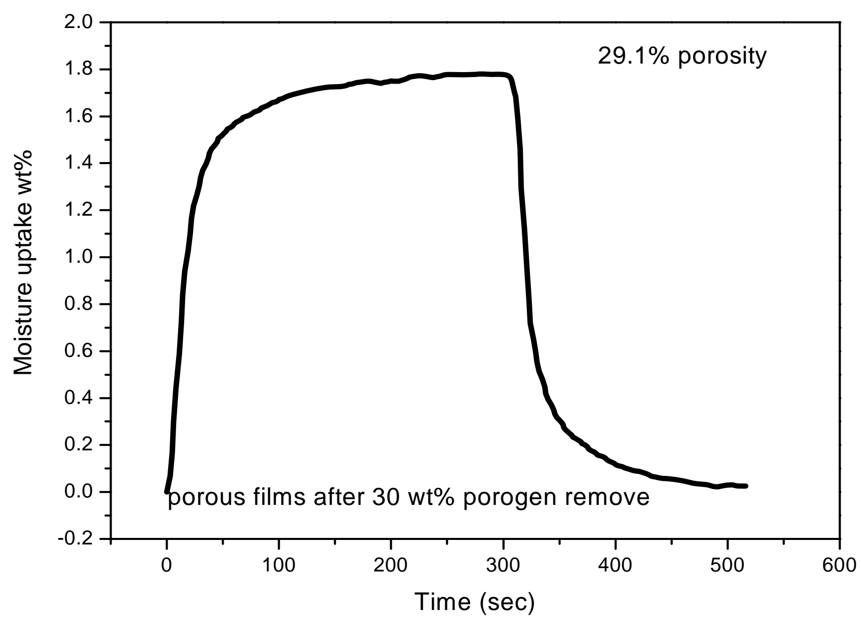

(f) Porous MSQ with 29.1 % porosity

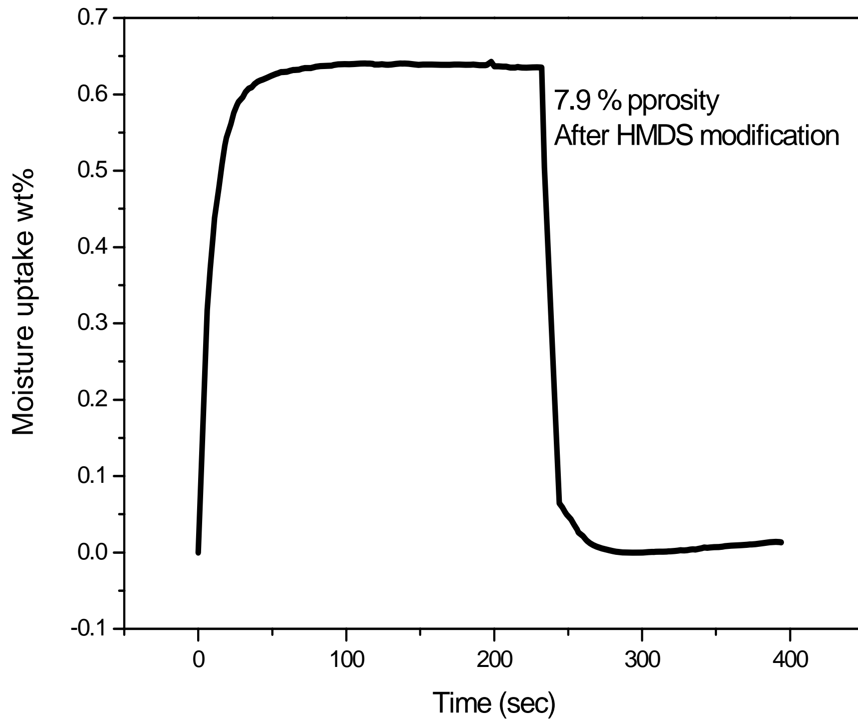

(g) Porous MSQ after HMDS modification

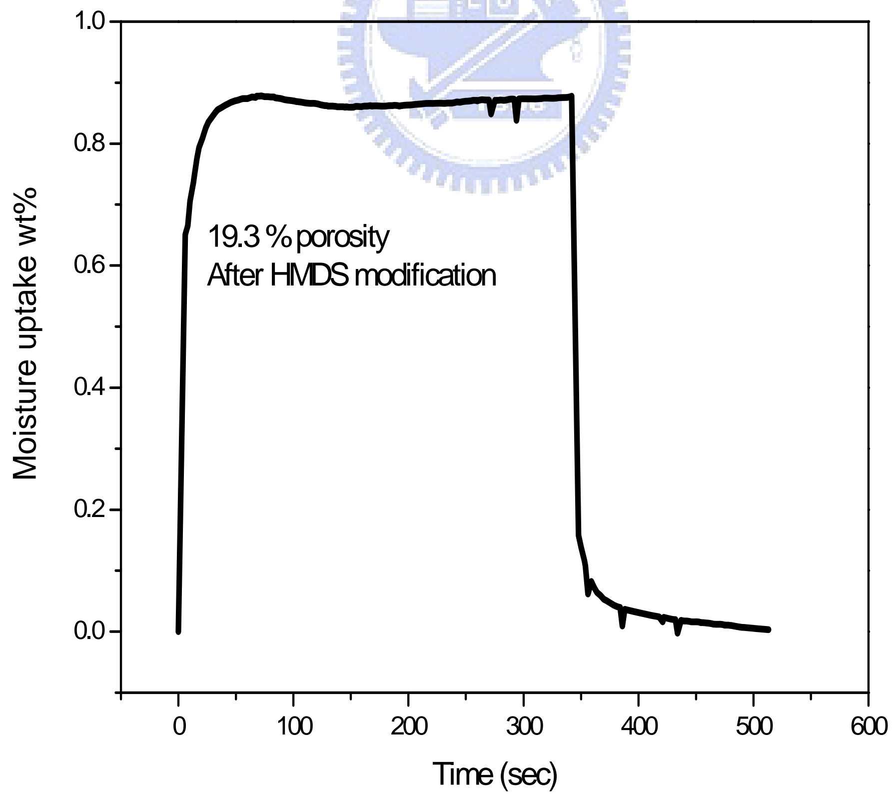

(h) Porous MSQ after HMDS modification

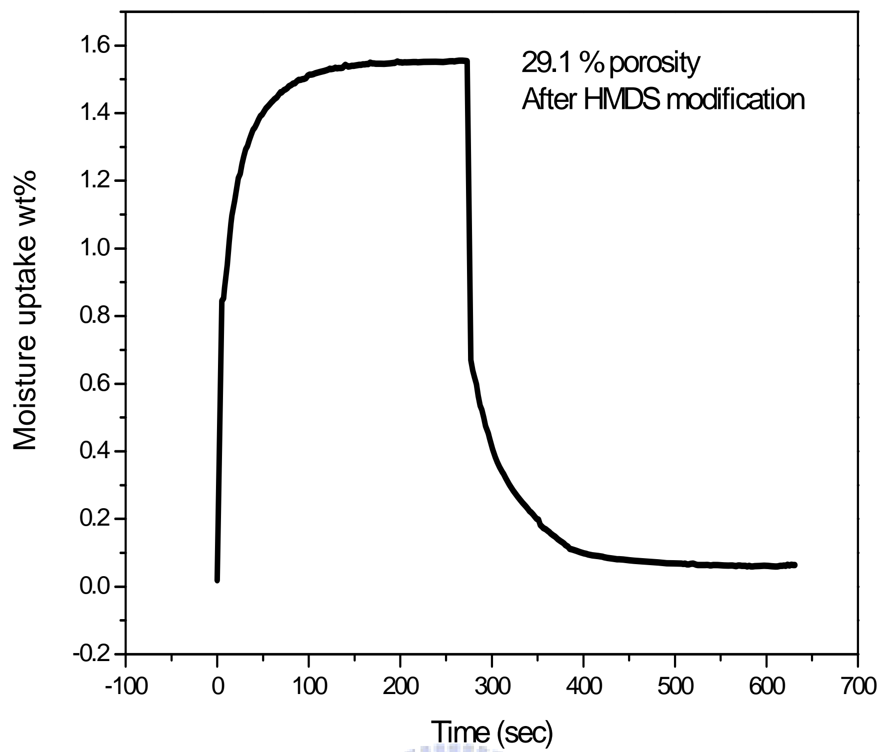

(i) Porous MSQ after HMDS modification

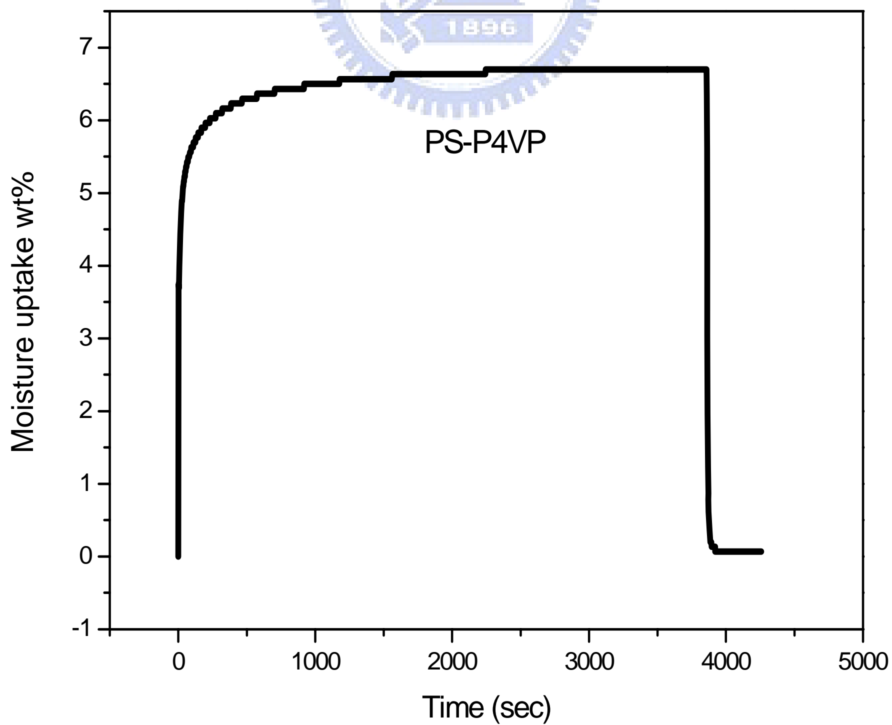

(j) Pure porogen

Appendix B

QCM data curve of Moisture uptakes of MSQ/PS-PB-PS hybrid film

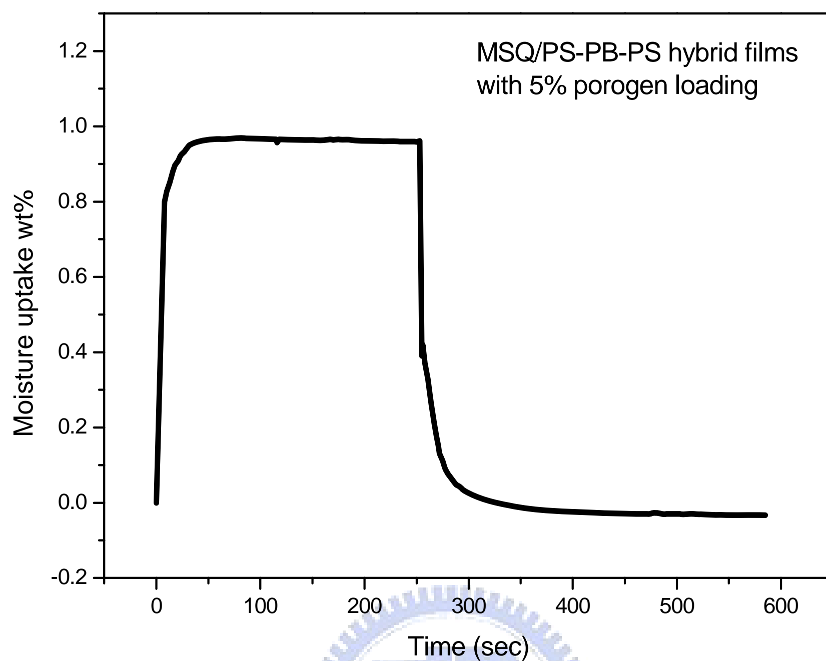

(a) Hybrid film with 5 wt% loading

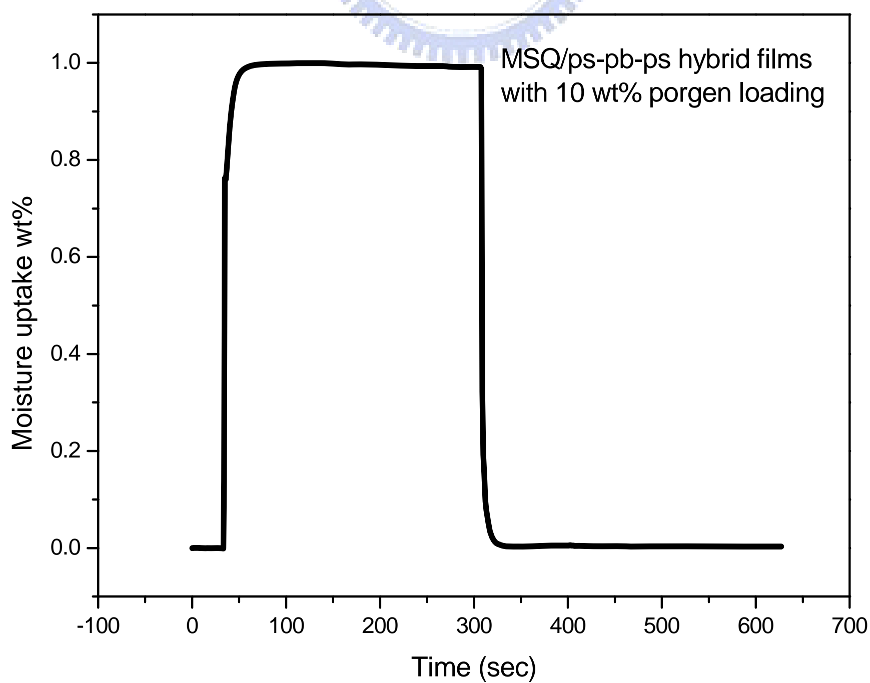

(b) Hybrid film with 10 wt% loading

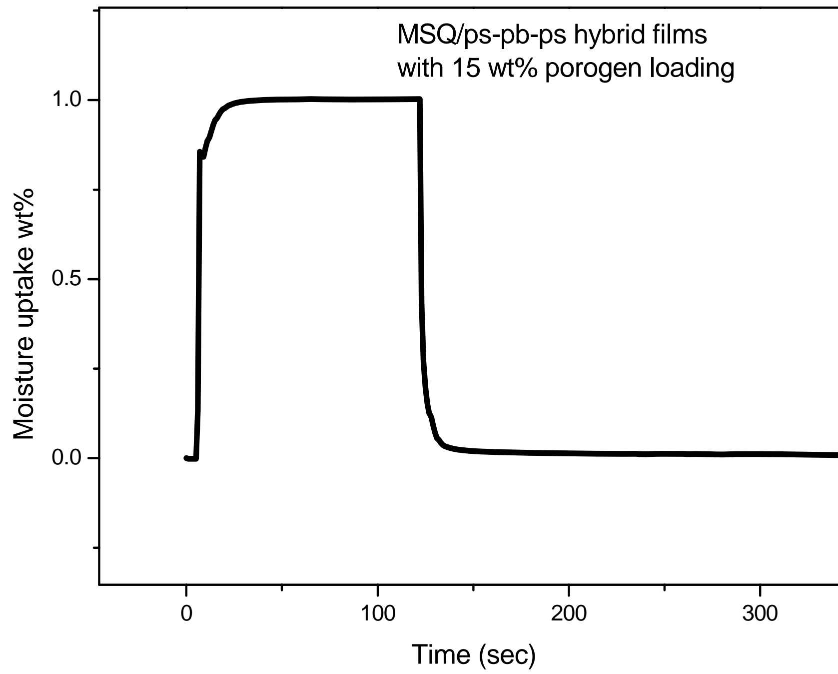

(c) Hybrid film with 15 wt% loading

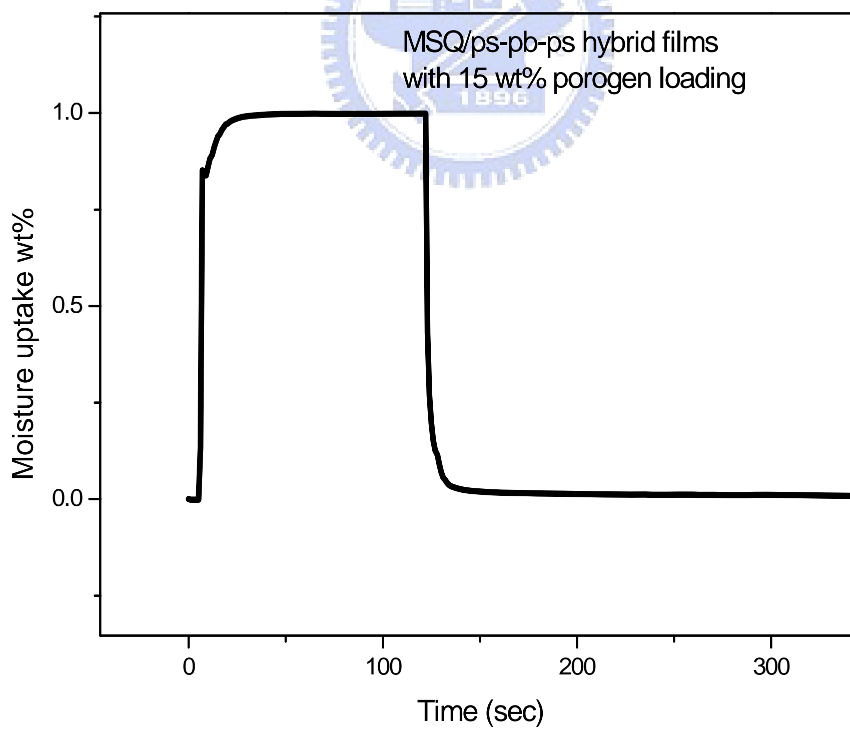

(d) Pure porogen